Fracture Mechanisms in PVC and Other Thermoplastics

by

Lidia Hsueh Lee

B.A., New York University (1979)
S.M., Polytechnic Institute of New York (1981)

Submitted to the
Department of Materials Science and Engineering
in partial fulfillment of the requirements
for the degree of

DOCTOR OF PHILOSOPHY

at the

Massachusetts Institute of Technology
August, 1984

Signature of Author ———————————————————————

Department of Materials Science and Engineering
August 10, 1984

Certified by ———————————

Professor Frederick McGarry
Thesis Supervisor

Accepted by ———————————

Professor Bernhardt J. Wuensch
Chairman, Department Committee on Graduate Students

Fracture Mechanisms in PVC and Other Thermoplastics

by

Lidia Hsueh Lee

Submitted to the
Department of Materials Science and Engineering
on August 10, 1984 in partial fulfillment of the requirements
for the Degree of Doctor of Philosophy.

Abstract

Multiple crazing was found to be the principle non-elastic deformation mechanism occurring at the crack tips of PVC pipe materials under plane strain conditions. A direction correlation between multiple crazing and fracture toughness value is established based on the study of fracture properties of several thermoplastic polymers. The results indicate that the formation of multiple crazes at the crack tip serves as an energy absorption mechanism which enhances the fracture toughness value of a polymer. The failure mechanisms of the polymers which form multiple crazes was shown to be broadly similar. A transition from multiple crazes to a single craze occurs prior to catastrophic failure. Associated with this transition is a changing of crack propagation mode from stable to unstable. The governing factors for this transition in PVC were investigated by studying craze initiation, craze growth and the velocities of crack propagation before and after the instability. The multiple-single craze transition was suggested to be due to the interaction among the crazes and the rate effect on the initiation of the multiple crazes. The fracture toughness value of PVC could be estimated successfully from the number of crazes and the craze properties determined by using interference microscopy and electron microscopy techniques. The effect of microstructures of PVC, in terms of the crystallinity and the molecular entanglements, on the properties of the crazes was investigated.

Thesis Supervisor: Frederick McGarry

Title: Professor of Materials Science and Engineering

Acknowledgments

I like to express my sincere gratitude to Professor F.J. McGarry, my thesis advisor, and Dr. J. Mandell for their guidance, invaluable suggestions and support through out the course of this study.

Thanks to Mr. A.P. Rudolph for his excellent assistance in machining. His genuine concern and encouragment as a spiritual friend will always be remembered. I am grateful to Mr. L.I. Sudenfield and Ms. E.L. Shaw for their kind and excellent help in the SEM lab.

I wish to extend my gratitude to my friends in the polymer group, for all their help and friendship. Special thanks to Anoop Agrawal for sharing his technical insight and experiences with me.

I am indebted to Mark Matson, without whose unsparing help the printout of this thesis would not have been possible.

I am most indebted to my parents for their love, care, and support. Lastly, special thanks to my dear husband, Daniel, who has supported me with his love, understanding and prayers all along the way.

Table of Contents

List of Tables

List of Figures

CHAPTER ONE

Introduction

The use of polymeric materials as structural components has increased significantly over the last decade, but the use often is limited by the tendency of these materials to fail in a macroscopically brittle manner.

Polyvinyl chloride (PVC) is one of the most widely used polymeric materials. One important application of PVC is in plastic pipes, where a major service problem is brittle fracture characterized by unstable extension of a crack when the pipe is pressurized under certain rate or temperature conditions. Linear elastic fracture mechanics (LEFM) has been found to be applicable to the study of the failure behavior of PVC pipe under certain testing conditions. In the theory of fracture mechanics, the fracture toughness property of a material can sometimes be defined by a single parameter K_c, the critical value of the stress intensity factor at which brittle fracture occurs in a material body containing a sharp defect, normally a pre-existing crack. Severals aspects of the fracture toughness of PVC pressure pipe materials have been addressed in the recent papers, such as the development of testing techniques and the applicability of linear elastic fracture mechanics [1], the effects of rate [1] and temperature [2], and fractographic analysis [2]. In these studies, the applicability of LEFM and the criteria for a valid plane strain fracture toughness test of PVC pipe material have been well established. It was shown that the fracture behavior of PVC pipe materials shifts from notch-insensitive, yield stress controlled to brittle linear elastic fracture mechanics controlled as the temperature decreases or the rate increases.

Although the macroscopic fracture toughness of PVC is directly related to the non-elastic deformation processes at the crack tip prior to fracture, little has been reported on the deformation processes involved in brittle fracture.

Fracture mechanics has developed as a branch of theoretical stress analysis and is a continuum theory with few apparent links to the fine-scale microstructure [3]. Cleavage in metals and polymers is always preceded and/or accompanied by some plastic deformation, however small. In metals, plastic yielding accompanied by strain hardening is the principal source of fracture toughness [4]. In polymers, the resistance to fracture arises from two nonelastic deformation processes at the crack tip: shear and cavitation. Shear processes, either diffuse shear yielding or the formation of more localized microshear bands, usually take place without the loss of intermolecular cohesion, and thus produce very little, if any, change in density. Cavitation processes, either crazing or isolated void formation, occur by a local loss of intermolecular cohesion and result in a significant decrease in the local density [5]. Whether a polymer would undergo shear yielding or cavitation depends on, in addition to the chemistry and structure of the material, the state of stress, time (or deformation rate), and temperature. [6]

Among typical polymers, the deformation mechanisms in Polystyrene(PS), Polymethyl methacrylate(PMMA), and Polycarbonate(PC) have been extensively studied. PS and PMMA have high propensities for craze development and are therefore very suitable for the study of crazing. PC exhibits comparatively high ductility, and the study of its deformation mechanism is often stimulated by commercial interest. The deformation mechanisms in PVC, however, has been studied less. Most of the results reported were obtained using thin specimens. The results usually led to the conclusion that PVC deforms by shear yielding and not by crazing. In fact, PVC at one time was classified as a non-crazing material [7, 8]. These results are not very useful for understanding the deformation processes occurring in PVC pipes, which have thick

pipe walls and generally fail under plain strain conditions. While the craze profile in other polymers, such as PS [9] and PMMA [10] , correlate well with the plastic zone at the crack tip expressed by the Dugdale model, discrepancies are reported for PVC [11] . Prediction of K_{Ic} for rigid PVC by calculations based on the crack tip craze and using a generalized model of the cohesive zone, as compared with measured values, has not been successful.

Usually, studies of the non-elastic deformation mechanism at the crack tip in polymers are done using transparent materials. Reports on the microscopic failure mechanisms of opaque material such as PVC pipes are scarce, possibly due to the absence of methods which can be used to study the nature of the yield zone. Consequently, physical interpretations of the results of macroscopic fracture properties of PVC pipes are subject to error from the lack of a clear understanding of the microscopic deformation processes occurring before crack propagation.

The objectives of this work were to study the micro-deformation processes related to the brittle fracture process of PVC pipe material and to investigate the fracture energy absorption mechanisms which are directly related to the non-elastic deformation processes at the crack tip prior to fracture.

CHAPTER TWO

Literature Review

2.1 Fracture Mechanics

Several different fracture theories have been applied to brittle crack propagation in glassy polymers. These can be divided essentially into energy criteria and stress criteria. A comprehensive treatment of these is outside the scope of this review (however, excellent reviews are given in [12] and [13]). A brief survey of their application to crack propagation in glassy polymers is given here.

2.1.1 Griffith Criterion

Griffith [14] stated that a necessary condition for new surfaces to form is that the change in the stored energy during crack growth is sufficient to provide the surface energy of the new crack surfaces. Using a stress field calculation by Inglis [15] for an elliptical flaw in an infinite plate with a tensile stress, σ, normal to the flaw, the Griffith equation is derived as

$$2\gamma = \frac{1}{2}\frac{dU}{dc} = \frac{\pi\sigma^2_c c}{E}$$

and the stress required for unstable fracture, σ_c, is

$$\sigma_c = \frac{2E\gamma}{\pi c}$$

where γ: Surface energy.

E: Young's modulus

C: Half the elliptical flaw length

U: Elastic stored energy

2.1.2 Critical Stress Intensity Factor

The stress intensity factor is a measure of the magnitude of the crack tip stress field. It depends on the gross section stress, σ, and the square root of the half crack length c. Thus, the stress intensity factor K incorporates both geometrical terms and the stress level. For various geometries with cracks of length 2c,

$$K = \sigma \sqrt{\pi c} \cdot Y$$

where Y: Geometrical factor which depends on geometry and loading conditions.

If the crack extends at gross section stresses significantly less than the yield stress, and K at fracture is found to be a constant for various specimen geometries, then this value of K is denoted as K_c, and provides a single parameter fracture criterion. K_c is the critical stress intensity factor at which the crack will extend rapidly, leading to fracture [16].

2.1.3 Elastic Strain Energy Release Rate

The elastic strain energy release rate, G, is defined as

$$G = \frac{dU}{dA}$$

where U: Elastic stored strain energy
A: Crack area

G can be presented as a function of the load and the change in compliance of the specimen C with respect to the crack area [16],

$$G = \frac{P^2 \partial C}{B \partial c}$$

The critical value of G corresponds to 2γ in the Griffith equation. The concepts of LEFM can be developed independently either in terms of G or K, but the two criteria are not independent; they are related by

$$K^2 = GE \quad \text{Plane stress}$$

$$K^2 = \frac{GE}{(1-\nu)} \quad \text{Plane strain}$$

where ν: Poisson's ratio.

2.2 Deformation and Fracture

In most cases, a suitable choice of temperature and deformation rate for each material brings all glassy polymers to a similar mechanical response. Referred to glass transition temperature (T_g), the effect of temperature on the tensile stress-strain behavior of glassy polymers shows a general phenomenology of deformation and fracture. Four distinct temperature ranges can be classified based on different characteristics of fracture mode, determined by the interaction between the flow (shear yield) stress and the fracture stress exhibited in each range. These are ductile, semi-

ductile, semi-brittle, and brittle fracture [6]. It should be noted that the intrinsic flow stress of polymer is represented by its compressive flow stress, since crazing, which could interfere with the bulk flow processes, is inhibited under compression.

In the temperature region described as ductile fracture, failure is usually accompanied by a significant amount of bulk flow. Although PVC pipe materials may fail in a ductile manner in service, only brittle failures are considered in this study.

At a temperature range immediately below the ductile fracture region is the region described as semi-ductile. Discontinuous yielding followed by essentially unlimited ductility is manifested in compressive deformation. In tensile deformation, however, both bulk flow and crazing occur simultaneously. The breakdown of crazes to form a crack preempts continued development of the more homogeneous deformation process and the polymer fails catastrophically before general yielding. In the semi-ductile region, the flow stress is below the fracture stress.

As the temperature is lowered from the semi-ductile region, the intrinsic flow stress increases and eventually exceeds the tensile fracture strength. As a result, in the semi-brittle region the flow stress is greater than the fracture strength and the crazes develop in the absence of bulk ductility.

The temperature and rate dependency of yield stress for PVC [17, 18] and PVC pipe material have been reported [1]. In unnotched tensile specimens, a transition from a discontinuous yielding to a brittle failure mode has been observed around -60 ^{o}C in several different PVC pipe materials [1]. This transition temperature, however, can be shifted by different processing treatments or testing conditions. Nevertheless, in the absence of compressive flow stress data for PVC, no comparison between the temperature dependence of the flow stress and the fracture stress can be made.

2.3 Crazing

The fracture of many polymers is preceded by the formation of a structure known as craze. A craze is initiated when an applied tensile stress causes microvoids to nucleate at points of high stress concentration in the polymer created by scratches, flaws, cracks, dust particles, molecular heterogeneities, etc [9]. The microvoids develop in a plane perpendicular to the maximum tensile stress component. The resulting localized yielded region consists of an interpenetrating network of voids and polymer fibrils and is known as a craze. Unlike a crack, it is capable of transmitting loads across its faces. Crazes weaken the polymer matrix in which they form, and are often involved in the processes of crack initiation and crack propagation. However, under certain circumstances crazes absorb a large amount of mechanical energy and therefore is beneficial to the fracture toughness.

2.4 Craze Morphology and Structure

The two major tools in characterizing craze microstructure have been X-ray scattering and electron microscopy. That crazes scatter X-rays strongly has been reported by several workers who have estimated the size of the scattering element [19, 3]. However, due to molecular orientation in the polymer elements, the interpretation of the X-ray scattering pattern due to craze matter becomes very difficult. Therefore, electron microscopy is more generally used in studying craze structure.

The success of transmission electron microscopy (TEM) often depends upon the ability to ultramicrotome thin sections and view them in the microscope without excessively damaging the craze structure. A summary of different techniques used in this regard has been presented in reference [20]. Based on TEM studies, it has been found that crazes generally consist of an open network of polymer fibrils between 100 Å and 400 Å in diameter, interspersed by pores between 100 and 200 Å in diameter. The craze is highly light reflecting because it has a refractive index which is much lower than

that of the bulk polymer. The importance of the craze refractive index is that it may be used with the Lorentz-Lorenz equation to calculate the polymer content of the craze [21]. Such calculations reveal that in the absence of residual stress, or under low stresses, the composition of "fresh crazes" lies in the range of 40-60 volume percent polymer, the remainder being air or liquid depending upon the craze-forming environment. [22]

In recent years, interference microscopy has been used as a powerful tool for direct observation of the profile at the crack tip in transparent thermoplastics. Essential requirements for the application of this method are : a) the crack opening and craze zone thickness should be comparable in order of magnitude to the wavelength of light , b) the refractive index of the crazed material should differ significantly from that of the bulk material, and c) the boundary between the two regions should be sharp [23].

Interference fringes of crazes at crack tips were first reported by Kambour [7]. He analyzed the fringe pattern using interference optics and was able to determine a craze-crack profile. A number of studies involving the use of the fringe patterns have since been completed. For example, this technique has been used in studying the effect of molecular weight and temperature on craze shape and fracture toughness in polycarbonate [24], craze growth and crack growth in PVC under monotonic and fatigue loading [25], Young's modulus of the craze in PMMA [26], and craze shape and fracture in PMMA [10]. Important information related to fracture, such as craze shape, craze extension ratio and strain at break, and stress at craze boundary become accessible with this technique. A comprehensive review on the optical interference measurements and fracture mechanics analysis of crack tip craze zones has been given by Doll [27].

2.5 Shear Yielding

The other mode of plastic deformation in polymers is a shear process consisting of a distortion of shape with little or no volume change. The degree of strain localization due to shear yielding varies, ranging from diffuse shear yielding to very localized, clearly defined shear bands. The localized banding is of particular interest in the toughening of rubber-modified systems and often serves to stabilize crazes which might otherwise lead to fracture.

Shear banding, like crazing, is an inhomogeneous deformation process. A high degree of strain softening in a glassy polymer leads to the formation of shear bands, which are thin planar regions of high shear strain usually inclined to the applied uniaxial tensile stress direction by an angle $45^{o} \pm 8^{o}$, in contrast to the 90^{o} orientation found in crazes. Shear bands are initiated in regions where there are heterogeneities of strain due to surface flaws or internal defects which can produce stress concentration. The conditions necessary for shear band formation are discussed by Bowden and coworkers [28, 29].

Shear bands may be created in tension as well as in compression, and have been observed in a wide range of glassy polymers, including PVC, PMMA, epoxy resins, and amorphous PET [29, 30, 31]. Shear bands have been characterized as coarse or fine [32, 33]. Coarse and thin bands were found to follow different yielding criteria and to respond differently to temperature, strain rate, and thermal history. More importantly, the coarse bands always lead to shear fracture without producing much macroscopic plastic deformation, while the fine bands result in ductile failure after considerable plastic strain [32, 33]. Various criteria for shear yielding have been proposed. These include: a) the Tresca yield Criterion [34]; b) von Mises Criterion [34]; c) Mohr-Coulomb Criterion [35]; d) Bowden Criterion [36]; and e) Sternstein-Ongchin Criterion [37]. The details of each criterion are described in the cited references and will not be discussed here.

2.6 Relationship Between Crazing and Fracture Toughness of Polymers

As mentioned earlier, crazing has a central role in determining the onset of instability in the process of continuous crack growth. If a large (area) craze pre-exists in a specimen prior to crack initiation, that craze will subsequently act as a preferred path for crack propagation; in this role, the craze is utilized as a lower energy crack path. A material such as PS at room temperature, and PMMA and PC at low temperature ($\simeq$ 78 ^{o}K) show this type of behavior [6]. Conversely, in materials which form only small (area) crazes, the crack will propagate with concurrent craze formation at its tip, and in this case crazing acts as an energy dissipation mechanism. An example of this type of behavior is PMMA at room temperature [6].

In the past two decades, many of the results of fracture toughness values of glassy polymers have been represented in terms of the Griffith energy γ. Summaries and reviews of fracture surface energy results for glassy polymers have been given by Berry [12]. Kambour [38] has attempted to analyze the various energy contributions which make up the overall measured value of γ reported by Berry from cleavage experiments on PMMA. The result showed that the major energy sink operative during crack propagation is the viscoelastic work of craze extension from unstressed state to its breaking point.

Continuum fracture energy theories ignore the details of specimen configuration and are so broad in scope that they shed little light on the mechanism of crack propagation. On the other hand, local stress theories deal with material response and crack geometry in specific ways. When successful, this class of theory may shed more light on the details of the fracture mechanisms than do simple energy theories.

One model which utilizes the local stress theory in the study of yielding at a crack tip is the Dugdale model [39], which can be applied to crack tip configuration. The length of the plastic zone (R) can be calculated as [40]:

$$R = \frac{\pi K^2}{8 \sigma_y}$$

or

$$R = \frac{\pi E G}{8 \sigma_y^2}$$

and $$V = \frac{G}{2 \sigma_y}$$

where V is half the maximum plastic displacement that develops, E is the modulus of the bulk material, σ_y the plastic yield stress (i.e. the craze formation stress), and G is the Irwin's strain energy release rate.

The shape of crack tip crazes has been examined for PMMA and shown to be an accurate fit to the Dugdale model [10, 41]. For the crack tip crazes in PVC, however, the Dugdale model is less applicable than for other polymers. The crack tip crazes were much more wedge shaped than would be predicted by the Dugdale model, and also the stress intensity factors calculated from the craze parameters using the Dugdale model were less than half of those observed experimentally [25, 42]. Several workers have attempted to explain these discrepancies. Mills and Waiker suggested that they might be caused by the existence of plastic yielding above and below the craze [25]. Brown and Stevens thought the use of the Dugdale model for the wedge shaped crazes might be the problem [42]. Lastly, the discrepancies could be caused by the coexistence of a shear yield zone with the craze which was observed by optical and scanning electron microscopy [43, 44]. A fairly similar discrepancy has also been observed in PC [45], which undergoes shear yielding easily. In addition, during fatigue crack propagation in PC, an "epsilon"-plastic zone, which consists of a pair of discrete shear bands and a single craze, has been observed [46]. For PVC it has also been suggested that both crazing and shear yielding might be involved in the fatigue crack propagation [9]. It is worth-noting that Dugdale model provides a fairly good approximation of crack propagation in glassy polymers when just one or two crazes are formed at the crack tip [9].

The amount of strain at the crack tip at the mid-thickness of plane strain fracture toughness specimens multiplied by the size of yield zone and the yield stress should approximate G_{Ic} [47]. This approximation has recently been used by Darwish [1] to estimate the fracture toughness value of PVC pipe material. The crack tip displacement was derived from the height of strained fibrils in the ductile zone of the fracture surface measured from SEM micrographs. The estimated K_{Ic}, however, was consistently lower than measured K_{Ic}. More discussion based on the results of this study will be made in a later chapter.

2.7 Craze Initiation

The stresses which are important in craze initiation may be characterized by the negative pressure σ_o and the deviatoric stress S_o. These are given by

$$\sigma_o = (\sigma_{11} + \sigma_{22} + \sigma_{33}) / 3$$

and

$$S_o = 1/6 [(\sigma_{11} - \sigma_{22})^2 + (\sigma_{22} - \sigma_{33}^2 + (\sigma_{33} - \sigma_{11})^2 + \sigma^2_{23} + \sigma^2_{13} + \sigma^2_{12}]^{1/2}$$

where the σ_{ij}'s are the components of the stress tensor.

The elemental step in craze formation is the opening of voids with aligned matrix. Different theories for craze initiation have been proposed. A complex mechanism of craze formation was proposed by Argon [48]. According to Argon, the event of crazing consists of three relatively distinct stages which are, in order: thermally activated production of stable microporosity under stress; formation of a craze nucleus by plastic expansion of holes in a small region while elastically unloading the surroundings; and extension of the craze nucleus in to a planar "yield" zone.

Kramer has put the stages of craze initiation proposed by Argon into a more descriptive picture [49]. In the picture, the first step with a polymer surface under simple tension, as shown in Figure 1a, is plastic deformation by shear at the surface in the region of stress concentration of a defect. The strain softening characteristic of most polymer glasses leads both to an acceleration of the strain rate and a localization of strain as the plastic strain increases. The localization of plastic strain also leads to the development of lateral stresses (σ_{22}, σ_{33}) in the plastic zone. At this stage one of two things can happen. If shear deformation is to continue, the applied tensile stress must be increased since the lateral stresses have reduced the local deviatoric stress s_0 which is driving the shear deformation. The increase in stress may be enough to cause global plastic shear deformation outside the initial localized zone, in which case the polymer glass sample, if thin enough, will probably neck and fail after large macroscopic plastic deformation. As the local lateral stresses increase, however, it becomes increasingly probable that voids nucleate in the zone due to the high local σ_0 there, as shown in Figure 1b. If this happens the voids can subsequently grow and interconnect with the remaining polymer ligaments between voids, as shown in Figure 1c. Finally the periphery of the voided sheet structure begins to extend within the zone and simultaneously this structure begins to thicken. Craze nucleation has been accomplished and craze growth has begun.

There has been some controversies regarding whether air crazes can nucleate when σ_0 is zero or even negative. Some studies [50, 51] have shown that a craze can develop in torsion, even with a superposed hydrostatic pressure [52] and therefore no macroscopic dilation. To explain these unconventional results, a model was proposed [38] which suggests a craze initiation criterion which is a function of the maximum principal stress only. However, no craze initiation has yet been seen in torsion in the absence of a liquid, thus suggesting the role of environmental factors in producing crazes without tension.

Bucknall [5] has found that the relationship between rate of craze initiation, temperature, and applied stress may be described by the Eyring theory of activated rate processes. He used the Eyring model to analyze data obtained by Maxwell and Rahm [53] for craze initiation in polystyrene. This yielded an activation energy of about 175 KJ/mole which was compared with the activation energy of thermal bond rupture in polystyrene, namely 230 KJ/mole. Thus, it was suggested that stress-activated chain scission is the rate-determining step in craze initiation.

2.8 Craze Growth

The theoretical studies of craze growth have been largely based on fracture mechanics approaches without much consideration being given to the mechanism of craze growth. One model which has shed much light in understanding the mechanisms of craze matter production as a craze extends was proposed by Argon [54]. The model suggests that craze growth occurs by the mechanism of meniscus instability, in which the yielded polymer at the concave air/polymer interface at the craze tip breaks up and produces new craze matter by repeated convolutions. Such convolution of the yielded polymer at the craze tip results from the basic instability of all fluid menisci advancing under the action of a suction gradient (negative pressure gradient) created in the fluid. This is because such interfaces are unstable to perturbations above a certain wavelength which decreases with increasing suction gradient causing break up into a series of fingers.

Finally, their work showed that while craze initiation obeyed a complex criterion involving both the deviatoric and dilatational components of the stress tensor, the craze growth rate via the meniscus instability mechanism was theoretically and experimentally governed only by the value of the maximum principal tensile stress.

2.9 Craze Fibril Breakdown

Craze breakdown which leads to crack extension is of vital importance to the failure process. It has been shown that the fibrils grow primarily by pulling fresh material out of the bulk rather than by increasing their draw ratio [55]. The draw ratio of the fibrils is nearly constant over the whole craze volume. Nevertheless, it is slightly higher in the so-called "mid-rib" region and also at the craze end and tip. [56].

Craze fibril breakdown and crack initiation clearly involves the breakage of interatomic bonds. Zhurkov and colleagues [57], from a molecular approach to fracture, have developed a model which views fracture as an activated rate process, i.e. one involving the surmounting of a potential energy barrier, and has a similar form to the Eyring model. The energy barrier may be surmounted because random thermal fluctuations ensure that the thermal or kinetic energy of an atom varies in time with a finite possibility of exceeding the potential barrier. The model envisages this barrier being lowered by the application of a tensile stress. Experimental results obtained using infrared, electron spin resonance, etc [58], provides strong support for main-chain bond scission as the rate determining step in the failure process.

Although chain scission can contribute to initial craze fibril breakdown, an equally, and perhaps more important contribution could be due to chain disentanglement by chain reptation or tube relaxation during localized creep of the fibrils. Such local creep of the fibrils could generate weak spots which lead to fibril failure [49, 59]. Haward et al [59] have suggested that if the majority of chain ends of the polymer molecules passing through the craze/bulk polymer interface terminate within the craze then the craze may fracture by a largely viscous flow mechanism, which is a molecular separation process involving the viscous and viscoelastic disentanglement of polymer chains, rather than by the breaking of covalent bonds. Experimental support for this mechanism comes from micrographs of craze breakdown [60] where

long drawn-out filaments which retract upon failure span the craze. These filaments possess a roughly globular tip, consistent with a viscous or viscoelastic rupture hypotheses. It has been suggested that whether crazes breakdown by chain scission or by chain disentanglement depends on the temperature. Above a certain critical temperature the craze breaks smoothly, probably in the mid-rib region, where the extension ratio is higher, leaving two craze layers on each fracture surface. Below that temperature, the craze breaks in a very irregular way, forming many side crazes and leaving a fairly rough fracture surface.

2.10 Slow Crack Growth

In recent years, Williams and co-workers [61], have successfully combined the viscoelastic aspect of polymers with fracture mechanics to explain the kinetics of stable crack propagation and crack instability. By employing the Dugdale model and replacing the elastic parameters with time dependent forms, they have established the relationship between the stress intensity factor, K_I, and crack speed, $(\dot{a})$ during stable crack growth as :

$$K_{Ic} = \sqrt{\delta_c^* e_y} \left(\frac{8 e \sigma}{\pi \delta_c^*} \right)^n E_o \dot{a}^n$$

where δ_c^* = crack opening displacement, e_y = yield strain,
and E_o = unit time modulus.

The value n is a measure of the degree of time dependence acting (e.g. $n=0$ for an elastic material),corresponding to the loss factor $\tan\delta$ for the β-molecular relaxation peak, i.e. $\tan\delta = \tan \pi n/2$. For most polymers, $n<0.1$ and frequently $n<0.05$. [62] The relationship was confirmed experimentally for PMMA [61]. Studies done on PC and PMMA support the notion that the stability of crack growth in slow growth is governed by n. Viscoelastic processes at the crack tip therefore assist in stabilizing crack extension.

2.11 Influence of Molecular Entanglements in Crazing

The importance of crazes both as a toughening mechanism and as the precursors of cracks and failure is now well established [9]. Consequently , it is crucial to obtain a clear understanding of which parameters control their growth and micromechanical properties. TEM has revealed that the craze microstructure consists of a dense array of fibrils which span the craze-matrix interface giving the raze its load bearing capabilities. The strength of the craze will therefore be determined by the properties of these fibrils. In particular, for a given level of stress S at the craze surface, the true stress born by the fibrils is S divided by the volume fraction V_f of fibrils. Since the plastic deformation of the fibrils occurs at approximately constant volume, the volume fraction is $V_f = 1/\lambda$, where λ is the extension ratio of the craze fibrils. The true fibril stress is thus given b

$$\sigma_t = \lambda S$$

Kramer in several studies [63, 64] has demonstrated that the extension ratio of a craze is governed by the properties of the entanglement network. One of the most prominent effects of molecular entanglement is the appearance of a rubbery plateau in the shear modulus G above T_g [65, 66]. Using the simple theory of rubber elasticity one can compute a molecular weight between entanglement crosslinks, M_c, from the level of G^o_N at the plateau,i.e.,

$$M_c = \frac{\rho R T_A}{G_N^o}$$

where ρ is the polymer density, R is the universal gas constant and T_A is the absolute temperature.

One of the parameters of the entanglement network is the chain contour length l_c between entanglements, which is given by

$$l_c = l_o M_c / M_o$$

where l_o is the average projected length of stiff units along the chain and M_o is the average molecular weight of these units.

Another parameter is the entanglement mesh size d, which is the straight line distance between entanglements. It is given by the root-mean-square end-to-end distance of a chain of molecular weight M_e, i.e.,

$$d = k (M_e)^{1/2}$$

where k is a constant, and for most polymer k lies between 0.05 and 0.09 nm/(mol wt)$^{1/2}$ [67].

Figure 2 is a schematic of a polymer chain in the entanglement network. If the chain is extended fully between entanglements, in the absence of slippage or breakage of entanglement network points or chains, the maximum extension ratio λ_{max} of the network is given by

$$\lambda_{max} = l_e/d$$

The result of several studies [63, 64], which covered a number of polymer systems with a wide range of l_e values, indicate that the ductile polymers were those with low l_e (e.g. PC and polyphenylene oxide(PPO)), whereas those with high l_e, and subsequently high values of λ_{max} and λ_{craze} (e.g. PS, and poly(ter-butylstyrene)(PTBS)) were the typically brittle polymers. Thus, chain entanglement is shown to be essential for craze fibril stability. Higher fibril stresses exist in crazes with higher extension ratio, and the fibril stress, rather than the applied stress, is the stress parameter which controls the rates of chain scission and/or reptation. The polymers with low l_e showed a tendency to form a relatively delocalized plane stress deformation zone. In addition, polymers form progressively shorter and fatter crazes as their l_e decreases.

The recently developed TEM technique for studying craze microstructure also

provides insight into the micromechanics of crazes [49]. With the known displacement profile for a craze at a crack tip, the method of Wang [68], which is based on the distributed dislocation theory of Bilby and Eshelby [69], allows the craze surface stress profile and the applied stress level to be computed. The only assumption required is that the material outside the craze can be treated as a linear elastic solid. The results show that for polymers such as PTBS and PS, classified as more "brittle" polymers based on their extension ratios, the stress is almost constant along the craze, rising to small stress concentrations at both the craze and crack tips. The average stress value lies close to, but slightly above the applied stress level. However, for polymers with low craze extension ratio, a much higher stress concentration exists at both the crack tip and the craze tip. These results are in variance with the Dugdale model, in which the craze surface stress is assumed to have a constant value. Therefore, the results based on Kramer's study indicate that the Dugdale model is a reasonable approximation for the polymers with widely spaced entanglement networks, but it becomes a progressively poorer one for crazes in the more densely entangled polymers.

2.12 Multiple Crazes

2.12.1 Phenomenology of Single-Multiple Craze Transition

While in some cases fracture is noted to proceed from a single craze ahead of the crack tip, in other cases multiple crazes are formed at the crack tip before and during the crack propagation. The presence of the multiple crazes could alter the stress distribution at the main crack tip and enhance the total amount of plastic energy absorbed.Therefore the analysis of fracture in glassy polymers involving the formation of multiple crazes is more complicated and difficult than the case where only a single craze is involved.

Schirrer et al [70] has studied the multiple-single craze transition in five polymers. Their results show that below a critical temperature, T_c, multiple crazes appeared ahead

of the crack and the fracture toughness increased. Above this critical temperature a transition from multiple crazes to single craze took place and $K_c(T)$ decreased. The transition T_c appeared to be sharp for PMMA, PS, PC and a triblock co-polymers of PS, polyisoprene and PS (SIS). However, for PVC, due to the anisotropic nature of the extruded sheet used, two different patterns of crazing behavior and two different T_c's were obtained, parallel and perpendicular to the direction of extrusion. The values of T_c at which multiple crazing appeared are given in Table 1. An attempt was made to correlate T_c with the β relaxation temperature of the polymer. However, there seems to be the lack of experimental evidence to support this correlation.

2.12.2 Crack Layer Concept

In addition to the phenomenological study of the single-multiple craze transition, a model termed "Crack Layer" (CL) has been proposed, which considers the main crack and the surrounding damage zone as a macroscopic entity. The CL theory, as proposed by Chudnovsky et al [71], has been advanced to model the event of crack propagation accompanied by disseminated microcrazes.

In the CL theory, a zone of nonzero rate of damage accumulation $\dot{}$ is defined as the active zone , as shown in Figure 3. In the wake of the active zone, due to unloading, an inert zone appears. The active zone movement can be decomposed into translation, rotation, isotropic expansion, and shape changes. While conventional fracture mechanics usually deals with the translational mode only, the CL approach offers three additional degrees of freedom. The rate of crack propagation (extensional) is directly influenced by rotational, expansional, or distortional active zone changes according the the CL theory. The ultimate goal of the development of the CL concept is to establish constitutive equations relating the crack layer elementary movements (thermodynamic fluxes) to their causes (thermodynamic forces) within the framework of irreversible thermodynamics. By setting up the energy balance and entropy balance of the system,

the critical energy release rate,in its final form, could be expressed as the product of the specific enthalpy of fracture (γ^*) and the critical CL translational resistance moment R, i.e.

$$G_c = \gamma^* R_{IC} \qquad (1)$$

The term γ^* was found to be of the same order as the heat of fusion of the material, and the term R is related to the amount of crazes in the active zone, or more generally, it expresses the intensity of transformation within the active zone which could be crazes, shear bands, recrystallization, etc. The specific enthalpy of fracture (γ^*)is a material parameter, and the latter term R_{Ic} depends on the history of loading.

By using the first and second law of thermodynamics, the rate of fatigue CL propagation has also been derived as:

$$\frac{dl}{dN} = \frac{\beta(\dot{W}^p - \dot{Q})}{(\gamma R_I - G_I)} \qquad (2)$$

where

$\dot{W}^p$: rate of total work dissipation,

$\dot{Q}$: rate of heat dissipation within the active zone,

β: the fraction of $(\dot{W}^p - \dot{Q})$ spent in the CL translation,

γ: specific enthalpy of crazing,

R_I: translational resistance moment,

and G_I : the energy release rate.

The established relationship in equation 1 has not been critically verified. However, the proposed formalism for fatigue CL propagation as indicated in equation 2 shows good agreement with the experimental results [72].

2.12.3 Craze Interaction and Fracture

Mill [73] has used a dislocation array method of two-dimensional stress analysis to study craze growth and craze interaction in the absence of a crack in glassy polymers. It was suggested that the growth kinetics of crazes is controlled by the potential energy changes in the surrounding elastic material, which in turn are affected by the geometric interaction of crazes. His analysis also shows that the length of the crazes depends on the ratio of craze length to the craze separation and the depth of penetration from the free surface into the bulk.

Although the event of crack propagation accompanied by the formation of microcrazes has been modelled, further progress requires knowledge of the stress field around the damage zone, i.e. understanding of the micromechanics of the crack layer. As already been noted in the previous sections, microcracks (or micro-crazes), interacting with the main crack and with each other, change the stress distribution in the vicinity of the macrocrack tip. Theoretical analysis of a two dimensional problem of elastic interaction of a macrocracks with a field of microcracks has been attempted by Chudnovsky et al [74]. The analysis was based on the self-consistent method (widely used in physics of many particles systems), and the technique of double layer potential, with crack opening displacements being the potential densities. A closed form solution of the effective stress field was presented.

2.13 Polyvinyl chloride

Polyvinyl chloride (PVC) is the second most extensively used polymer after polyethylene. Emulsion or bulk polymerization produces polyvinyl chloride primary particles about 0.2-1.5μm in size. Powder grains with diameters of about 100μm will include primary particles and cavities of various size [75].

In general, PVC is nearly structureless and amorphous; however, a careful

structure analysis indicates the presence of crystalline domains in PVC with a degree of crystallinity below 10% [75]. The glass transition temperature of PVC is about 83 °C, and the melting temperature is in the range of 180 ± 10 ° C. The use of processing aids and stabilizers is necessary to reduce the temperature required for fusion of PVC and to allow for processing without degradation.

Rigid pipe material contains about 93-94% PVC and 6-7% processing aids, stabilizers, impact modifiers and fillers. Extensive review of PVC structure and properties is available in the PVC encyclopedia [75].

CHAPTER THREE

Experimental Methods

3.1 Materials

3.1.1 Preparation of Pure PVC Sheets

A thermostabilizer (Thermolite 31), 2% by weight, was dissolved in hexane and the resulting solution was mixed with the PVC powder (Geon Vinyl, 103EP.F-76; B.F. Goodrich; M_w=150,000 and M_N=60,000) with constant manual stirring. After the complete evaporation of hexane, thermostabilized PVC powder was compression-molded at a pressure of 700 psi and a temperature of 204 °C(400°F) for 10 minutes, into sheets 7mm thick. The molded sheets were cooled by quenching in water. Any residual stress due to quenching was annealed out at a later stage. The sheets passed the acetone and methylene chloride immersion tests (following ASTMD2152-80 Standard Test Methods), which were performed for examining the degree of fusion. The pure PVC sheets were transparent and slightly yellowish.

3.1.2 Calcium Carbonate Filled PVC Sheets

Calcium carbonate ($CaCO_3$, Thompson,Weinman,Inc Company), 3% by weight, was mixed with thermostabilized PVC powder in a mechanical blender for 5 minutes. The mixing was stopped periodically for the dissipation of heat built up during mixing.

3.1.3 PVC Pipe Material

The PVC pipe material used in this study was taken from pipes of the standard 1120 type intended for water distribution. The pipe , wall thickness of 11.6mm, was purchased from a local store. The composition of the pipe compound is proprietary, but it contained approximately 93-94% of PVC pure resin, plus processing ingredients and about 3% calcium carbonate, following the ASTM 12454A classification.

3.2 Specimen Preparation

To test the plane strain fracture toughness of pure PVC, compact tension(CT) specimens were made from the compression-molded sheets. The CT specimens, as shown in Figure 4a , were initially notched with a slotter having a cutter of 1.7mm thickness and edge angle of 60^{o} . The tip of the notch was then sharpened with a razor blade for a depth of 1mm. To eliminate any residual stress due to machining and blade-notching, specimens were annealed at $95^{o}C$ ($T_g=83^{o}C$, determined by DSC at a heating rate of $10^{o}C$ /min) for 40 minutes to one hour. After slow cooling, the sheets were tested for birefringence under an optical microscope, to be certain of the absence of any residual stress due either to machining or quenching.

The CT specimens of the PVC pipe material were made from PVC pipes which were flattened by heating sections of the pipe above T_g for 15 to 30 minutes and then pressing under two parallel steel plates while they were air cooled.

To test the yield strength of the material, standard tensile specimens were made, as shown in Figure 4b.

3.3 Microscopy Study

The morphology at the crack tip was examined by optical and scanning electron microscope. The sections containing the crack tips were cut off from the specimens, and further polished down to the central planes using coarse sand paper under wet conditions, to where the deformation occurred under plane strain conditions. The surfaces then were polished with Al_2O_3 polishing solution, according to the standard polishing procedures for metals.

3.4 Testing Equipment

A servohydraulic Instron (Model 1331) was used for mechanical testing. An electronic peak detector was used to determine the maximum force; the output displacement rate and force displacement curve were determined by a Tektronix Model 564 storage oscilloscope or using a Nicolet Explorer II digital oscilloscope. A Bascom-Turner recorder and Analyzer (4120) was used to record the load and resistance increase in the crack propagation tests. A Reichert Zetarpan microscope with both transmission and reflection modes was used for light microscopy work. A scanning electron microscope (Cambridge) was used to study fracture surfaces and crazes structure. An eccentric rotating disc rheometer (Rheometrics, Inc.) was used to measure the shear modulus of PVC in the rubbery region.

3.5 Crack Speed Measurement

Crack propagation gages obtained from Micro-measurements were used to determine the crack speed. The gages (25.4mm x 5.1mm) consist of 20 resistor strands connected in parallel, with 0.25 mm interval in between the centerline of each strand. The gage is bonded unto the CT specimen using conventional strain gage installation techniques with adhesives, positioned on the projected path of the crack and perpendicular to the direction of crack propagation. Progression of a surface crack

through the gage pattern causes successive open-circuiting of the strands, resulting in an increase in total resistance. Figure 5a shows the increase in resistance vs. strands fractured chart supplied by the company, and Figure 5b illustrates the circuitry used in measuring the increase of the resistance during crack propagation. The known spacing between each strand allows the crack length to be determined precisely.

The length of time for each strand to break was obtained from the trace on the digital oscilloscope (Nicolet) or X-Y recorder. A typical voltage vs time recording is shown in Figure 6. From the gage resistance chart supplied by the company and the circuitry used in the experiment, the voltage value corresponding to the breaking of individual strands can be calculated, as listed in Table 2. Thus, from the voltage level on the recording chart, the number of strands that have broken can be precisely determined.

3.6 Data Analysis

3.6.1 Fracture Toughness Calculations

For CT specimens, the maximum load to fracture was used to calculate the critical stress intensity factor, K_Q, according to formulas given in ASTME399:

$$K = \frac{\Delta P}{B\sqrt{W}} \frac{(2+\alpha)}{(1-\alpha)^{3/2}} (.886 + 4.64\alpha - 13.32\alpha^2 + 14.72\alpha^3 - 5.6\alpha^4)$$

where $\alpha = a/W$

The resulting value was designated K_Q, indicating that it was a candidate value for K_{Ic}.

3.7 Test Validity Considerations

The fracture toughness validity conditions as stated for CT specimens in metals [76] includes the condition that the thickness, crack length and other dimensions should satisfy

$$C \text{ and } B \geq 2.5\left(\frac{K_{Ic}}{\sigma_y}\right)^2 = S$$

Therefore, S/c, S/B<1.0 ,where c is the crack length and B is the specimen thickness.

These requirements are to ensure that the plastic zone size is small relative to the specimen geometry, so that the plane strain condition along the crack front through the thickness is dominant. If the K_Q value satisfies the above validity condition, then K_Q is designated as K_{Ic} in this study. Other validity criteria in ASTM E399 were not applied. The application of validity criteria for PVC has been discussed in [1].

CHAPTER FOUR

Nature of the Yield Zone in PVC

To study the nature of the yield zone in PVC, CT specimens were loaded close to the maximum load required for fracture in a valid test, then unloaded. The test was done using a triangular load-time waveform.

For all pure PVC and $CaCO_3$ filled specimens, multiple crazes were observed in the yield zone ahead of the crack tip under a light microscope. Due to the light-scattering nature of $CaCO_3$, multiple crazes are less easily seen in the PVC-$CaCO_3$ specimens, but they were still evident. Figure 7 illustrates the morphology of the multiple crazes observed at the crack tip of the pure PVC specimen, and Figure 8 shows the multiple crazes growing along a crack in a $CaCO_3$-PVC specimen.

To confirm the nature of the apparent crazes, the region that contained the crack tip was sectioned out from the specimen and immersed in OsO_4 :H_2O solution for several days. After the top surface layer was microtomed away, the immersed blocks were analyzed by the energy dispersive X-ray analysis (EDAX) technique. Strong signals of the heavy element osmium were found inside these crazes and little on the surface, indicating that the observed deformation process is of the type of cavitation with local pore formation, and not of the type of shear yielding, for which there is no porosity.

Some shear yielding was evident on the surfaces of the specimens, as shown in Figure 9. In addition, shear yielding in PVC could occur under compression. Localized

shear bands, initiated from the notch root, are formed at an angle of about 45^{0} to the compression axis, as seen in Figure 10. Nevertheless, at the mid-section of the CT specimen, under plane strain conditions, no shear yielding was evident in PVC, as indicated by the absence of birefringence.

Although optical microscopy can be used to examine the general features at the crack tip, electron microscopy is needed to study the detailed structure of the crazes. The sample preparation technique for this study generally involved the procedures of sectioning the specimens, polishing, and coating the surfaces with conductive metals. These procedures could damage or destroy the morphological details of the crazes. For instance, Figures 11 and 12 illustrate the craze morphology after these procedures. For both pure PVC and PVC pipe material, only some fine lines could be observed. There is little or no structural details of the crazes that could be discerned. To solve this problem, two surface treatment techniques were employed, which were intended to remove the damaged surface layer in order to reveal the crazed material underneath it. Firstly, chemical etching technique was used. It was found that suitable solvents could preferentially etch the amorphous part of the craze material and reveal the fibrillar structure in the crazes, as reported by Jang for the case of polypropylene [20]. Xylene and acetone were used as the chemical etchant for pure PVC. The results show that these solvents did not perform the expected etching effect. The etched crazes, rather, appeared to be in a closed form as seen in Figure 13. The effect of plasticization by the solvents could possibly cause fusion of the material, giving the observed closed form. More success was achieved by etching the polished specimens with activated gaseous species, referred to as the plasma etching technique. This technique is based on feeding a gas into a vacuum chamber where an electromagnetic field causes the gas to assume an excited state. The activated gaseous species can break covalent bonds on the polymer surface. Eventually, the top decomposed layer is stripped off from the polymer by the vacuum in the system, rendering the craze structure beneath the sample surface ready to

be examined. Different gaseous media, such as air, argon and oxygen were used; the best results were obtained from the specimens etched in oxygen. Figure 14 shows the morphology of a crack tip in pure PVC after being plasma etched in oxygen gas, with the structural details of the crazes shown at higher magnification in Figure 15. The fibrillar structure of the crazes , as revealed by the plasma etching technique, is evident. The thickness of the crazes varies from one to two μm in the unloaded state. Figure 16 illustrates the craze morphology observed in PVC pipe material after plasma etching. Although not as clear as in pure PVC, the fibrillar structure of crazes in PVC pipe material is still discernible. The crazes appear to be smaller than the crazes seen in pure PVC, and are more numerous. The particles are fillers incorporated in the pipe material and aluminum oxide particles used during polishing , which remained on the surface even after ultrasonic bath cleaning. Due to the internal instability of the plasma generator used in this study, etching conditions can not be easily controlled. As a result, changing the plasma etching conditions could give rise to variations in the appearance of the crazes. Figure 17 shows the morphology of the crazes in a PVC pipe specimen, for which it was observed that heat had built up in the sample after the plasma etching. The crazes appear to have healed and closed up due to the heating, giving a clear contrast to the uncrazed materials. Heating specimens containing crazes to a temperature higher than T_g also results in healing and closing up of the crazes, as shown in Figure 18. It thus appears tl plasma etching can serve to reveal the cra e morphology underneath the top damaged surface and , in some instances, decorates the crazes to make them more visible.

The technique of plasma etching is most valuable in the studying of the materials which are opaque. At present, there is no other direct evidence showing the morphology of the deformation zone in an opaque system, such as PVC pipe materials, due to the limited microscopic techniques that can be used.

4.1 Multiple Crazing-an Intrinsic Property

Crazing is known to be an energy absorption mechanism in thermoplastic materials. Formation of multiple crazes can enhance the fracture toughness of PVC and be directly involved in the fracture process. However, before making any correlation , the question of whether the formation of multiple crazes at the crack tip is an artifact due to blade-notching, or is an inherent material property must be clarified.

Marshall et al. [77] found that the method of notching in PS strongly affected the observed K_c values; in particular slow razor notching produced a craze bunch at the notch tip and a high K_c value, whereas cracks grown by fatigue at 30 cycles/sec, had a single craze at their tip and gave a low K_c value. Moreover, the stress field around a crack tip produced by blade-notching method may be different from that around a natural crack tip. In view of these concerns, a set of CT specimens were fatigued over a broad range of K_{max} values (maximum K_I during cycling) to produce fatigue crack tips, which are considered natural crack tips. The fracture toughness values of these specimens were then determined and compared with the toughness values of the blade-notched specimens. The same type of tests were also done for $CaCO_3$ filled PVC specimens to elucidate the effect of $CaCO_3$ on the fracture properties of pure PVC matrix. The results of these tests are shown in Figure 19, in which the fracture toughness of pure PVC and $CaCO_3$-PVC is plotted as a function of the ratio of K_{max}, used in producing the fatigue crack, to K_c(fracture toughness value). For both pure PVC and $CaCO_3$-PVC, the fracture toughness values showed only small variation with different levels of fatigue loading. In addition, the toughness values for fatigued specimens and blade-notched specimens are about the same in both materials, as also shown in the Figure. Loading a specimen containing a fatigue crack tip to a point before its critical load for fracture, multiple crazes again were observed at the crack tip. Based on these experimental facts, the following conclusions could be drawn: a) fracture toughness values obtained from blade-notched specimens can be used reliably

as the fracture toughness value for PVC containing a natural crack (similar results were found for pipe PVC in [1]); b) Multiple crazing is an intrinsic material property of the PVC matrix, which occurs in the interior of the specimen under plane strain condition.

4.2 Effect of $CaCO_3$ on the Fracture Toughness of PVC

While the yield strength, tested as a function of displacement rate, (Figure 20) , for pure PVC and $CaCO_3$-PVC are about the same, the presence of $CaCO_3$ generally decreases the toughness of the PVC matrix, as has been shown in Figure 19. The decrease of the toughness of PVC matrix could be due to $CaCO_3$ agglomerates which might be present and act as zones of concentration of stresses locally, or the poor adhesion between filler and the PVC matrix. In PVC pipe material, micro voids were shown to nucleate around the additive particles prior to brittle failure [1]. On the $CaCO_3$-PVC fracture surface, many dimples with particles at the center were observed, as will be seen in a later chapter.

CHAPTER FIVE

Phenomenology of Multiple Crazing

In polymers, the mechanism of crazing involves large plastic strain and considerable local energy absorption by the materials. The formation of multiple crazes increases the volume of the material involved, and can thus affect the fracture toughness. The presence of multiple crazes can also alter the stress distribution at the main crack tip and directly influence the fracture processes. To verify and support these concepts, several polymers covering a broad range of fracture toughness values were selected. The goals were to examine the nature of the yield zone at the crack tip of the selected polymers and to correlate with their fracture toughness values. Further, the fracture processes in these polymers ,which are governed by the deformation mechanisms occurring at the crack tip, have been studied. Polymers selected for these purposes include nylon 66, polycarbonate(PC), polysulfone(PSF), polystyrene(PS), and polymethyl methacrylate(PMMA).

• The experimental approach is similar to the study of deformation mechanisms in PVC. Compact tension (CT) specimens were made out of compression molded sheets of each material, except for the specimens of PSF and nylon 66 (Zytel 101), which were made from injection molded plates. After machining, the specimens were annealed at a temperature a few degrees higher than T_g. To ensure that the initial crack tips had the same properties as natural crack tips, each specimen was fatigued at an appropriate K_{max} at a frequency of 10 Hz, to generate a fatigue crack tip ahead of its notched tip. The specimens then were subsequently loaded to a load which is about 80-90% of their

fracture load. The regions which contain the crack tips were sectioned out for further microscopic studies.

5.0.1 Fracture Toughness

The fracture toughness value of each material used in this study is listed in Table 3. The K_c value of PMMA obtained agrees with the value reported in the literature [41] , and appears to be the lowest among all the polymers tested. The relative fracture toughness of each polymer compared with PMMA is also listed. Overall, the K_c values of nylon 66, PVC,PSF, PC and PS are about two to 3.6 times higher than the K_c value of PMMA.

Nylon 66, a semi-crystalline polymer, has the highest K_c value. For PC and PSF, the values are slightly lower than expected [77], which could be due to the high rate of loading. The K_c value of PS obtained is higher than expected. To test if the higher K_c of PS obtained in this study could be lowered by varying the fatigue condition, as has been demonstrated by Marshall [77], the frequency was increased from 10 Hz to 30 Hz. The results indicate that the K_c values of PS did not show a decrease but rather it increased from 1.94 $MN/m^{3/2}$ to 2.80 $MN/m^{3/2}$. This could be due to hysteretic heatings at the crack tip. The K_c value of PS obtained in this study could therefore reflect its true intrinsic property and be reliably used. Lower literature values may result from differences in the type of PS.

5.0.2 Nature of the Yield Zone

The results of microscopic studies indicate that there is only one single craze present at the crack tip of PMMA after loading. Multiple crazes are formed at the crack tips of the rest of the selected materials under valid plane strain fracture toughness testing conditions. Figure 21 shows the optical micrographs of the multiple crazes formed in PC, PSF, PVC and PS. Figure 22 shows the morphology of the crack tip in

PMMA after loading. The crack tip morphology of nylon66, which is opaque due to its crystalline nature, is shown in Figure 23. A better view of the morphology of the crazes is shown in Figure 24. Recalling the fact that the fracture toughness value of PMMA is the lowest among the polymers studied, these results confirm that the formation of multiple crazes has a direct correlation with fracture toughness of a material.

5.1 Mechanism of Fracture

The mechanisms of fracture for the polymers forming multiple crazes before brittle failure are broadly similar. When the load reached to a certain level,the crack started to propagate in a stable manner while more multiple crazes were formed at the crack tip. When a critical condition was reached, the crack propagation mode changed from stable to unstable. Examining the side profile of the fracture pieces reveals that a transition from multiple craze to single craze is associated with this changing of the crack speed. Figures 25 and 26 illustrate such transition in PVC and PC, with the corresponding fracture surface morphology included for comparison. Few or no multiple crazes could be found beneath the fracture surface in the region where rapid crack propagation had occurred. The results reported on the studies of plane-strain fracture in polysulfone [78] and PC [79] using different specimen geometries agree with the present finding. As about eleven crazes were found in the stable crack growth region of SEN polysulfone specimens and fifty crazes in DCB PC specimens, no crazes were observed in the region where crack instability had set in.

It is evident that the mechanisms responsible for the transition from multiple crazes to single craze govern the final catastrophic failure of the material. To maintain the utility of the material for service, it is necessary to delay or prevent this transition from occurring. The understanding of the governing factors for the transition therefore is crucial for the control of brittle fracture in glassy polymers which form multiple crazes. It is speculated that the observed multiple to single craze transition could be

determined by the strain rate at the crack tip since craze initiation and craze growth are both time dependent processes. Further, interaction among the crazes could alter the stress distribution at the crack tip, thus directly affecting the crack growth. In fact, propagation of a crack, which eventually results in the failure of the structure, is a consequence of the following steps: craze initiation, craze growth and the breakdown of craze fibrils. In each of these step, parameters such as material properties, time, temperature and load are involved. The following chapters will be devoted to the studies of craze initiation, craze growth and crack propagation in PVC. The results will be used for the understanding of the brittle fracture processes involving the multiple-single craze transition.

Due to its transparent nature which facilitates experimental observation, pure PVC matrix was used in these studies. The results could be used as a base for understanding the more complicated PVC pipe system, which undergoes similar deformation mechanisms at the crack tip and shows similar S-N and fatigue crack growth data to that of the pure PVC matrix [80].

CHAPTER SIX

Craze Initiation in PVC

The kinetics of craze initiation was studied by using CT specimens under static loading conditions. Any residual stress due to blade-notching was annealed out before testing. The crack tips were examined through a stereo-microscope. Craze initiation is characterized by tiny shining spots appearing at the blade-notch tip uniformly across the crack front. The time for such event to occur is taken as the craze initiation time. SEM study of one of the specimens in which the event had occurred showed that a single craze had grown at the crack tip for about 28 μm long. Craze initiation time as a function of the stress intensity factor is shown in Figure 27. As observed in other polymers, craze initiation appears to be a time dependent process. Lower the K_I applied, longer the time it takes for a craze to initiate. On the plot of log time vs. log K_I , the data essentially fall on a straight line, with a little uncertainty near the very low K_I region. A slope of eight was obtained in the straight line section. In polysulfone a slope of 15 was reported under the same static loading condition using unannealed specimens [81]. However,the slope of craze initiation study could be lowered if annealed specimens were used, as supported by the fact that the slope is two times larger for unannealed specimens tested under cyclic loading conditions. Crazing occurs less readily in more ductile resins and requires a longer initiation time [82]. The propensity of a material to form multiple crazes could be reflected by the magnitude of slope of craze initiation tests of the material. However, at present no craze initiation data are available for a single craze system such as PMMA tested under similar conditions. It is difficult to draw any definite conclusions about the importance of craze initiation

conditions in determining the tendency to form multiple crazes. The number of crazes that initiate in PVC depends on the K_I level at the crack tip. The higher the K_I, the more crazes initiate. This trend is also observed during fatigue crack growth in PVC. The number of crazes initiated increases with increasing K_{max} as crack propagates, as shown in Figure 28. The importance of the craze initiation process in the fatigue failure of PVC has been demonstrated in a separate study [80]. The results suggest that the fatigue lifetime of PVC unnotched specimens at low applied stresses is dominated by the craze/crack initiation process, as evidenced by the similarity in the power law exponent (~6) for initiation and failure. It was suggested that the initiation process is dominant because of the many craze/cracks which must initiate before failure occurs, while none can individually propagate to cause failure. The craze initiation process is also critically involved in the brittle failure of notched PVC. As is shown by the craze initiation study, craze initiation in PVC depends very much on time and load. If the crack propagates slowly enough, new (multiple) crazes could have sufficient time to initiate at the crack tip. Formation of multiple crazes could stabilize the propagating crack and slow down the crack propagation rate. However, when the point of instability is reached, the crack accelerates rapidly, accompanied by a rapidly dropping load. The strain rate at the crack tip at this point could get so high that there is not enough time for multiple craze to initiate. The dropping load similarly could no longer maintain the growth of the multiple crazes. These are consistent with the previously noted fact that a transition from multiple crazes to single craze occurs upon the changing of crack propagation mode from stable to unstable.

Fracture instability has been rationalized in terms of the interplay of shear deformation with crazing in the crack-tip plastic zone [82]. In poly(xylenyl ether) (PXE) , which fails by shear flow in uniaxial tension at room temperature [38], the crack at high speed is preceded by two short crazes on the average, contrary to that observed in PVC and other thermoplastics studied in this work. It is possible that by modifying the resin ductility, for example by using polymer blends or rubber toughening techniques,

one could increase the fracture toughness value defined by the on-set of crack instability by delaying the transition to a single craze from occurring,or increase the dynamic fracture toughness of the system by increasing the number of the crazes formed in the high speed region.

CHAPTER SEVEN

Craze Growth

Once a craze is initiated, it will grow in length and in thickness. The maximum thickness of a craze has been used as a fracture criteria for PMMA [27], analogous to the maximum crack opening displacement criterion for metals. The growth of a craze is clearly an important process leading to the final failure. In this chapter, the effects of load and time on the growth of the crazes will be described. In a constant loading or displacement rate test, the load increases with increasing time. To separate the effects of time and load on the growth of crazes, two approaches were taken. First,the effect of time on the growth of crazes was studied by loading CT specimens at different rates to the same K_I using a half triangle wave function, as shown in Figure 29. Secondly, the effect of load was characterized by loading the specimens to different K_I values, while keeping the cycle time constant, as shown in Figure 30. Table 4 lists the corresponding loading rate for each half cycle time used. The range of the loading rate is due to the different K_I levels reached. The growth of the crazes under different loading conditions was examined by both SEM and light microscopy.

The results reveal that multiple crazes were formed when the load was higher than 30% of K_Q. Below that , only a single craze was observed, irrespective of the half cycle time used. The effect of load on the number of crazes for a loading rate about 1 lb/sec is illustrated in Figure 31. An increase of about 40% in K_I results in a four to five times increase in the number of crazes. The effects of load and time on the extensional growth of the crazes are summarized in Figure 32. Each point represents a single

loadings-unloading experiment with subsequent sectioning and viewing in a microscope. In the figure, a line was drawn through the results of the same half cycle time. Due to the overlapping of the data for the half cycle times of 0.5 and 5 seconds, a single line was drawn through the results of these half cycle times. It can be seen that for each K_I value, the length of the craze zone, taken as the distance between the notch tip and the tip of the longest craze, increases with longer half cycle time; for each fixed half cycle time, the length of the craze zone increases with increasing K_I. The length of the crazes is thus shown to be a direct function of both load and time.

The increase in craze length with K_I appears to be more pronounced between the half cycle time of 5 to 50 seconds. A plot of the craze zone length at different K_I levels vs. the total cycle time, is shown in Figure 33. As craze zone length shows a slight increase in the range of total cycle time of 0.1 to 10 seconds for each K_I level, a more pronounced increase is noted as the total half cycle time is changed to 100 seconds. The trend is most clear at a higher K_I level. It has been suggested that molecular relaxation could play a role in the behavior of craze growth [70] , the disentanglement time of the craze fibrils [83], and the slow crack growth behavior in thermoplastics [61] . It is desirable to see if the observed transition corresponds to some kind of molecular relaxation process in PVC bulk material. Generally, molecular relaxation corresponds to some sort of molecular movement which produces a damping peak on a temperature or a frequency spectrum. Hysteresis tests on pure PVC tensile strips were performed over the same time range to see if there is correspondingly a transition of the amount of hysteresis. The hysteresis results indicate that depending on whether the samples were loaded to the same absolute stress or if the samples were loaded to the same percentage of the yield strength under different half cycle times, a transition or a minimum peak was observed. The results are therefore hard to interpret and give little insight to the growth behavior of the crazes.

For a half cycle time longer than 5 seconds, corresponding to a loading rate less

than 100 lb/sec., fracture toughness tests are invalid. At these slower rates, crack lengthening by breaking down the pre-existing crazes and propagating through the newly formed crazes is significant enough that the calculated K_Q values based on the final crack length is affected, as will be discussed in more details in a later chapter. The tests of the craze growth for each half cycle time used however are valid, due to the relatively low K_I applied for generating crazes at the crack tips. While the fracture toughness values of the PVC pipe materials [1] and pure PVC (as will be shown later) are insensitive to the loading rate in the valid region , the rate of extensional growth of the crazes is governed by the rate of loading. As shown in Figure 34, the faster the loading rate the higher the growth rate of the crazes.

As the temperature dropped down from room temperature to -65°C the extensional craze growth is less for each half cycle time. Table 5 lists the results of low temperature tests of crazes growth. There is no clear trend with time for all K_I levels at -65 °C.

As been noted in chapter 1, interference microscopy has been used as an important tool for direct observation of craze growth in transparent thermoplastics. Important information related to fracture as a result of craze growth have been successfully obtained from a single craze system [24, 25, 26, 10]. In this study, the technique is used to study the growth patterns of crazes in the multiple craze zones in PVC.

The regions containing crack tips were sectioned out from the pre-loaded pure PVC CT specimens and viewed under a light microscope after polishing the top surfaces parallel to the crack planes. The crack tip regions were reopened in a wedging device attached to the stage of the optical microscope. Figure 35 illustrates the set-up for this study. The distance between the crack plane (defined as the (1 3) plane in Figure 35) and the top surface was kept long enough so that plane strain condition

remains at the crack tip during the reopening of the specimen in the device. Wedging was stopped at the point when crazes were about to extend.

Upon incidence of monochromatic light in a direction normal to the crack plane, a fringe pattern can be observed. The observed fringe pattern is a result of the recombination of two beams, one of which is a reflection from the upper surface of the craze and the other from the lower surface, as shown in Figure 36. The alternating black and white fringe pattern is a result of the increasing craze thickness, δ, as it opens toward the crack region, as predicted by the theory of interference optics [84],i.e.

$$\text{for bright fringes } \delta = \frac{(f+1/2)\lambda}{2\mu} \quad f=0,1,2$$

$$\text{for dark fringes } \delta = \frac{f\lambda}{2\mu} \quad f=1,2,3$$

where λ: wavelength of the monochromatic light, which is 546nm for the green light used in this study.
f: fringe number, taking f=1 for the first dark fringe at the craze tip.
μ: refractive index of the craze.

In the case where two crazes are present, the resulting fringe pattern depends on the angle of the two crazes relative to each other. When two crazes of different thickness are relatively parallel, the light goes through the crazes without changing its phase appreciably, as shown in Figure 37. The fringe pattern , however, is dominated by the thicker craze which has more densly spaced fringes. The beams reflected from the thin craze have large spacings, which at best modulate the intensity of the fringe pattern from the thick craze. In the case that the angle between the two crazes is relatively large, interference of the light beams from the crazes will occur and the resulting fringe pattern appears confused and distorted. Figure 38 shows the fringe pattern and the side view ((1 2) direction) of the craze zone in a specimen loaded to 1.87 $MN/m^{3/2}$ (~47% K_Q) at a loading rate of 1500 lb/sec. While three crazes are present,

the individual fringes are still easily resolvable, except near the crack tip. The span of the fringes coincides with the length of the longest craze. The smaller crazes act to diffuse the fringes of the main craze and cause distortion of the pattern in some places. As the load further increases, more crazes are formed and fringe pattern becomes rather confused, as illustrated in Figure 39 . It is possible to differentiate the fringe patterns arised from different crazes. The growth pattern of the crazes at the notch tip before the onset of stable crack growth can be schematically illustrated in Figure 40. Most of the crazes do not grow completely across the crack front but are more concentrated in the central region, where the triaxial stress is the highest. Similar growth pattern of crazes was observed ahead of the tip of a crack growing stably, except that more crazes were opened up, conceivably due to the higher stress field at the crack tip. The growth pattern of the crazes is an important factor involved in determining the onset of catastrophic failure, as will be discussed in a later chapter.

CHAPTER EIGHT

Crack Propagation

8.1 Slow Crack Growth

As K_I approaches K_c, craze fibrils start to rupture, and the crack propagates through the crazes while forming new crazes at its tip. In PVC, the initiation of the crack appears to be rate dependent in that the crack initiated at a lower K_I at lower rates, similar to results reported for PMMA [61]. Figure 41 illustrates the growth of a stable crack in a specimen loaded to about 90% of K_C. The growth of the stable crack through the multiple crazes is evident. A more magnified view of the end of the crack tip is also shown in the Figure. SEM micrographs of the same region, Figures 13 and 42 reveal that the propagation of the crack could have involved the rupture of more than one craze. It is likely that two or three crazes broke and coalesced as the crack propagated through. Jumping of the crack among the crazes is also evident in these electron micrographs. The amount of stable crack growth, taken as the distance from the end of notch tip to the fracture origin found at the end of slow crack growth region (to be discussed in details later), increases with temperature and decreases with displacement rate, as shown in Figures 43 and 44 respectively. Studies done on PC and PMMA support the notion that the stability of crack growth at low growth rates is governed by the viscoelastic processes at the crack tip, specifically the β relaxation, which assists the stabilization of crack extension [85]. The β relaxation in PVC pipe material occurs over a broad range from -80 ^{o}C to 50 ^{o}C, with a maximum peak around -20 ^{o}C [1]. Although the amount of stable crack growth shows an increase at -20 ^{o}C,

there is not enough evidence to support its correlation with the β relaxation in PVC. On the fracture surfaces of PVC pipe material, ductile bands, which appear white to the eye on the surfaces of the grey material, were also observed [1]. Figure 45 gives the width of the ductile band as a function of temperature, with the average value of K_Q . The ductile band diminishes in width as the temperature is decreased, despite a nearly constant K_Q below 0°C.

8.2 Crack Instability

As has been mentioned, the transition of a growing crack from multiple crazes to a single craze could be governed by the strain rate at the crack tip, which in turn, depends on the speed of crack propagation. Therefore, determining the crack velocity profile from initial loading to the point of fracture is essential for an understanding of the fracture processes involved. An attempt was made to use DCB specimens to determine the crack speed. However, reliable results were not obtained using this type of specimen due to the fact that either extensive yielding occurred during crack propagation when the thickness was too low, (no longer under plane strain conditions), or , with thicker section , the crack deviated from the original crack plane causing the failure of the arms of the specimen. Another method attempted was by oscillating the load with high frequency and low amplitude while manually increasing the load on the specimen in the Instron until the specimen failed. The technique in principle is similar to the ultrasonic fractography technique used by Takahashi [86] for PMMA. It was hoped that each oscillated load would generate marking on the fracture surface, allowing the crack length as a function of time to be determined. Due to the irregular nature of the fracture surface morphology of PVC, as will be shown later, no visible marking could be identified. This method did not prove to be useful for crack speed determination in PVC. Successful results were obtained by employing crack propagation gages which measure the increase of the resistance as the crack propagates through the strands of the gage. Experimental details of this technique have been described in the experimental section.

As described in Chapter 7, the rate of extensional growth of crazes is a function of the loading rate applied. It is desirable to know if the rate of crack propagation, particularly at the transition to unstable growth, also is governed by the rate of loading during the test. Therefore, the crack propagation velocity profiles for specimens of pure PVC fractured under different loading rates were determined. Figure 46 gives the crack velocity before the instability vs. the crack length from the end of the pre-cut notch. It can be seen that the crack accelerates when it first starts to grow, then levels out to a plateau in the range of 18 mm/s to 100 mm/s. The initial acceleration could be due to the propagation of the crack through the pre-formed crazes. As new crazes are formed at the crack tip, crack acceleration diminishes and crack speed levels out. The final crack length at which the crack becomes unstable is shorter for higher loading rates. However, the crack velocities just before the instability all seem to reach approximately the same value, independent of the loading rate. It is expected that increasing the loading rate causes the speed to rise more quickly initially, but the final critical velocity is not affected. These results suggest that the beginning of the crack growth is controlled by the applied loading rate, while the high crack velocities are a result of the elastic energy field in the specimen, which is similar at each loading rate.

The load increased very little once the crack speed had reached the plateau region, but the K_I level at the crack tip increased continuously due to lengthening of the crack. The relationship between the velocity of the stable crack and the instantaneous K_I at the crack tip is shown in Figure 47. Growth rates of craze zones (prior to crack growth) under two different loading rates, as determined by the microscopic techniques, are also included in the Figure. It can be seen that at relatively low K_I, crazes start to grow at a relatively constant and slow rate. A higher loading rate results in a higher craze growth rate. As the K_I increases further, cracks start to propagate, following a crack speed profile similar to that plotted against the crack length, but with a less prominent plateau region. Again, it is seen that crack speed rises faster at higher loading rates; however, within the limit of the scattering of the data, the final velocity

before the instability showed little sensitivity to the loading rate. The scattering of the data could be due to the nature of the mechanisms involved in craze formation and craze break down in a multiple craze system. Further, propagating crack sometimes caused debonding of the crack growth gage from the CT specimen, which could also contribute to the scattering . Figure 48 shows the relationship between the crack speed and K_I/K_Q. As K_I increases to about 60% of K_Q, the crack starts to accelerate and eventually becomes unstable at K_Q. The determination of the dynamic crack velocity after the instability is very much limited by the sampling interval (SI) of the digital oscilloscope used, due to the fact that after instability all the remaining strands broke in a time interval which was much shorter than the smallest practical SI. The minimum dynamic velocity determined at a loading rate of 100 lb/sec, averaged among the strands broken after the instability at an SI of 100 microseconds, is 17.5 m/sec. Although this is much slower than the 3/10 of the speed of sound in the resin [87] which is 481 m/s as determined in Table 6, the magnitude of the increase in velocity at the transition from slow crack growth to fast crack growth is still over two orders of magnitude.

CHAPTER NINE

Multiple Crazing and Fracture Toughness in PVC

9.1 Fracture Surface Morphology

The fracture surface morphology of PVC pipe materials has been described previously [1]. The surface morphology under conditions where K_{Ic} just becomes valid can be separated into three steps. Just ahead of the crack tip, a band of highly drawn material is observed, with micro voids nucleated around some additive particles, as shown in Figure 49. Ahead of this band the surface appears brittle with little yielding or drawing evident. Between these two distinctive modes a transition stage is observed.

For pure PVC, the surface morphology under conditions where K_{Ic} becomes valid can be separated into three regions, similar to those in PVC pipe materials. Figure 50 is a schematic representation of a fracture surface from a valid K_{Ic} test of pure PVC and $CaCO_3$-PVC material, and Figure 51 is an SEM micrograph of fracture surface morphology. In the region just ahead of the fatigue pre-crack tip, Region I, the surface topology mainly consists of dimples, lips or ridges, which reflect a plastic mode of deformation of craze material, as illustrated in the SEM micrographs of the fracture surface morphology of PVC and $CaCO_3$-PVC in Figure 52 and 53 respectively. In Figure 53 , the formation of dimples around some filler particles is evident. A minor part of the fracture surface in Region I appears to be relatively featureless and smooth. This could result from the detaching of the craze-bulk interface. In addition, zones of different elevations could be observed, which could be due to the jumping of the crack

from one craze to the next on a different plane. These features suggest that crack nucleation in pure PVC and $CaCO_3$-PVC begins with the development of crazes and that crack propagation at subcritical velocity is attributable to the coalescence of the microvoids within these crazes. In PC, PSF and PS, the stable crack growth region is characterized by the appearance of a river pattern, possibly due to the splitting of the craze in different planes.

At the end of Region I is a mirror zone in which the origin of unstable fracture can be identified. This localized failure initiation was observed in all the polymers in which multiple crazes are formed prior to brittle fracture. It is generally found that the unstable fracture origin is located in the interior of the specimen near the center, and the shape of the mirror zone resembles the shape of a secondary craze which hasn't grown completely across the specimen thickness. Figure 54 illustrates the fracture origin identified in a pure PVC specimen, and Figures 55 and 56 show the fracture surface morphology of PC and polysulfone respectively. The fracture origins can also be observed in these micrographs. The mirror zone appears relatively smooth with little craze material seen. It is likely that the failure occur along the craze/bulk boundary. Beyond the mirror zone is a region where crack rapidly accelerates and spreads radially forward. In Region III, the fracture surface of pure PVC is characterized by rough, fast crack propagation.

Based on the results of fractographic analysis and on the results of craze initiation/growth and crack velocity measurements, the mechanisms involved in the event of crack instability can be summarized as follows. At low K_I, there is a single craze formed at the crack tip of PVC, (as it may be generally true in all polymers which craze). As K_I is increased to be higher than 1 $MN/m^{3/2}$, the stress field at the crack tip becomes sufficiently high to initiate secondary crazes. In a multiple craze zone, the stress and strain in any individual craze is smaller than that which would be in a single craze system, which gives rise to the stability of the multiple-craze system. At K_I ~

$0.6K_c$, crack begins to grow from the major craze which has the best orientation. It's possible that more than one craze rupture and coalesce to form a crack, depending upon the orientation of the crazes. The secondary crazes surrounding the major craze are less stressed and remain unruptured at this K_I level. As crack propagates, the high stress field at the crack tip causes new crazes to form, which has the effect of stabilizing the propagating crack. At a higher enough K_I, associated with some $\dot{a}$, the secondary crazes are highly enough stressed and opened. The fracture stress may be easily reached in one of the secondary crazes which does not grow completely across the specimen thickness but grow near the central region where the triaxial stress is the highest and craze interaction is most intensive. When this occurs, a flaw is initiated along craze/buck boundary on one side of the crack near the bulk, as schematically illustrated in Figure 57. The newly initiated crack near the bulk gets driven unstably due to the releasing of the large amount of elastic strain energy stored in the bulk. The strain rate at the tip of the accelerated crack gets high enough that there is no sufficient time for the initiation of multiple crazes. The crack propagates at a high speed, led by a single craze at its tip, resulting in the catastrophic failure of the specimen.

The mechanism suggested here can be generally applied to the plane strain fracture of polymers in which multiple crazing occurs before the catastrophic failure. The fracture stress of the crazes is determined by the craze shape, craze stress and modulus, which are rate dependent. In addition, it depends on the stress interaction which alters the stress field at the crack tip. An attempt was made to study the change of the stress field due to the presence of the secondary crazes by comparing the stress distribution around a single craze and a multiple craze zone using photoelastic method. Specimens which were previously loaded to have either a single craze or multiple crazes, determined by the loading conditions, at the crack tips, were reopened in the wedging device. The fringe patterns developed around the crack tip while it was been reloaded were photographed. Unfortunately, the individual stress fields could not be resolved.

Developing a criterion for such fracture event requires knowledge of the stress distribution among the crazes and the above mentioned local properties of the crazes. Although an effort has been made in modelling the elastic interaction of a macrocrack with a field of microcracks [74], the solutions are of great complexity mathematically, and are not directly useful here.

9.2 Multiple Craze Zone and Fracture Toughness

As previously described, stable crack growth occurs in the multiple craze zone before catastrophic fracture. Since the stress continues to rise during this slow growth, the stress at fracture must be related to the true crack length at failure - - that is, the initial crack length plus the slow crack growth. The usual procedure of calculating plain strain fracture toughness, ASTM-E399, uses the initial crack length before loading. For a material having a crack growing stably before the critical fracture load is reached, this procedure would give an erroneously low value of K_Q. Figures 58 and 59 illustrate this point; the calculated fracture toughness values with and without the stable crack length are plotted as functions of displacement rate and temperature, respectively. The amount of stable crack growth as a function of temperature and displacement rate has already been shown in Figures 43 and 44. The calculated fracture toughness values which take the length of stable crack growth into account are higher and also show a much greater dependency on the displacement rate and temperature. The validity of a plane strain fracture toughness test based on the K_Q with stable crack growth distance included (i.e. $S/B < 1$; the thickness B is smaller than the crack length C in all cases and is therefore more critical), is also shown in these Figures. The correspondence between the displacement rate and the loading rate can be obtained directly by recording the displacement and the load simultaneously on the digital oscilloscope. Table 7 shows the correspondence between different displacement and loading rates, with time to failure and the yield strength of each rate included.

In the fracture toughness tests it was observed that when the displacement rate is changed from 0.85 mm/s to 0.085 mm/s the crack propagated stably throughout the specimen without catastrophic failure occurring. In such case, the load increased to a maximum load then slowly dropped down as the crack continued propagating stably. At a temperature above 60 ^{o}C, extensive shear flow occurred as the crack propagated stably to the end of the specimen.

The results of the fracture toughness tests of pure PVC and PVC pipe materials [1] show a noticeable amount of scatter. It is known that the technique of notching could affect the fracture toughness values. However, the specimens which were fatigued under similar conditions to generate fatigue crack tips also show some amount of data scattering with their K_{Ic} values, as can be seen in Figure 19. It thus appears that the observed scattering is due to the nature of PVC pipe materials to form multiple crazes before fracture. Comparing the side profiles of the specimens fractured under the same condition, it was found that higher K_{Ic} is associated with longer slow crack growth and more crazes underneath the surfaces; in addition, the crazes tend to grow deeper into the bulk. Figure 60 shows the side profiles of two specimens fractured under the same condition for comparison. In the specimen of higher K_c, crazes can be easily seen underneath the fracture surface. Crazes are small and barely resolvable under the light microscope in the specimen of lower K_c. It is not understood, however, why there is variation with the growth of the crazes in the same material tested under similar conditions.

Although some scatter is evident, the fracture toughness values in the valid test region remain relatively insensitive to both the displacement rate and the temperature, which agrees with the results obtained for the PVC pipe system [1]. However, the results of the low temperature tests at -60 ^{o}C showed that the fracture toughness value of pure PVC depends on the loading rate rather significantly. The value decreases as the loading rate is increases, as demonstrated in Table 8. Due to the increase in yield

strength at low temperature all the tests were valid with s/B < 1. In PMMA, the fracture toughness value was also shown to be rate sensitive when the temperature is dropped down to that below -80 °C. Below this temperature, a higher cross-head rate gives a lower K_c value, similar to the trend observed in PMMA [61]. The morphology of the stable crack zone appeared to be smoother for the specimen fractured at -60 °C than that fractured at the room temperature, as shown in Figure 61.

9.3 Estimation of Fracture Toughness

Darwish [1] has attempted to estimate the fracture toughness of the PVC pipe material from the measured height of fibrils observed in the ductile band and the yield stress of the pipe material. The estimated values turned out to be less than the measured K_{Ic} by a factor of several fold. Moreover, under valid K_{Ic} conditions the ductile band width is shorter than the Dugdale zone, calculated using the measured K_{Ic} and yield stress, by more than a factor of five for some pipe materials. The fracture surfaces of pure PVC do not show the fibrillar appearance, although the value of K_{Ic} is similar to that of pipe materials. These results suggest that much of the fracture toughness is derived from plastic deformation processes not evident on the fracture surface.

Results of microscopic studies in the previous chapters have established that the formation of multiple crazes is the principle energy absorption mechanism in PVC pipe material and pure PVC matrix under plane strain conditions. It is possible that by determining the craze properties and the number of crazes G_{Ic} can be estimated. Kambour [79] has proposed a model for calculating the work involved in forming an stretching to the breaking point of all the crazes at the crack tip as

$$G_{Ic} = N \varepsilon_b l_o \sigma$$

where N: number of crazes

ε_b: total strain in each craze at break.
l_o: the "gauge" length of polymer of normal density that is transformed into the craze
σ: average stress for the entire deformation process.

Based on the model, the properties of a craze which are important for the estimation of energy absorption include craze extension ratio, strain at break, and craze thickness.

The mechanical properties of a single craze in PC has been determined by Kambour [38]. The technique used involving subjecting a stressed tensile bar to a crazing agent under a carefully controlled condition to obtain a few well-spaced crazes growing completely through the specimen. Similar technique was used in an effort to determine the craze properties of a single craze in PVC. The results indicate that an appropriate condition for obtaining a single craze developed through the specimen in PVC is difficult to achieve. No crazes were observed in the specimens subjected to a low stress level for a minimum during of three weeks. However,crack easily developed and propagated through the specimens when the bars were subjected to high stresses.

Estimating G_{Ic} of PVC based on the properties of a craze obtained from a single craze system has the following disadvantages. The condition under which a single craze is statically formed is very different from the formation of multiple crazes at a moving crack tip. It has been reported that the craze thickness deceases with strain rate [27]. Secondly, the stress field in a multiple craze zone is different from that in a single craze system, as a result,the properties of the individual crazes in a multiple craze zone are different from the properties in a single craze system. These factors could give rise to errors in estimating G_{Ic} of PVC. An alternative approach in determining the craze properties is by using interference microscopy method, as has been attempted by other workers [7, 24, 25]. As discussed previously, the fringe pattern of a multiple craze zone can be confused . In most cases, however,small areas of clearly aligned fringes, resembles the fringe pattern of a single craze, can be found. These areas could be where the main craze is much more opened up than the secondary crazes and the angle

between them is relatively small. Quantitative analysis of the craze properties were made using the fringes in these areas. Experimental approach of this study is the same as that described in the study of craze growth in Chapter 7. The craze thickness, one of the important parameters needed for the calculation of the energy absorbed by a craze, can be determined by applying the theory of interference optics, which has been shown in page (57). The refractive index of an unloaded craze μ_0 can be determined from the critical angle for the total internal reflection at the craze/matrix interface, which is 1.3 for PVC as reported in the literature [25]. The refractive index of a loaded craze was obtained through Lorentz-Lorenz relationship, which relates the refractive index to the polarizability and the density of the craze material, under the assumption that the craze extends with lateral constraint [21, 25]. The procedure for determining this value is shown in the Appendix I. The determined refractive index of the loaded craze in PVC is about 1.14 at the crack tip where the density of the material inside the craze is the lowest,and about 1.18 at the craze tip. The variation is small enough that the refractive index of the loaded craze can be taken as a constant, 1.14. With the known μ of the craze and the fringe number as a function of the distance from the craze tip, the craze thickness can be calculated from the theory of interference optics. Figure 62 shows the calculated craze thickness as a function of the distance from the crack tip, for a specimen previously loaded close to the onset of stable crack growth at a loading rate of 100 lb/sec. The maximum craze opening thickness, extrapolated to the crack tip, is about 4.3 μm for a loaded craze and 2 μm for an unloaded craze. For a craze at the tip of a stable crack in a specimen previously loaded to 90% K_Q, the maximum thickness is very close to that before the crack had advanced. Figure 63 shows the interference pattern of such craze and Figure 64 shows the craze thickness profile calculated, with the fringe number indicated on the left axis and the craze thickness on the right axis.

The strain to break of a craze, another parameter necessary for the energy calculation, can be determined from the number of fringes at the breaking point of a craze under loaded and unloaded states, based on the method used by Brown et al. [10].

The calculated ε_b for pure PVC is 1.3, with the calculation procedure listed in Table 9. The gage length l_o, determined from the craze thickness and extension ratio of unstressed craze, is calculated to be 2.68 μm, as shown in Table 10. Weidmann et al. [23] have determined that the crazing stress of PVC is close to but slightly lower than the yield stress. Therefore, in calculating the G_{Ic} ,the yielding stress of pure PVC, 70 MN/m^2 for a loading rate of 100 lb/sec at room temperature, is taken as the average stress for the deformation process.

With all the values of the parameters acquired, the amount of energy absorbed by the crazes can then be calculated using Kambour's model. The energy required to extend one craze to its breaking point is

$$\begin{aligned} G &= N \alpha_b l_o \sigma \\ &= (1)(1.3)(2.68\mu m)(70\ MN/m^2) \\ &= 244\ J/m^2 \end{aligned}$$

The fracture toughness value,K_{Ic}, of PVC obtained under valid test conditions is around 3.3 $MN/m^{3/2}$. The corresponding G_{Ic} value calculated, as shown in Table 11, is equal to 2703 J/m^2. Dividing this number by the amount of energy absorbed by one craze, 244 J/m^2, it is estimated that about 11 crazes should have been formed at the point of fracture. Examining the crack tip of the specimen loaded close to the fracture point, as shown in Figures 41 and 42, about 8 to 10 crazes were present at the crack tip.

One major assumption made in the calculation is that the values of the crazes properties are the same in each craze. In fact, some crazes are opened up more than others and not all the crazes are brought to the same point of failure. In view of the inherent error made in the assumption, the estimation based on the present model still is much better than the estimation made based on the measured height of fibrils in the ductile band of the PVC material pipe, for which the estimated values were less than the

measured K_{Ic} by several factors. A significant amount of energy not evident on the fracture surface was absorbed by forming numerous small crazes in PVC pipe material.

CHAPTER TEN

Effect of the Microstructure on the Properties of Crazes

In the previous chapters, it has been shown that craze properties are critically related to the fracture processes and fracture toughness of thermoplastics. This chapter will address the questions of what factors govern craze properties in different polymers with different chemical structure, and how the molecular structure influences the mode of deformation in different polymers.

There is, at present, no theoretical vehicle for assessing whether or not a particular polymer will craze under a given set of conditions. However, many links between chemical structure and deformation by crazing have been successfully brought out by different studies. For instance, Wellinghoff and Baer et al [88, 89] classify glassy polymers into two major types. Vinyl polymers with bulky side chains, such as PS and PMMA, (Type I polymers), craze at all temperature below their glass transition temperature. The chemical structure of Type II polymers is generally characterized by the presence of a main chain aryl unit connected by flexible heteroatom linkages, eg. PC,PET and PPO. Although it is claimed that Type II polymers craze in a temperature range just below their T_g's and fail by shear banding below this temperature range, it has been observed that PC crazes at room temperature, which is extensively below its T_g [24]. Results based on Argon's molecular kink model [48] and Yannas' strophon model [22] indicate that plastic flow in Type I polymers is much more of a highly localized nature than of Type II polymers. The fact that PVC is a relatively tough

polymer and forms multiple crazes which could be considered as a form of strain delocalization might put PVC into the classification of Type II polymers. However, crazing in PVC at a temperature around -100 ^{o}C was observed in this study. Its low temperature crazing behavior is in contrast with the characteristics of the type II polymers.

Kramer has further demonstrated that the craze properties are closely associated with the properties of the entanglement network characteristic of that polymer or polymer blend, as has been mentioned in the literature review. In particular, the craze fibril extension ratio was shown to increase approximately linearly with the chain contour length l_e between entanglements [63]. Kramer has suggested that a useful way to increase the brittle fracture stress and decrease the ductile-to-brittle transition temperature of a glassy polymer is to decrease its entanglement contour length, which is similar to decreasing the fibril extension ratio.

As already shown, the toughness of PVC is related to the properties of its crazes, which in turn could be governed by the properties of the entanglement network, as has been demonstrated in other polymers. It is desirable, therefore, to investigate the characteristics of the entanglement network in PVC, such as entanglement molecular weight, extension ratio and entanglement mesh size, as have been described in the Chapter 1, to elucidate the effects of molecular entanglement on the properties of the crazes in PVC.

The entanglement network theory, applicable to amorphous polymers, is based on the fact that long chain molecules randomly cross among each other, and the entanglement points act as crosslinks, capable of bearing certain amount of load. This gives rise to the prominent effect of a rubbery plateau in the shear modulus, G, above T_g. In this study, an eccentric rotating disc rheometer ,(Rhemotrics Inc.), was used to determine the values of G as a function of temperature in the rubbery region.

Subsequently, the molecular weight between entanglements, M_e, the extension ratio (λ) and entanglement mesh size (d) can be calculated based on the experimentally determined value of G.

A disc shape sample of pure PVC (~ 1 inch in diameter) was inserted in a heating chamber between two circular plates, rotating at a selected frequency under a fixed strain. The shear storage modulus can be determined from the force measured by the force transducers connected to the plates based on the following relationship:

$$G = \frac{\text{force}}{\text{area x strain}}$$

The values of G determined at three different temperatures at a fixed strain of 1% and a frequency of 0.016 Hz are listed in Table 12. The value of G drops significantly over a temperature range of 117 °C to 159 °C. The results obtained from a similar pipe resin also reveal a constant drop of the modulus [90]. A study on the effect of plasticization on the modulus of PVC shows that the shear modulus of unplasticized PVC drops from 1.3×10^6 N/m^2 at 120 °C to 5.3×10^5 N/m^2 at 160 °C [91], comparable to the results obtained in this study. These results indicate that there is a structural change occurring over the rubbery region in PVC.

In commercial PVC, although generally described as amorphous, a range of 5-15% crystallinity has been reported [92]. It was shown that the crystallinity of rigid PVC is greatly influenced by the type of stabilizer added [92]. Moreover, the amount of crystallinity has considerable effects on the mechanical properties of rigid PVC after U.V. irradiation. Crystallinity in commercial rigid PVC comes mostly from the annealing process, during which the residual frozen stresses, built in as a result of quenching from molten state after molding, is relieved. Witenhafer [93] has shown that 110°C is the optimum crystallization temperature for PVC. It was also shown by Chartoff et al [94] that while the quenched PVC is amorphous, crystallinity would

increase rapidly during the first half hour of annealing at a temperature of 100 °. The PVC pipe materials used in this study have gone through the process of annealing at 95 ° (T_g = 83 °C) for 40 minutes to one hour before testing. The percent of crystallinity accumulated during this process could be close to 10. The crystallites in PVC is known to have a wide melting range, with a more pronounced peak at 180 ± 10 °C [46, 95]. The dropping of the modulus therefore can be attributed to the graduate melting of the crystallites, which act as more effective crosslinks than molecular entanglements, in PVC at temperatures above its T_g.

Table 13 lists the information needed for the calculation of the characteristics of entanglement network in PVC. The calculated M_e, l_e, d and λ_{max} based on the G values obtained at different temperatures are listed in Table 14. Table 15 demonstrates the calculation procedure using the G value obtained at 117 °C. As more crystallites are melted with the increasing of temperature, the extension ratio of the molecules increases. At 117 °C, a least amount of crystallite melting is expected and the λ_{max} is the shortest. The amount of crystallites present should be very close to that at room temperature. Comparing λ_{max} at this temperature,3.51, with the values of other 11 polymers reported by Kramer et al. [63], as shown in Table 15, the λ_{max} of PVC falls in between the values of the tough (PPO, PC) and brittle polymers (PS, PTBS).

The properties of the crazes in PVC, however, are not simply governed by the characteristic of the entanglement network. The small crystallites which act as physical crosslinks are more likely to govern the fracture properties of the craze. The morphology of crazes in semi-crystalline polymers, such as polypropylene, have been studied [20]. Crazes were seen to develop ahead of the crack preferentially at the boundaries of the crystallites when the crystallites are small. Wenig [95] by using a wide angle X-ray scattering technique has determined the size of average crystallite in PVC to be 41 Å x 41 Å x 7 Å. These crystallites , spaced at 100 Å , are connected together by tie molecules, forming a three-dimensional network, as proposed by Summers [96].

Crazes would preferentially develop within these tie molecules when a load is applied. The growth of the crazes could be governed by the size and the spacing of the crystallites and the extent of entanglement among the tie molecules. Furthermore, the chemical structure of PVC - $(CH_2\text{-}CHCL)\text{-}_n$ give the material a high polarity constant. The Van der Wall force for separating the molecules would be relatively high compared with other less polar polymers, which could also contribute to the toughness observed in PVC.

CHAPTER ELEVEN

Conclusions

The results of the present study on the mechanisms of fracture in PVC and other thermoplastics are concluded as follows. Under plane strain fracture toughness testing conditions, the deformation mechanism which leads to the toughness of PVC pipe materials is the formation of multiple crazes. The thickness of the craze extended to breaking point is about 4.5μm. In the unloaded state, the craze thickness is about 2 μm. The number of the crazes formed at the crack tip of pure PVC is about 8~10 prior to brittle fracture. The fracture toughness value can be successfully estimated based on the number of crazes formed and craze properties. In PVC pipe materials, more crazes are present at the crack tip than in pure PVC , and the size of the crazes is relatively smaller. The presence of $CaCO_3$ particles decrease the fracture toughness of the matrix slightly, although the yield strength of the pure PVC and $CaCO_3$-PVC materials are about the same. Nucleation of microvoids around the additive particles in $CaCO_3$-PVC material is evident.

The formation of multiple crazes has a direct correlation with fracture toughness of a material, as evidenced by the fact that a single craze at the crack tip in PMMA gives rise to a lower fracture toughness value compared to those polymers which form multiple crazes at the crack tips, such as Nylon 66, PVC, PC, PSF and PS. The mechanisms of fracture for the polymers forming multiple crazes before brittle fracture are broadly similar. Upon loading, the crack starts to propagate in a stable manner until the crack instability occurs when a transition from multiple crazes to a single craze at

the crack tip takes place. Although the extensional growth rate of the crazes is governed by the loading rate applied, the velocity of the crack before the instability showed little sensitivity to the loading rate. The changing of the crack propagation mode corresponds to a change of the crack velocity from about 18 mm/s ~ 100 mm/s to a minimum of 17.5 m/s.

Microscopic analysis indicates that most of the secondary crazes do not grow across the whole crack plane, but are smaller in size and concentrate at the center of the specimen. It is suggested that due to the constraint of the craze shape and the high triaxial stress at the center of the specimen, a disk-shaped crack would initiate in the secondary crazes when the stress at the crack tip is high . The large amount of strain energy stored in the system causes the crack to accelerate rapidly as it is released.

The properties of the crazes in PVC do not seem to be simply governed by the characteristics of the entanglement network . The small crystallites which act as physical crosslinks are more likely to govern the fracture properties of the craze.

CHAPTER TWELVE

Recommendations

(1) The toughness of the material with stable cracks could be increased by forming more crazes at the crack tip. It is possible that by modifying the resin ductility, for example by using polymer blend or rubber toughening technique, more crazes could be formed. Chemical modification of the resin could also delay or prevent the transition from stable multiple crazes to an unstable single craze . Further study along this line would be interesting and profitable.

(2) The crack velocity profile at temperatures other than the room temperature should be determined to elucidate the effect of temperature on the critical velocity before the crack instability.

(3) A model which would predict the critical condition for the multiple-single craze transition based on the material parameters would be of great value. As mentioned previously, the development of such a model would require the knowledge of the stress distribution among the crazes, and the local properties of the crazes such as craze shape, craze stress and craze modulus. These local properties would, in turn, depend on the strain rate at the crack tip.

(4) The effect of crystallinity on the fracture toughness in PVC has not been quantitatively studied. Such knowledge could facilitate selecting optimal conditions for material processing in order to achieve the most desirable fracture properties of PVC pipe materials.

References

1. A. Darwish, *Fracture Analysis of PVC,* PhD dissertation, MIT, 1981.

2. J. F. Mandell, A. Y. Darwish, and F. J. McGarry, *Polym. Eng. and Sci.,* vol.22, 1982, p. 826.

3. F. A. Johnson and J. C. Radon, *J. of Polym. Sci., Polym Chem.ed.,* Vol. 13, 1975, p. 495.

4. J. Eftis and J. M. Krafft, *Journal Basic Eng. (Trans. ASME),* Vol. 87, 1965, p. 257.

5. C. B. Bucknall, *Toughened Plastics,* Applied Science Publishers, London, England, 1977.

6. S. Rabinowitz and P. Beardmore, *Craze Formation and Fracture in Glassy Polymers,* CRC Press, 1972.

7. R. P. Kambour, *J. Polymer Sci., A-2,* Vol. 4, 1966, p. 17.

8. P. L. Cornes and R. N. Haward, *Polymer,* Vol. 15, 1974, p. 149.

9. R. P. Kambour, *Macromol Rev.,* Vol. 7 1873, p. 1

10. H. R. Brown and I. M. Ward, *Polymer,* Vol. 14, 1973, p. 469.

11. Hans Bergkvist and Hans Anderson, *Int. J. of Fr. Mech.,* Vol. 8, No. 2, 1972, p. 139.

12. J. P. Berry, in *Fracture Processes in Polymeric Solids,* B.Rosen ed., Interscience Publishers, New York, 1964, ch. II.

13. J. F. Knott, *Mater. Sci. Eng.,* Vol. 7, 1971, p. 1.

14. A. A. Griffith, *Proc. Intern. Congr. Appl. Mech. (Delft),* 1924, p. 55.

15. C. E. Inglis, *Trans. Inst. Naval Architects,* Vol. 55, 1913, p. 219.

16. J. F. Knott, *Fundamentals of Fracture Mechanics,* Butterworths Publishers, London, 1973.

17. C. Bauwens-Crowet, J. C. Bauwens, and G. Homes, *J. of Polymer Sci., A-2,* 1969, p. 735.

18. J-P. F. Chevaillier, "Fatigue of PVC-Pipe Material," Master's thesis, MIT, 1980.

19. B. D. Lauterwasser and E. J. Kramer, *Phil. Mag.,* Vol. A39, 1979, p. 469.

20. B. Z. Jang, PhD dissertation, MIT, 1982.

21. R. P. Kambour, *Polymer,* Vol. 5, 1964, p. 143.

22. J. F. Jansson and I. V. Yannas, *J. Polymer Sci., Phys.,* Vol. 15, 1977, p. 2103.

23. G. W. Weidmann and W. Döll, *Int. J. of Fracture,* Vol. 14, 1978, p. 189.

24. G. L. Pitman and I. M. Ward, *Polymer,* Vol. 20, 1979, p. 895.

25. N. J. Mills and N. Walker, *Polymer,* Vol. 17, 1976, p. 335.

26. R. Schirrer and C. Goett, *J. of Mat. Sci. Letter,* Vol. 1, 1982, p. 355.

27. W. Döll, *Advances in Polymer Science,* Springer-Verlag, Berlin, Heidelberg, 1983.

28. P. B. Bowden, *Phil. Mag.,* Vol. 22, 1970, p. 455.

29. P. B. Bowden and S. Raha, *Phil. Mag.,* Vol. 22, 1970, p. 463.

30. P. B. Bowden and J. A. Jukes, *J. Mat. Sci.,* Vol. 3, 1968, p. 183.

31. T. E. Brady and G. Yeh, *J. Appl. Phys.,* Vol. 42, 1971, p. 4622.

32. J. Wu and J. Li, *J. Mater. Sci.,* Vol. 11, 1976, p. 434.

33. J. Li and J. Wu, *J. Mater. Sci.,* Vol. 14, 1976, p. 445.

34. S. Crandall, N. Dahl and T. Larder, in *An Introduction to the Mechanics of Solids,* McGraw-Hill, Inc., N.Y., 1978, ch. 5.

35. C. A. Coulomb, *Meim, Math. et Phys.,* Vol. 7, 1973, p. 343.

36. P. B. Bowden, Appl. Sci. Publishers, 1973, p. 279.

37. S. S. Sternstein and L. Ongchin, *ACS Preprints,* Vol. 10, 1969, p. 1117.

38. R. P. Kambour, *The Role of Crazing in the Mechanism of Fracture of Glassy Polymers,* Interscience, New York, 1968, p. 215.

39. D. S. Dugdale, *J. Mech. Phys. Solids,* Vol. 8, 1960, p. 100.

40. B. Cotterell, *Inter. J. Fracture Mech.,* Vol. 4, 1968, p. 209.

41. G. P. Morgan and I. M. Ward, *Polymer,* Vol. 18, 1977, p. 87.

42. H. R. Brown and G. Stevens, *J. Mater. Sci.,* Vol. 13, 1978, p. 2373.

43. H. R. Brown and Tan Hea Chin, *J. Mater. Sci.,* Vol. 15, 1980, p. 677.

44. I. Narisawa, M. Ishikawa, and H. Ogawa, *J. of Polymer Sci., Physics,* Vol. 15, 1977, p. 2227.

45. R. A. Fraser and I. M. Ward, *Polymer,* Vol. 19, 1978, p. 220.

46. M. T. Takemori and R. P. Kambour, *J. Mater. Sci. Letters,* Vol. 16, 1981, p. 1108.

47. A. S. Tetelman, *Fracture of Structural Materials,* John Wiley and Sons, New York, London, Sydney, 1967.

48. A. S. Argon, *J. Marcomol. Sci.-Phys.,* Vol. B8 (3-4), 1973, p. 573.

49. E. J. Kramer, *Advances in Polymer Science,* Springer-Verlag, Berlin, Heidelberg, 1983.

50. S. H. Joseph and R. A. Duckett, *Polymer,* Vol. 19, 1978, p. 844.

51. R. A. Duckett, B. C. Goswami, L. S. A. Smith, I. M. Ward, and A. M. Zihlif, *British Polymer J.,* Vol. 10, 1978, p. 11.

52. R. A. Duckett, S. H. Joseph, J. Summer, and Z. Stachurski, *Fourth International Conference on Yield, Deformation, and Fracture of Polymers,* Plastic Institute, London, 1979.

53. B. Maxwell and L. F. Rahm, *Ind. Eng. Chem.,* Vol. 41, No. 1988, 1949, p. 4.

54. A. S. Argon and J. G. Hannoosh, *Phil. Mag.,* Vol. 36, 1977, p. 1195.

55. A. M. Donald and E. J. Kramer, *Phil. Mag. A.,* Vol. 43, 1981, p. 857.

56. H. H. Kausch, *Polymer Fracture,* Springer-Verlag, Berlin, Heidelberg, New York, 1978.

57. S. N. Zhurkov and V. E. Korshukor, *J. Polym. Sci., Polym. Phys. Ed.,* Vol. 12, 1974, p. 385.

58. E. H. Andrews and P. E. Reed, Adv. *Polym. Sci.,* Vol. 27, 1978, p. 3.

59. R. N. Haward, H. E. Daniels, and L. R. G. Treloar, *J. Polym. Sci., Polym. Phys. ed.*, Vol. 16, 1978, p. 1169.

60. P. Beahan, M. Bevis, and D. Hull, *Proc. R. Soc.*, Vol. A343, 1975, p. 525.

61. G. P. Marshall, L. H. Contts, and J. G. Williams, *J. of Mat. Sci.*, Vol. 9, 1974, pp. 1409-1419.

62. J. G. Williams, "Applications of Linear Fracture Mechanics," in *Advances in Polym. Sci.*, H. J. Cantow and G. Dall Ada, eds., Springer-Verlag, Berlin, Heidelberg, 1978.

63. A. Donald and E. J. Kramer, *J. of Polymer Sci., Polymer Phys.*, Vol. 20, 1982, p. 899.

64. A. M. Donald and E. J. Kramer, *Polymer*, Vol. 23, 1982, p. 461.

65. R. S. Porter and J. F. Johnson, *Chem. Rev.*, Vol. 66, 1966, p. 1.

66. W. W. Graesley, *Adv. Polym. Sci.*, Vol. 16, 1974, p. 1.

67. M. Kurata, Y. Tsunashima, M. Iwama, and K. Kamada, in *Polymer Handbook*, J. Brandrup and E. Immergut, eds., Wiley, New York, 1975, ch. IV-4.

68. W. C. V. Wang, PhD dissertation, Cornell University, 1981.

69. B. A. Bilby and J. D. Eshelby, *Fracture*, Academic, New York, 1972, p. 111, H. Liebowitz, Ed.

70. R. Schirrer and C. Goett, J. of Mat Sci., Vol. 16, 1981, p. 2566.

71. A. Chudnovsky, A. Shraiber, and J. Yu, *J. of Mechanics of Solids*, Vol. 3, 1974, p. 336.

72. A. Chudnovsky and A. Moet, *Conference on Fatigue in Polymers*, London, June 1983.

73. N. J. Mills, *J. of Mat. Sci.*, Vol. 16, 1981, p. 1332.

74. A. Chudnovsky and M. Kachanov, *Int. J. of Eng. Sci.*, 1984, in press.

75. L. I. Nass, editor, *Encyclopedia of PVC, vol. I, II, and III*, Marcel Dekker, Inc., 1977.

76. ASTM, "Standard Method of Test for Plane-Strain Fracture Toughness of Metallic Materials," Tech. report, ASTM Designation E399-74, Part 10.

77. G. P. Marshall, L. E. Culver, and J. Williams, *Int. J. Fract. Mech.*, Vol. 9, 1973, p. 295.

78. R. D. R. Gales and N. J. Mills, *Eng. Fracture Mech.*, Vol. 6, 1974, p. 93.

79. R. P. Kambour, A. S. Holik, and S. Miller, *J. of Polym. Sci., Polym Phys. ed.*, Vol. 16, 1978, p. 91.

80. J. F. Mandell and J.-P. F. Chevaillier, *Polymer Eng. and Sci.*, 1984, in press.

81. C.-G. Li, Master's thesis, MIT, 1983.

82. R. P. Kambour and S. A. Smith, *J. of Polym. Sci., Polym. Phys. ed.*, Vol. 20, 1982, p. 2069.

83. P. Trassaert and R. Schirrer, *J. of Mat. Sci.*, Vol. 18, 1983, p. 3004.

84. D. R. Khanna and H. R. Gulati, *Fundamentals of Optics*, Asia Book Center, Delhi, India, 1965.

85. M. Parvin and J. G. Williams, *J. of Mat. Sci.*, Vol. 10, 1975, p. 1883.

86. K. Takahashi, M. Kimura, and S. Hyodo, *J. of Mat. Sci.*, Vol. 13, 1978, p. 2718, letter.

87. D. Broek, *Elementary Engineering Fracture Mechanics*, Sijthoff and Noordhoff, Netherlands, 1978.

88. S. Wellinghoff and E. Baer, *J. Appl. Polym. Sci.*, Vol. 22, 1978, pp. 2025-45.

89. A. Moet, E. Baer, and S. Wellinghoff, "Irreversible Deformation Processes in Amorphous Polymers and Their Blends," *Structure and Properties of Amorphous Polymers, Proc. of the Second Symp. on Macromol.*, 1978, pp. 23-45.

90. S. A. Iobst, *Molecular Structure and Relaxation Behavior of Polyvinyl Chloride*, PhD dissertation, Lehigh University, 1970.

91. *Plasticization and Plasticizer Processes*, Vol. 98, 1965, Advances in Chemistry Series.

92. I. M. EL-Hennawi, M. Y. A. Younan, and M. A. EL-Rifai, "PVC Compounding and Degradation Physical-Chemical and Mechanical Effects," Tech. report 122, Cairo University -- MIT Technological Planning Program, 1983, Engineering Applications for the Egyptian Plastics Industry

93. D. E. Witenhafer, *J. Macromol. Sci.-Phys.*, Vol. B4, 1970, p. 915.

94. R. P. Chartoff, T. S. K. Lo, E. R. Harrel, Jr., and R. J. Roe, *J. Macromol. Sci.-Phys.*, Vol. B20(3), 1981, p. 287.

95. W. Wenig, *J. Polym. Sci.-Phys.*, Vol. 16, 1978.

96. J. W. Summers, *J. of Vinyl Technology,* Vol. 3, No. 2, June 1981.

97. J. Brandrup, E. H. Immergut, editors, *Polymer Handbook,* John Wiley and Sons, 1975.

98. H. Lee, PhD dissertation, MIT, 1983.

Tables

Table 1 — The critical temperature for the transition from multiple crazes to a single craze for several polymers Ref [70]

Polymer	T_c (°C)
PMMA	-20 ± 2
PS	+46 ± 2
PS-polyisoprene-PS	+65 ± 2
PC	-95 ± 2
PVC	+7 or +30

Table 2 — Number of strands broken vs. the resulting voltage level

no. of strands broken	voltage level (mv)
0	.921
1	.964
2	1.012
3	1.065
4	1.124
5	1.190
6	1.264
7	1.348
8	1.444
9	1.555
10	1.683
11	1.836
12	2.018
13	2.241
14	2.518
15	2.875
16	3.349
17	4.010
18	4.996
19	6.625
20	9.644

Table 3 — Fracture toughness values of several different polymers

	loading rate (lb/sec)	average Kc ($MNm^{-3/2}$)	Kc / (Kc of PMMA)
NYLON 66	500	3.9	3.6
PVC	500	3.18	2.9
PSulf.	500	2.91	2.7
PC	500	2.83	2.6
PS	5	1.94	1.8
PMMA	5	1.08	1.0

Table 4 — The loading rates corresponding to different half cycle time used in studying craze growth

half cycle time(sec)	loading rate (lb/sec)
0.05	975 - 1632
0.5	68 - 138
5	7 - 14
50	0.7 - 1.4
500	0.002 - 0.113

Table 5 - Results of the low temperature tests of craze growth

half cycle time (sec)	K_I(MN/m$^{3/2}$)	craze zone length (mm)
5	0.85	0.063
	1.47	0.039
	1.86	0.025
50	0.9	0.019
	1.41	0.040
	1.82	0.066
500	0.95	0.11
	1.47	0.046
	1.91	0.095

Table 6 — Calculation of the Predicted Terminal Crack Velocity in PVC Resin

E: Young's Modulus of PVC

ρ: Specific density of PVC

$$\text{Longitudinal Velocity} = \sqrt{\frac{E}{\rho}}$$

$$= \sqrt{\frac{3447 \times 10^6 \text{ Kgm/sec}^2\text{m}^2}{1.343 \times 10^3 \text{ Kg/m}^3}}$$

$$= 1600 \text{ m/sec}$$

$$\text{Terminal Crack Speed in PVC resin} = \frac{1}{3}\left(\sqrt{\frac{E}{\rho}}\right) \text{ (Ref. [87])}$$

$$= \frac{1}{3}(1600 \text{ m/sec})$$

$$= 481 \text{ m/sec}$$

Table 7 — Correspondence between various displacement rates and loading rates

Displacement Rate (mm/s)	Loading Rate (lb/s)	Time to Failure (sec)	Yield Strength (Psi)
8.6×10^{-3}	.8	132	8,600
8.6×10^{-2}	7.6	12	9,300
8.6×10^{-1}	78	1.3	10,100
6.9	381	.26	11,000
60	846	.12	12,170
100	1508	.065	12,400

Table 8 — Results of fracture toughness tests at -60 °C

loading rate(lb/sec)	stable crack growth(mm)	critical load for fracture(lb)	calculated K_{Ic} ($MN/m^{3/2}$)
0.07	.861	164	4.71
	2.67	143	4.47
11.6	1.37	164	4.62
	.03	93	2.32
500	.26	108	3.2
	.12	88	2.6
	.09	78	2.3

Table 9 — Calculation of the strain to break of a craze in PVC

Assuming that the craze extends with complete lateral constraint and using Lorentz-Lorenz relationship:

$$\frac{\mu^2-1}{\mu^2+2} = \frac{\mu_o^2-1}{\mu_o^2+2} \cdot \frac{1}{l}$$

where l = extension ratio of the craze

With known refractive index of unloaded craze $\mu_o = 1.30$, then

$$\frac{\mu^2-1}{\mu^2+2} = \frac{0.19}{l}$$

which gives

$$\mu^2 = \frac{0.38+l}{l-0.19}$$

Let n_b and n_o be the number of fringes in the craze at break and unloaded respectively, then

$$\frac{n_b}{n_o} = \frac{\mu_b l_b}{\mu} = \left(\frac{0.38+l}{l-0.19} \right) \cdot \frac{l}{1.30}$$

$$= 1 + \frac{l-1}{1.30} \text{ (to a good approximation)}$$

or

$$\varepsilon_b = l_b - 1 = 1.30 \left(\frac{n_b}{n_o} - 1 \right)$$

In PVC, $\frac{n_b}{n_o} \approx 2$ for a craze loaded to the rupture point.

$\therefore \varepsilon_b = 1.30\,(2-1) = 1.30$

Table 10 — Calculation of the gage length of the craze

$$\text{gage length } l_o = \frac{\text{craze thickness at break}}{\text{extension ratio of unstressed craze}}$$

craze thickness of PVC at break $\approx 4.5\ \mu m$

Applying Lorentz-Lorenz relationship:

$$\frac{\mu_o^2-1}{\mu_o^2+2} = \frac{\mu_1^2-1}{\mu_1^2+2} \cdot \frac{1}{l}$$

where μ_o: refractive index of unstressed craze

μ_1: refractive index of bulk PVC material

l: extension ratio of unstressed craze

then,

$$l = \left(\frac{\mu_1^2-1}{\mu_1^2+2} \right) \left(\frac{\mu_o^2+2}{\mu_o^2-1} \right)$$

Since

$\mu_1 = 1.54$ (ref [97])

$\mu_o = 1.30$ (ref [25])

therefore

$l = (0.314)\,(5.348) = 1.68$

The gage length l_o can then be determined:

$$l_o = \frac{4.5\mu m}{1.68} = 2.68\mu m$$

Table 11 — Conversion of K_{Ic} to G_{Ic}

K_{Ic} = 3.3 x 1.^{6} N/m$^{3/2}$ (experimentally determined)

ν: Poisson's ratio = 0.38 (ref. [97])

E: Young's modulus = 3447 x 10^6 N/m^2 (experimentally determined)

$$G_{Ic} = \frac{K_{Ic}^2(1 - \nu^2)}{E}$$

$$= \frac{(3.3 \times 10^6 \text{N/m}^{3/2})^2 (1-(.38)^2)}{3447 \times 10^6 \text{N/m}^2}$$

$$= 2703 \text{ N/m (or J/m}^2\text{)}$$

Table 12 — Shear modulus of PVC determined at different temperatures in the rubbery region

Temperature	Shear modulus (N/m^2)
117 °C (390 °K)	1.2×10^6
147 °C (420 °K)	9.2×10^5
159 °C (432 °K)	7.3×10^5

Table 13 — Information for calculating the characteristics of entanglement network of PVC

parameter	denotation	value	reference
ρ	specific density of PVC	1.343 (390 °K) 1.325 (420 °K) 1.317 (432 °K)	[98]
c	characteristic ratio of PVC	6.7	[97]
M_o	molecular weight of PVC monomer	62 gm/mole	calculated
l_o	length of a fully extended chain unit of a monomer	5.12 Å/2	[97]
l	length of a bond in the monomer	1.54 Å	[97]

Table 14 — Molecular parameters of PVC calculated based on G values obtained at different temperatures

Temperature	Me (g/mole)	le (Å)	d(Å)	λ_{max}
117 °C	3,645	151	43	3.51
147 °C	5,075	210	51	4.11
159 °C	6,480	268	58	4.62

Table 15 — Calculation of the characteristics of the entanglement network in PVC

molecular weight between entanglements:

$$M_e = \rho R T_A / G^o_N = \frac{1.343 \times 10^3 kg/m^3 \times 8.314 J/mole^o K \times 393^o K}{1.2 \times 10^6 N/m^2}$$
$$= 3645 \text{ gm/mole}$$

chain contour length between entanglements:

$$l_e = \frac{M_e \cdot l_o}{M_o} = \left(\frac{10970 gm/mole}{62 gm/mole} \right) \left(\frac{5.12 Å}{2} \right) = 151 Å$$

mesh size (end-to-end root mean square distance) between the entanglements:

$$d = (n c l^2)^{1/2} = [6.7 \times 2 \times \left(\frac{10970 gm/mole}{62 gm/mole} \right) \times (1.54 Å)^2]^{1/2}$$
$$= 75 Å$$

maximum extension ratio:

$$\lambda_{max} = l_e/d = 151 Å / 43 Å = 3.51$$

Table 16 — Molecular and craze parameters of different polymers [63]

Polymer	M_e (g/mol)	l_e (Å)	d (Å)	λ_{max}	λ_{craze}
poly(tert-butylstryrene)PTBS	43,400	600	125	4.8	7.2
poly(para-vinyltolunene)PVT	25,000	470	107	4.4	4.5
polystyrene PS	19,100	410	96	4.3	3.8
poly(styrene-maleic anhydride)PSMLA	19,200	400	101	4.0	4.2
poly(styrene-acrylonitrile)PSAN1	11,600	270	82	3.3	2.7
poly(methyl methacraylate) PMMA	9,150	190	73	2.6	2.0
poly(styrene-methyl mathacrylate)PSMMA	8,980	190	61	3.1	2.0
poly(styrene-acrylonitrile) PSAN2	6,380	180	67	2.7	2.0
poly(2,6-dimethyl-1,4-phenylene oxide) PPO(E)	4,300	165	55	3.0	2.6
poly(2,6-dimethyl-1,4-phenylene oxide) PPO(M)	7,400	284	72	3.9	2.6
polycarbonate PC	2,490	110	44	2.5	2.0

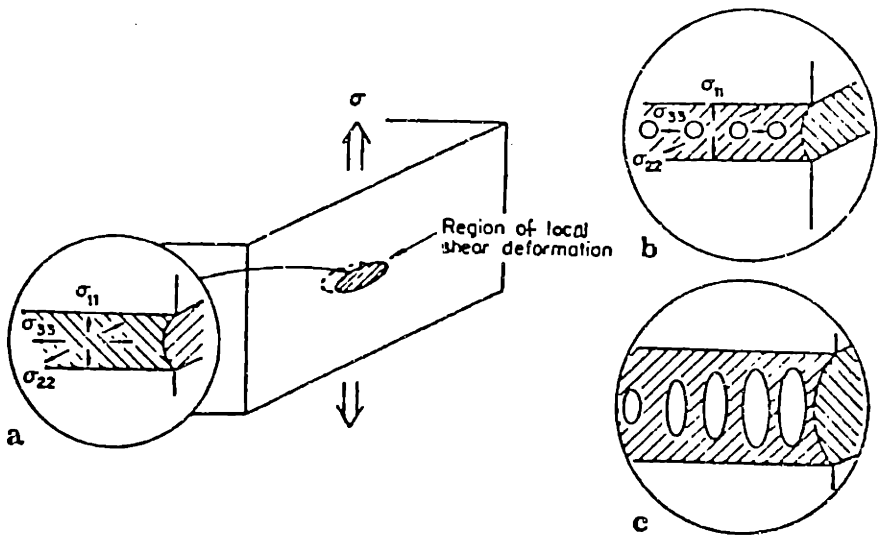

Fig. 1a—c. Schematic drawing of several postulated microscopic steps in craze nucleation: a Formation of a localized surface plastic zone and buildup of significant lateral stresses. b Nucleation of voids in the zone to relieve the triaxial constraints. c Further deformation of polymer ligaments between voids and coalescence of individual voids to form a void network (ref.49).

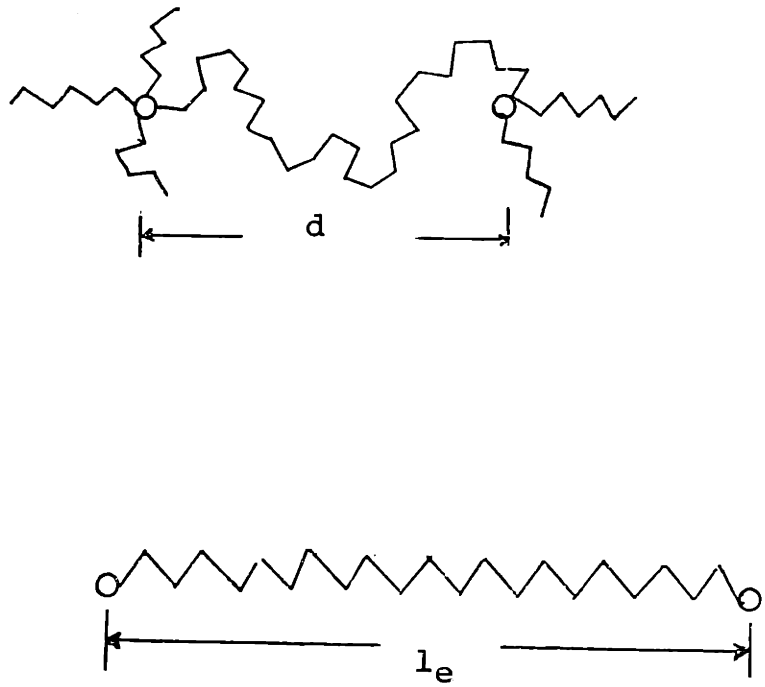

Figure 2. Idealized drawing of a polymer chain between entanglements in (a) the isotropic, undeformed state, and (b) the final strain-hardened state.

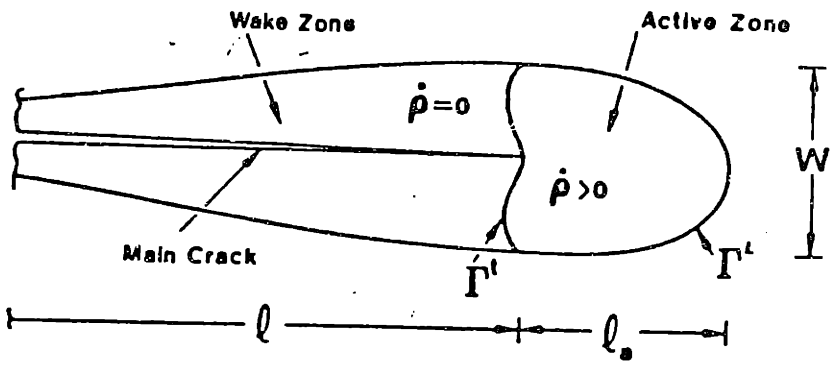

FIG. 3 A schematic illustrating characteristics of the crack layer, the active zone, and related parameters ref. (71).

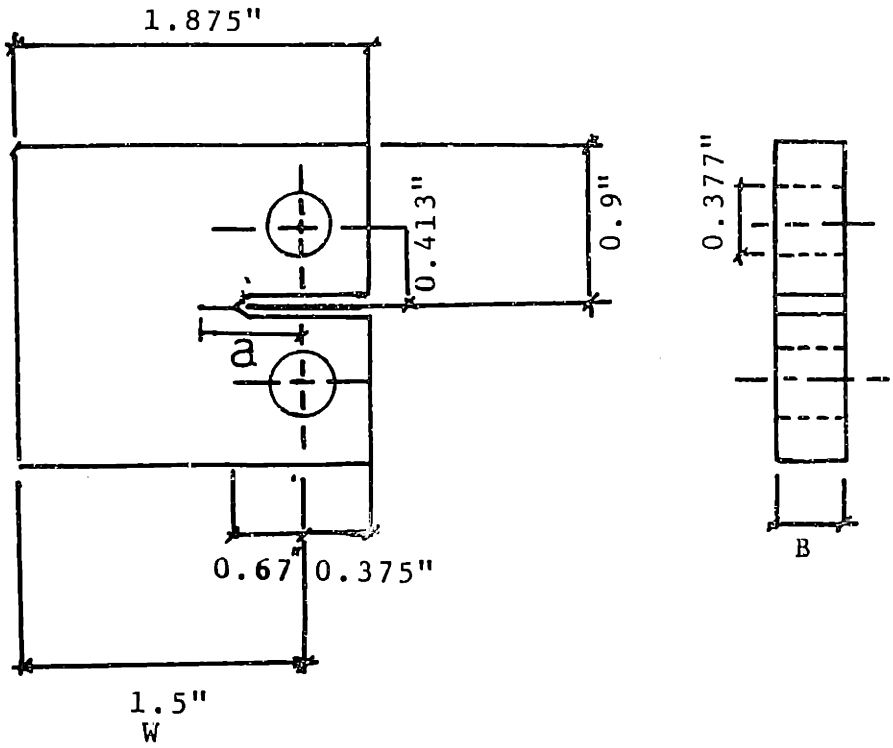

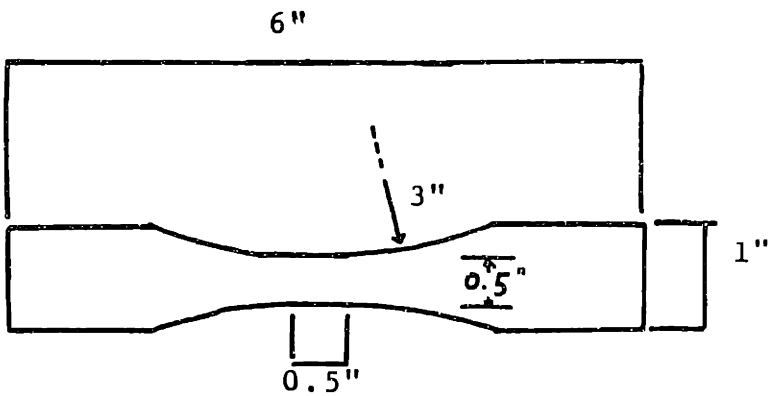

FIGURE 4

a) CT SPECIMEN GEOMETRY UNDER ASTM E 399-81
b) TENSILE SPECIMEN GEOMETRY

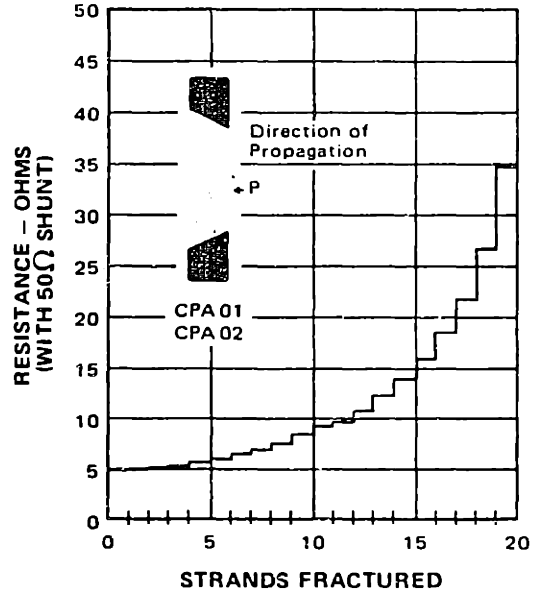

Figure 5a Resistance vs. strands fractured chart of the crack propagation gage.

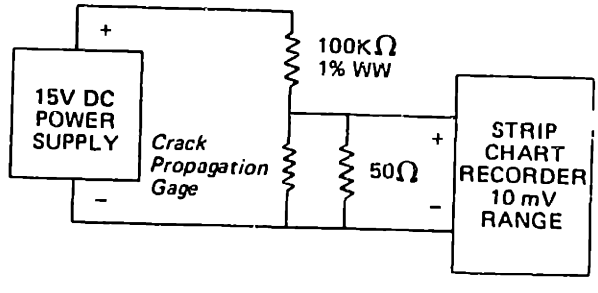

Figure 5b. Schematic presentation of the circuitry used in measuring the change of resistance during crack propagation.

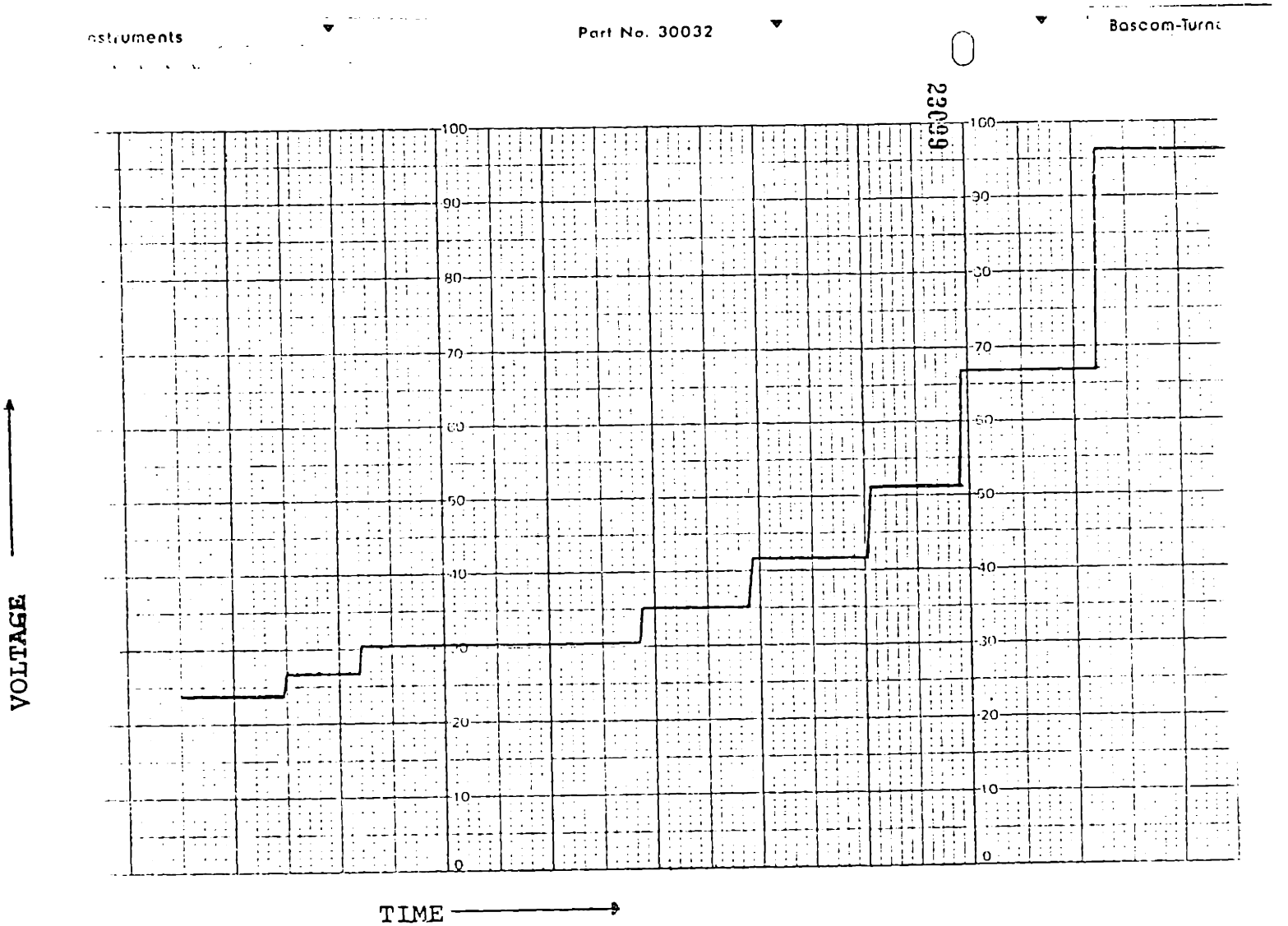

Figure 6. A typical recording of voltage vs. time for the breakage of the strands

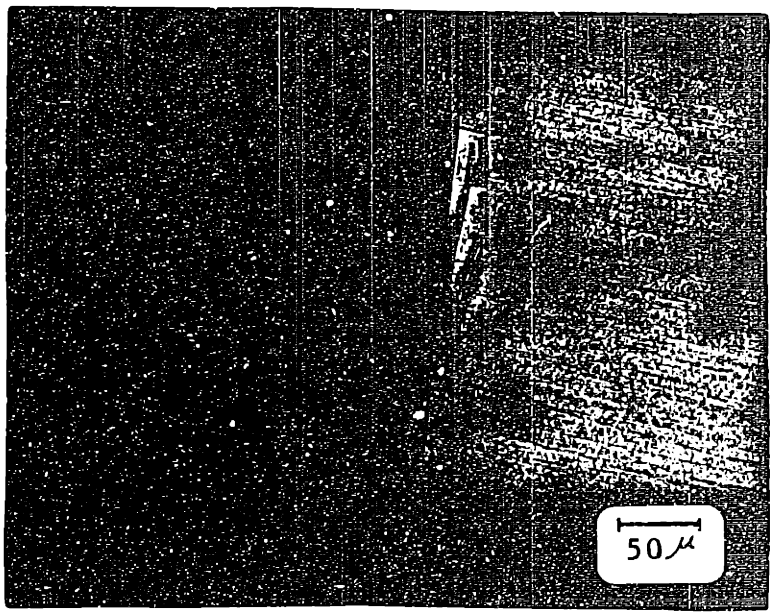

Figure 7 Crack tip of PVC showing distinct multiple crazes; loaded to 62% of K_Q.

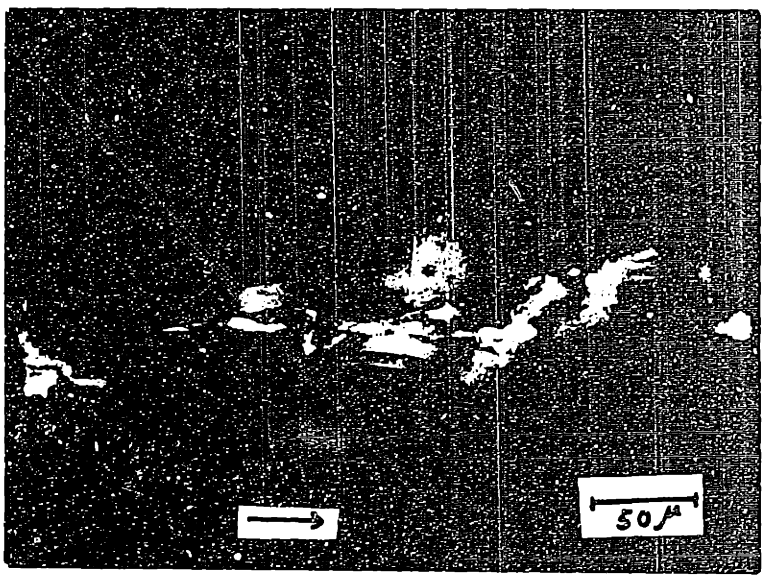

Figure 8 Optical micrograph of the multiple crazes along the main crack in a $CaCO_3$ (3% by weight) filled PVC. The specimen was loaded and polished without further treatment.

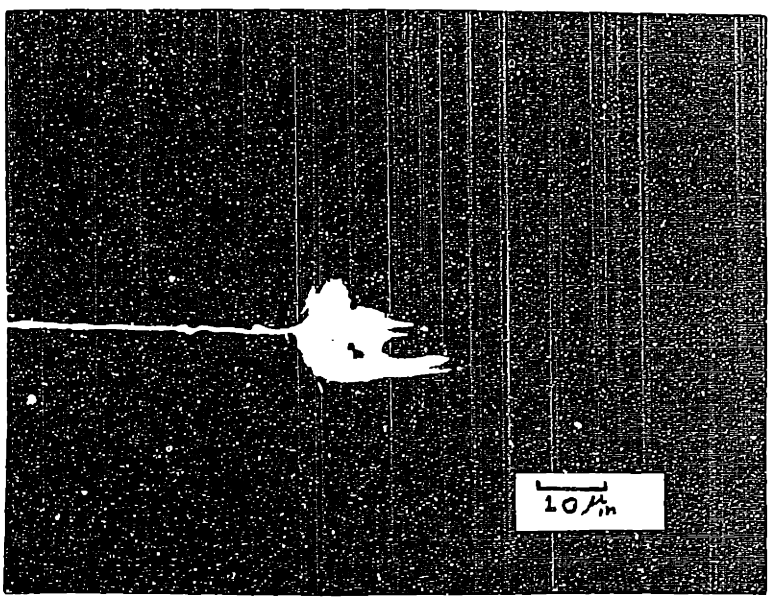

Figure 9 Optical micrograph showing shear yielding on the surface of a pure PVC CT specimen.

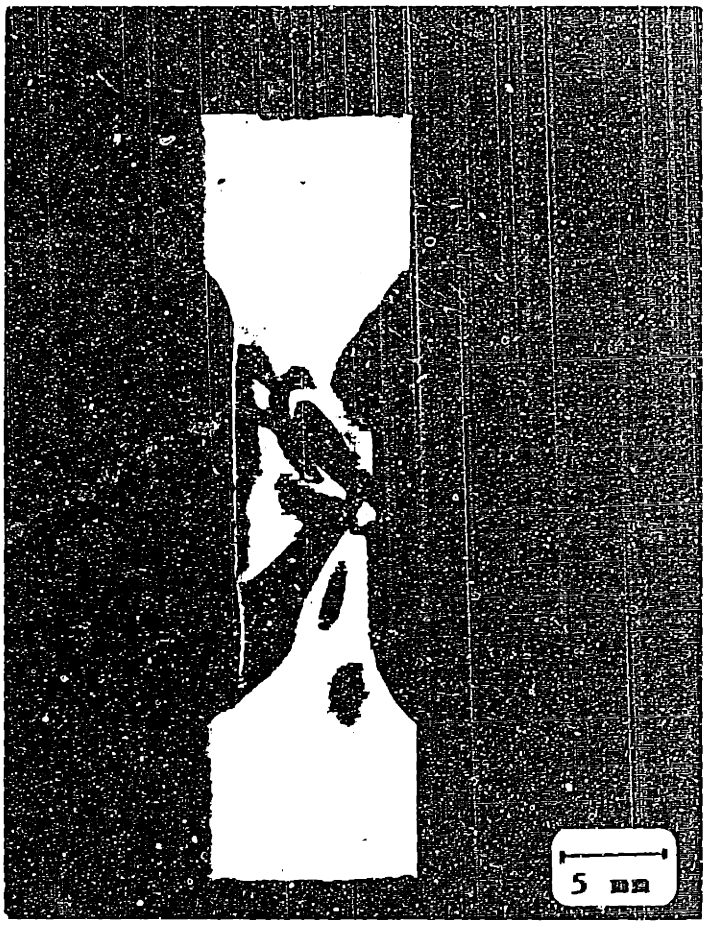

Figure 10. Optical micrograph of a compression specimen of pure PVC, showing the formation of shear bands.

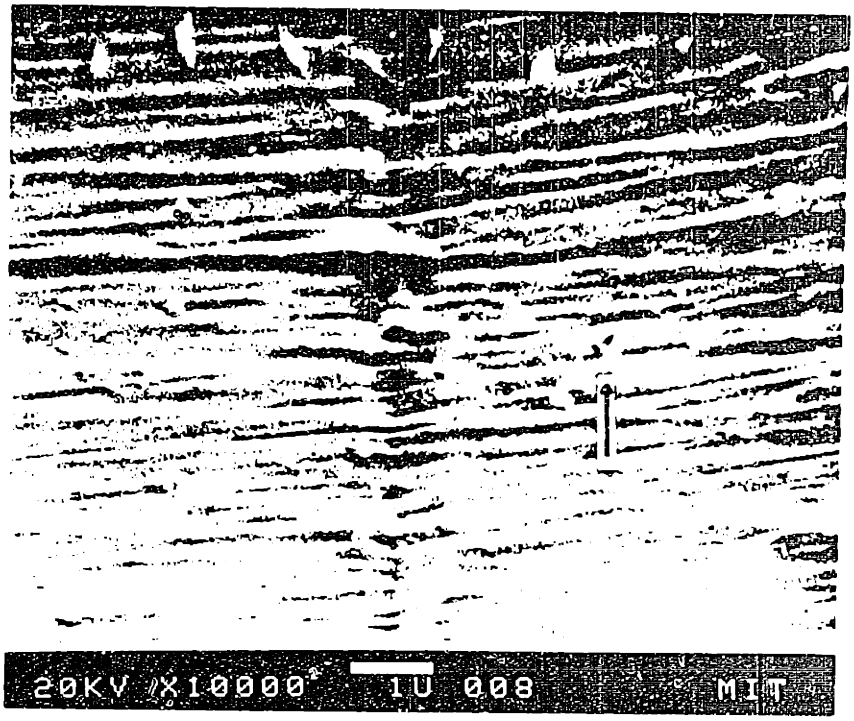

Figure 11. SEM micrograph of a craze line in a pure PVC specimen which received no surface treatment after polishing.

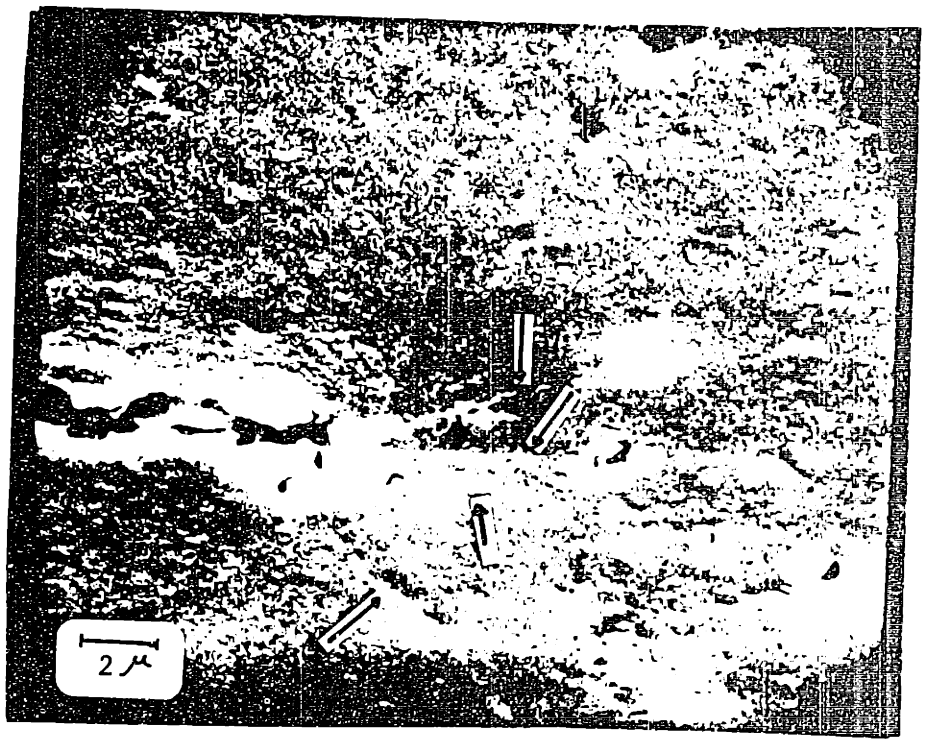

Figure 12. SEM micrograph of a crack tip of PVC pipe specimen shows some fine lines present at the crack tip.

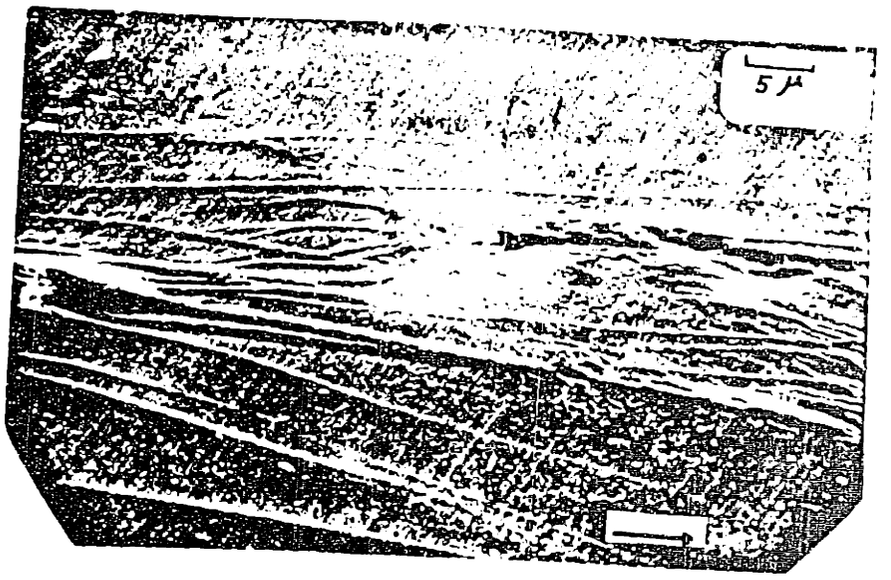

Figure 13 . Morphology of the crazes in a pure PVC specimen which was immersed in xylene for three minutes.

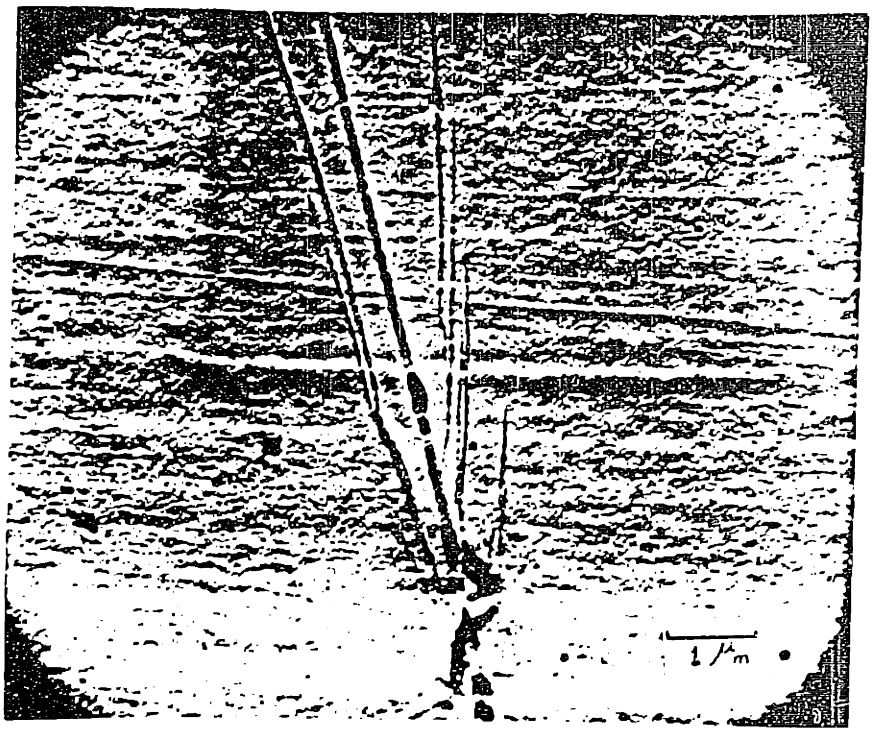

Figure 14 SEM micrograph of the morphology of multiple crazes at the crack tip of the pure PVC specimen, which was plasma etched in O_2 under the conditions of 50 watts and 0.3torr for 2.5 minutes.

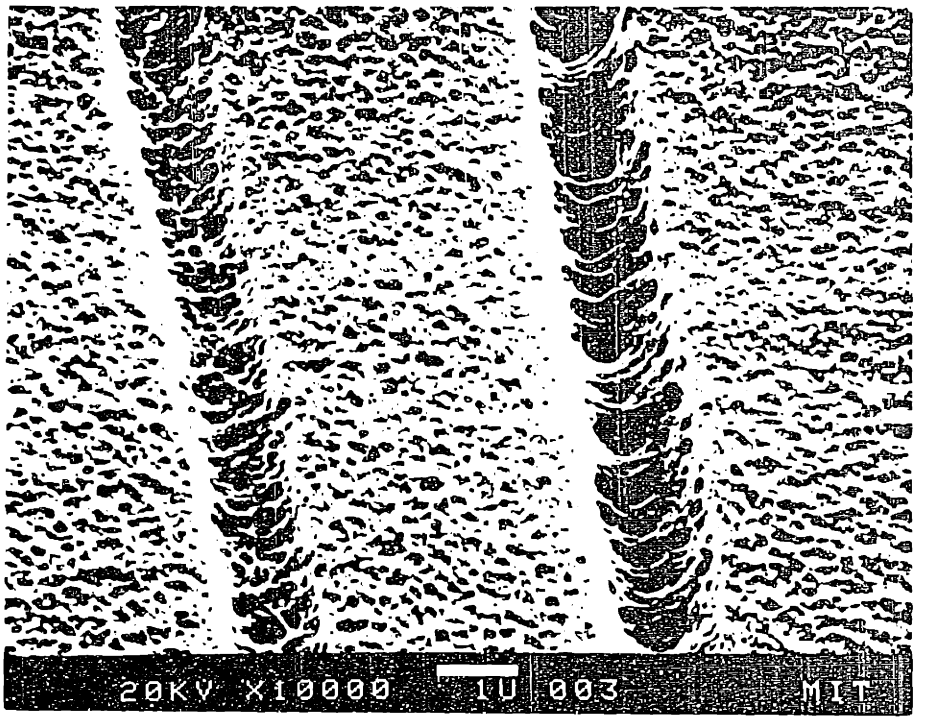

Figure 15 SEM micrograph of the morphology of crazes in pure PVC. The specimen was plasma etched in oxygen under the conditions of 50 watt and 0.5 torr for 2 minutes after loading, sectioning, and polishing.

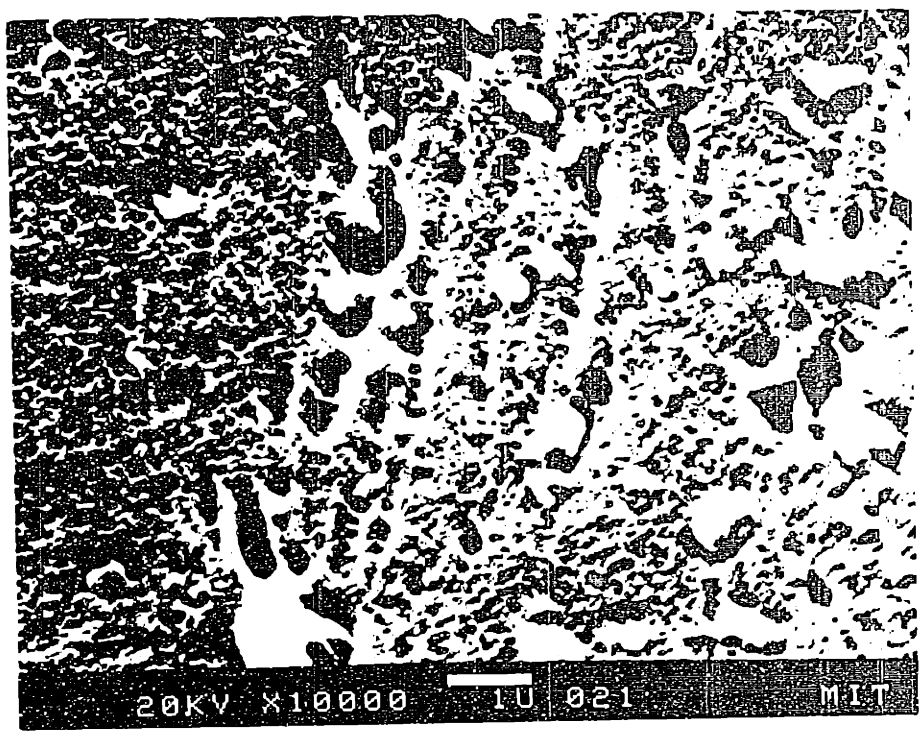

Figure 16 SEM micrograph of the morphology of the crazes in a PVC pipe specimen. The specimen was plasma etched in oxygen under the conditions of 50 watts, o.5 torr for 1 1/2 minutes after loading, sectioning, polishing.

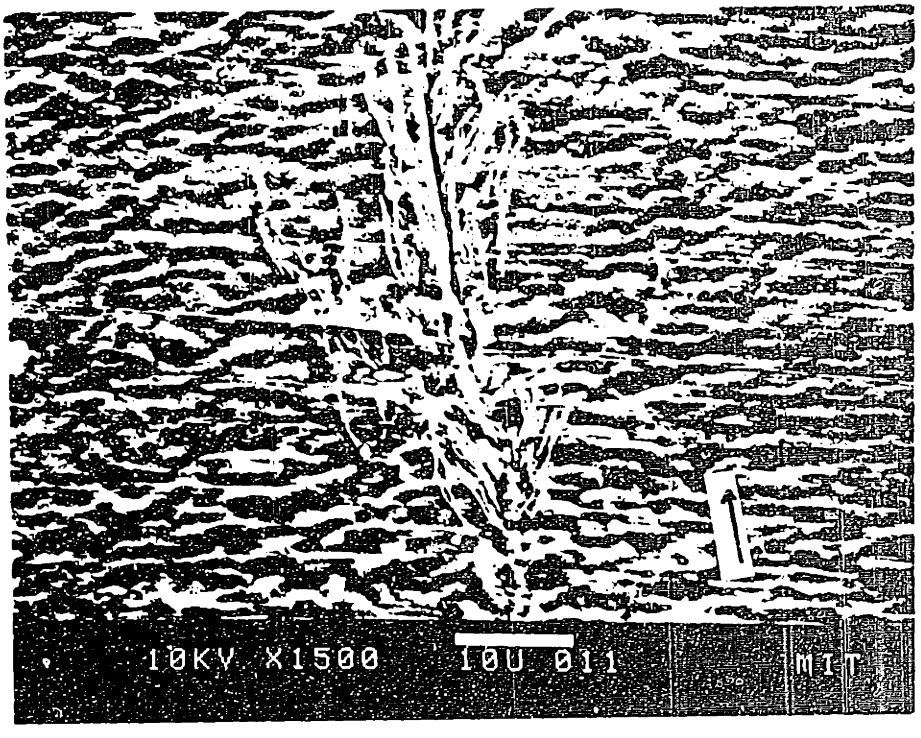

Figure 17 SEM micrograph of a crack and multiple crazes in a PVC pipe specimen. The specimen was plasma etched in air under the conditions of 100 watts and 0.5 torr for 2 minutes after loading, sectioning, polishing.

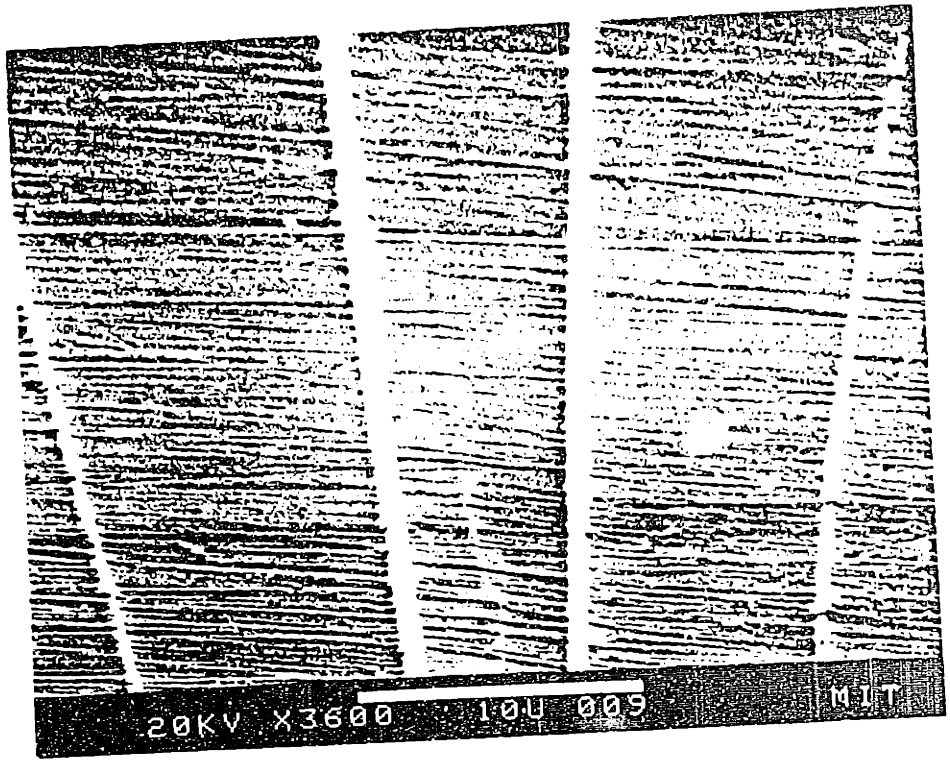

Figure 18 SEM micrograph of the crazes in a pure PVC specimen. The specimen was heated to a temperature above T_g for half hour after loading, sectioning, and polishing.

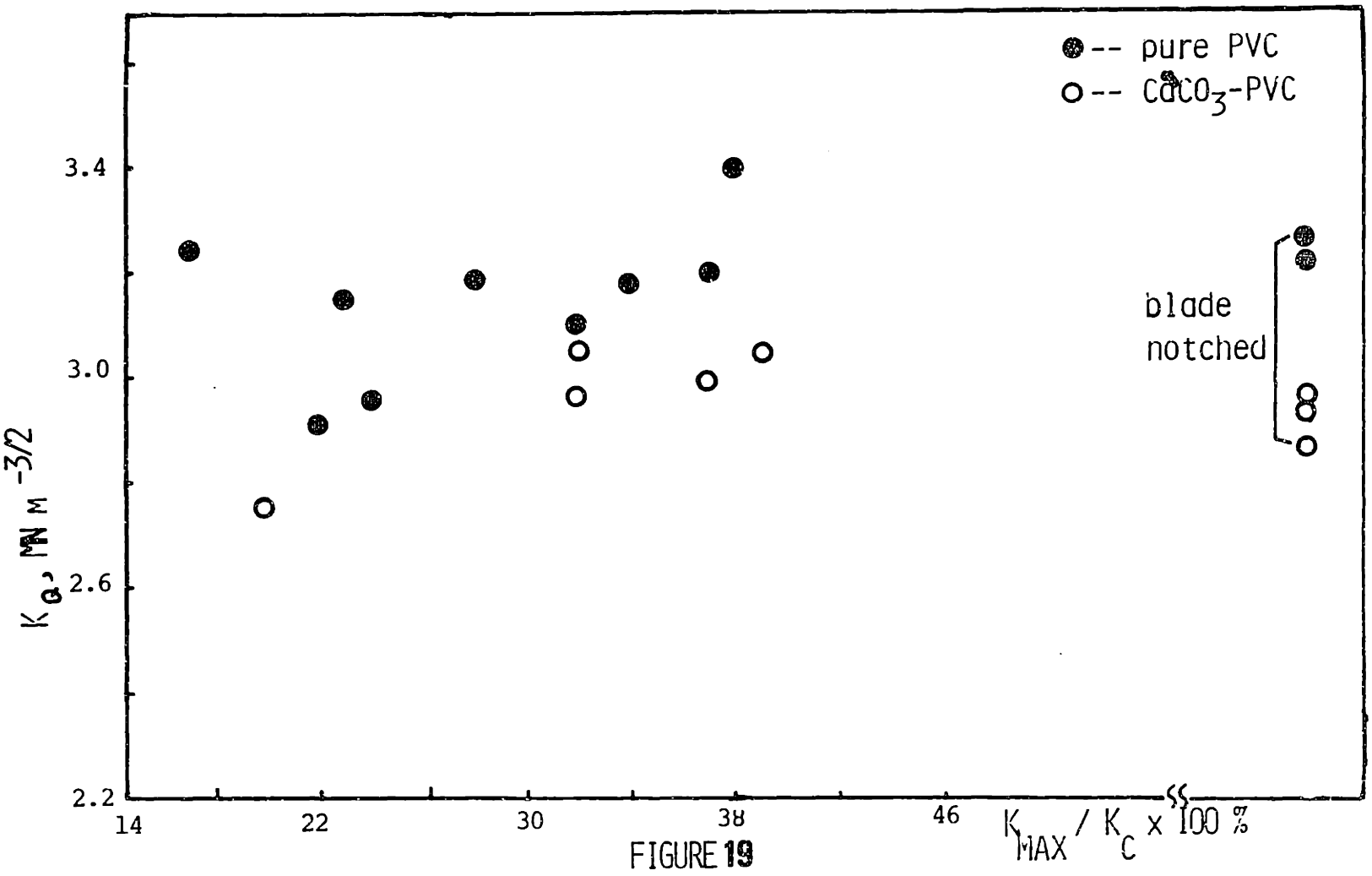

FIGURE 19

FRACTURE TOUGHNESS VS. THE PERCENTAGE OF K_C USED IN GENERATING FATIGUE CRACK.

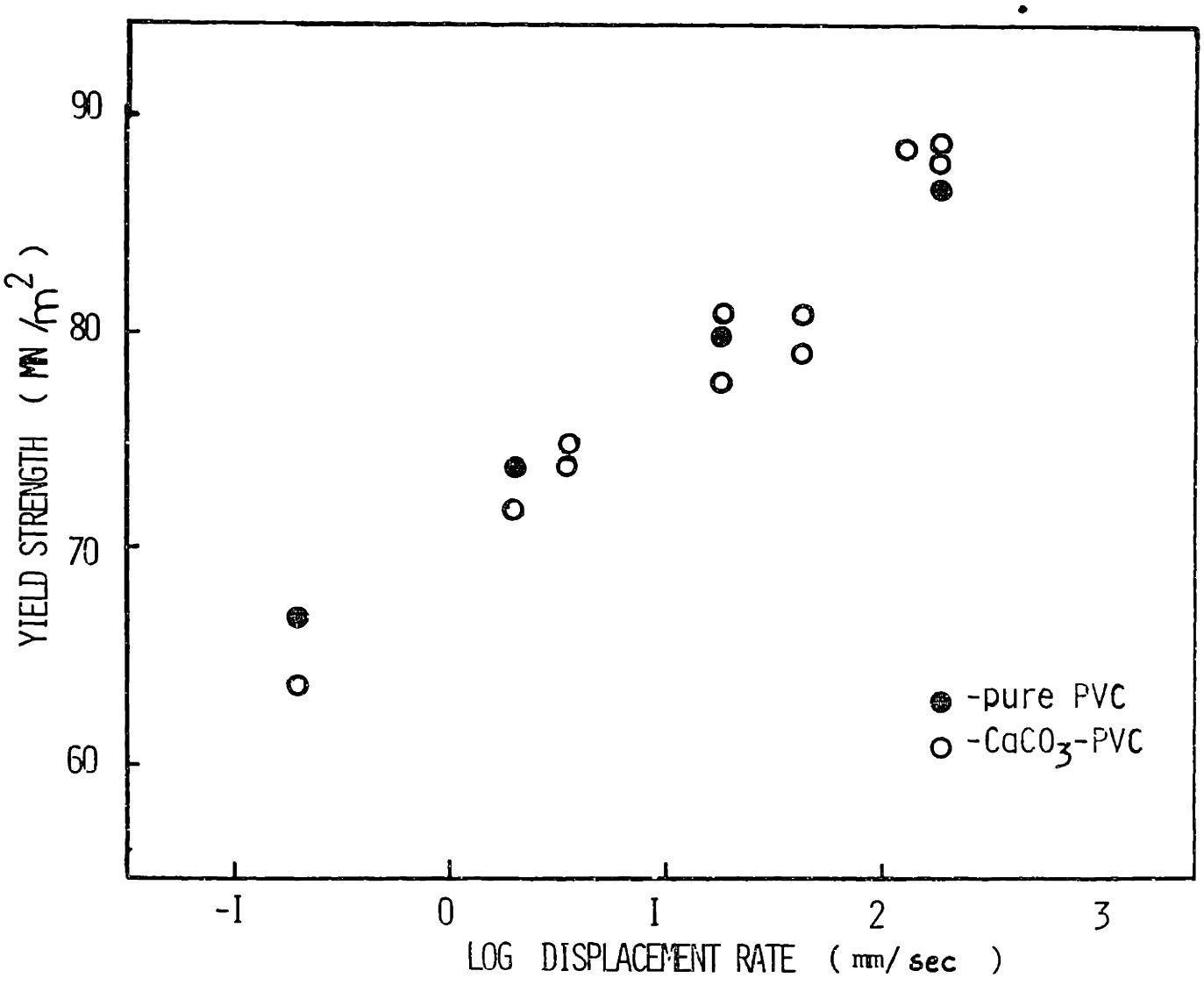

FIGURE 20

YIELD STRENGTH VS. LOG DISPLACEMENT RATE FOR PURE PVC AND $CaCO_3$-PVC MATERIALS.

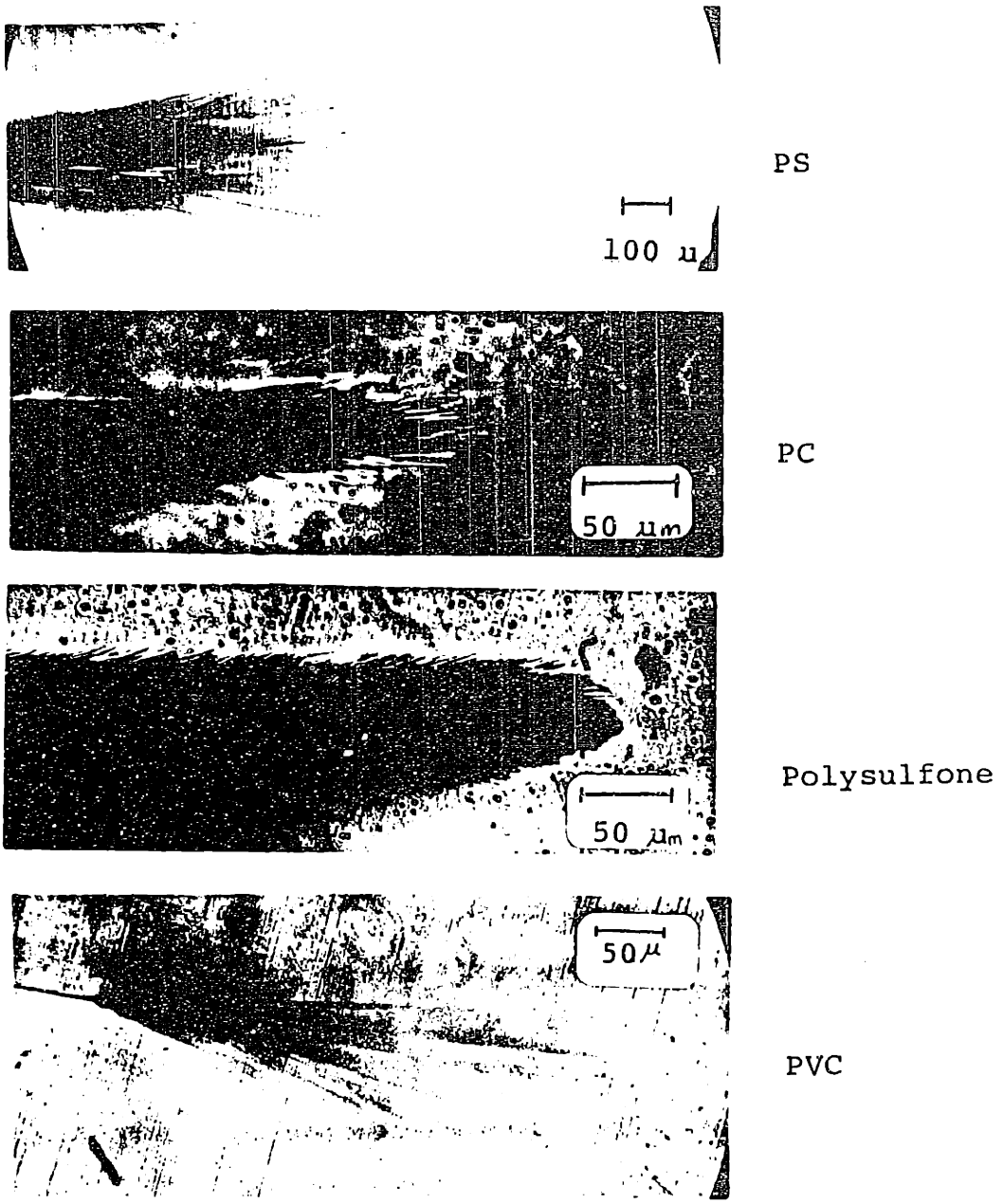

Figure 21 The morphology of the multiple crazes at the crack tips of several polymers.

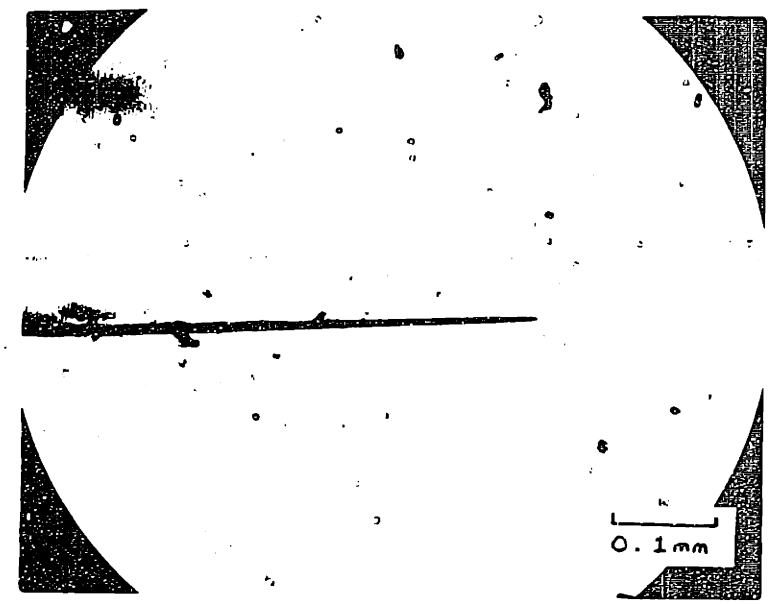

Figure 22 The morphology of the single craze at the crack tip of PMMA.

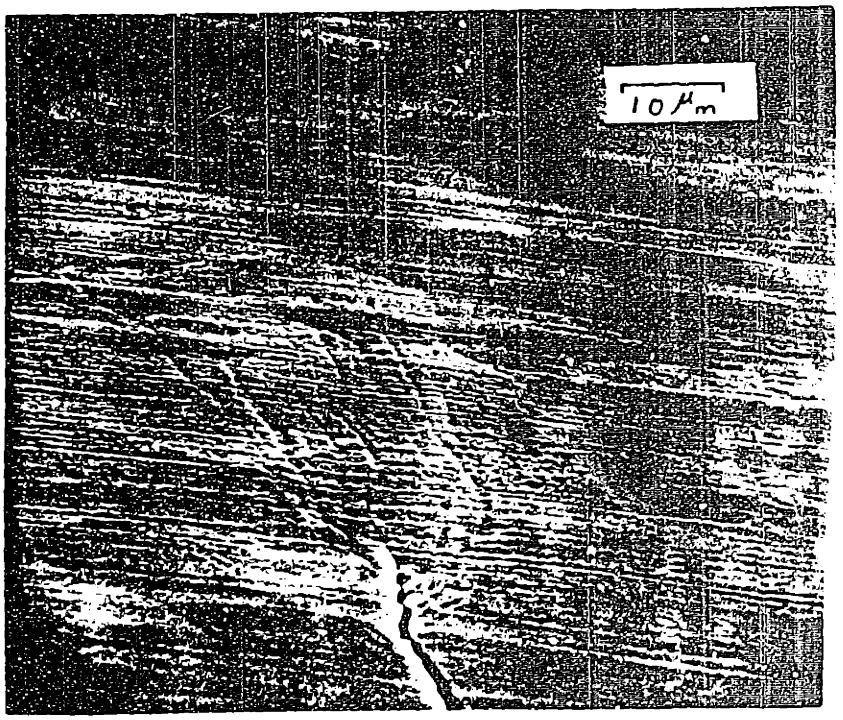

Figure 23 SEM micrograph of the morphology of the yield zone at the crack tip in nylon 66 specimen, loaded to 92% K_c at a loading rate of 500 lob/sec. The specimen was plasma etched in O_2, under the conditions of 500 watts and 0.5 torr for 5 minutes.

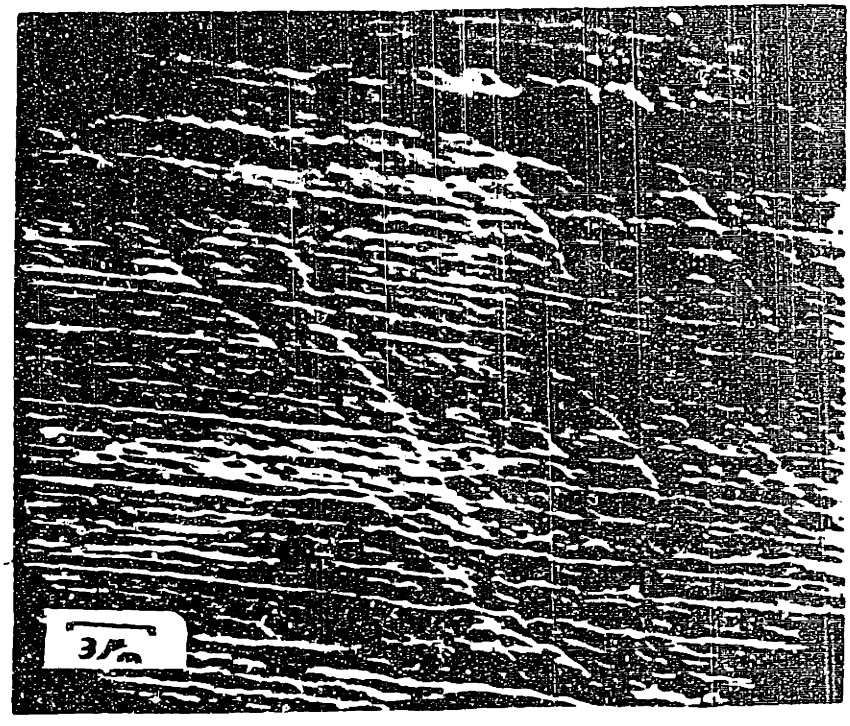

Figure24 SEM micrograph of the craze morphology in nylon 66. The specimen was plasma etched in O_2 under the conditions of 50 watts and 0.5 torr for 5 minutes.

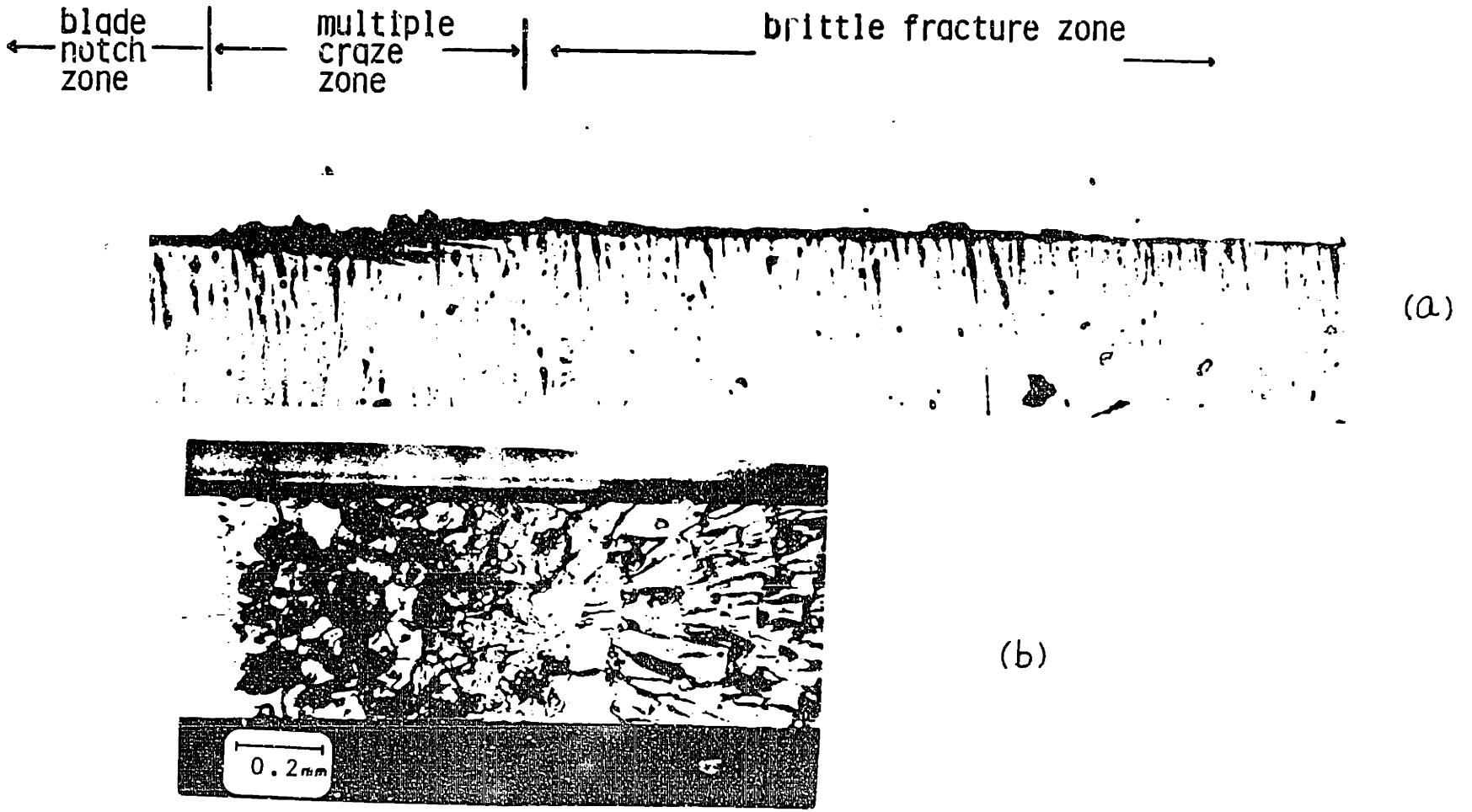

Figure 25. a) Side-view of a fractured piece of pure PVC
b) Top-view of the fracture surface of the same piece.

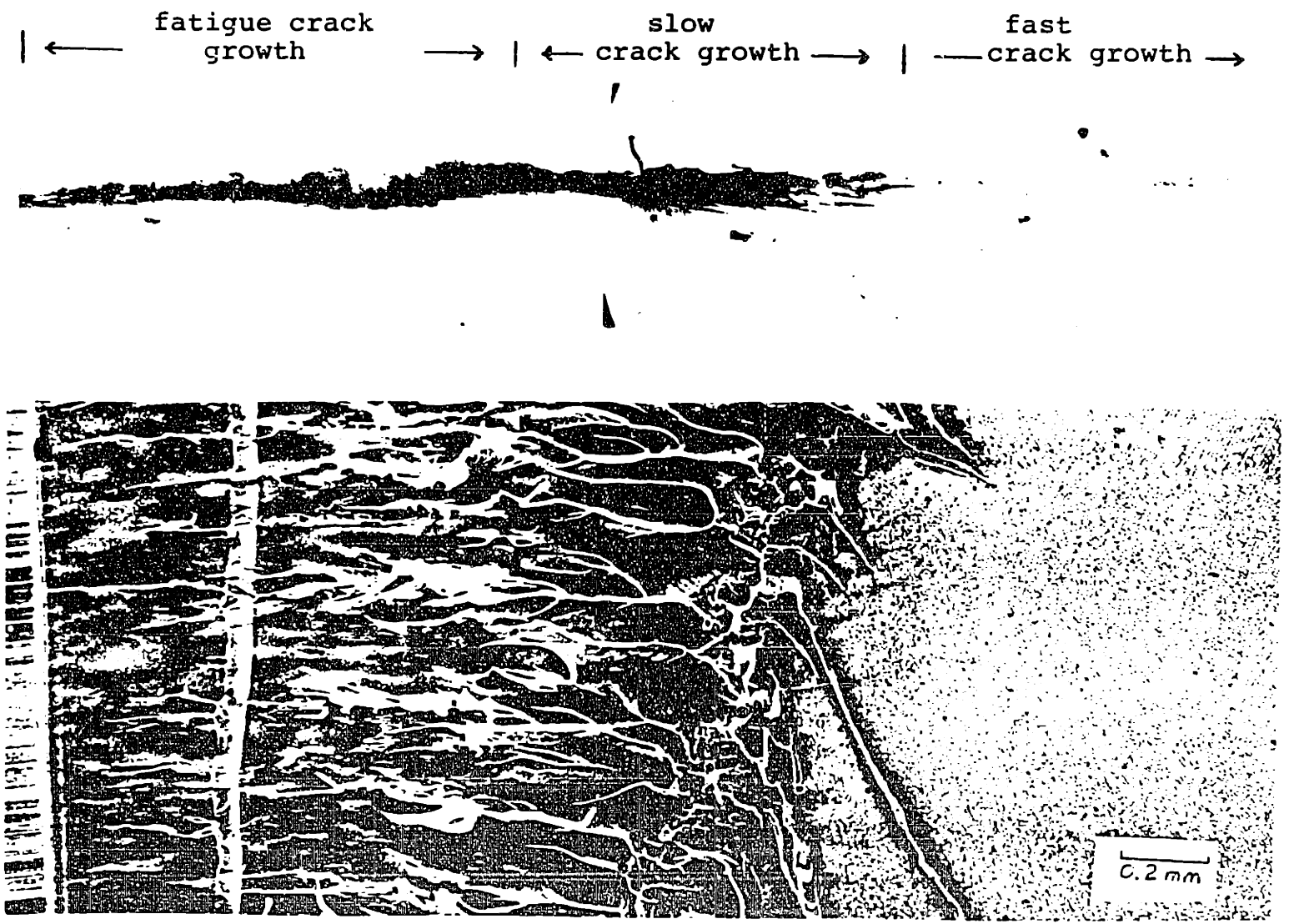

Figure 26 Top: side-view of a fractured piece of polycarbonate
Bottom: top-view of the fracture surface of the same piece.

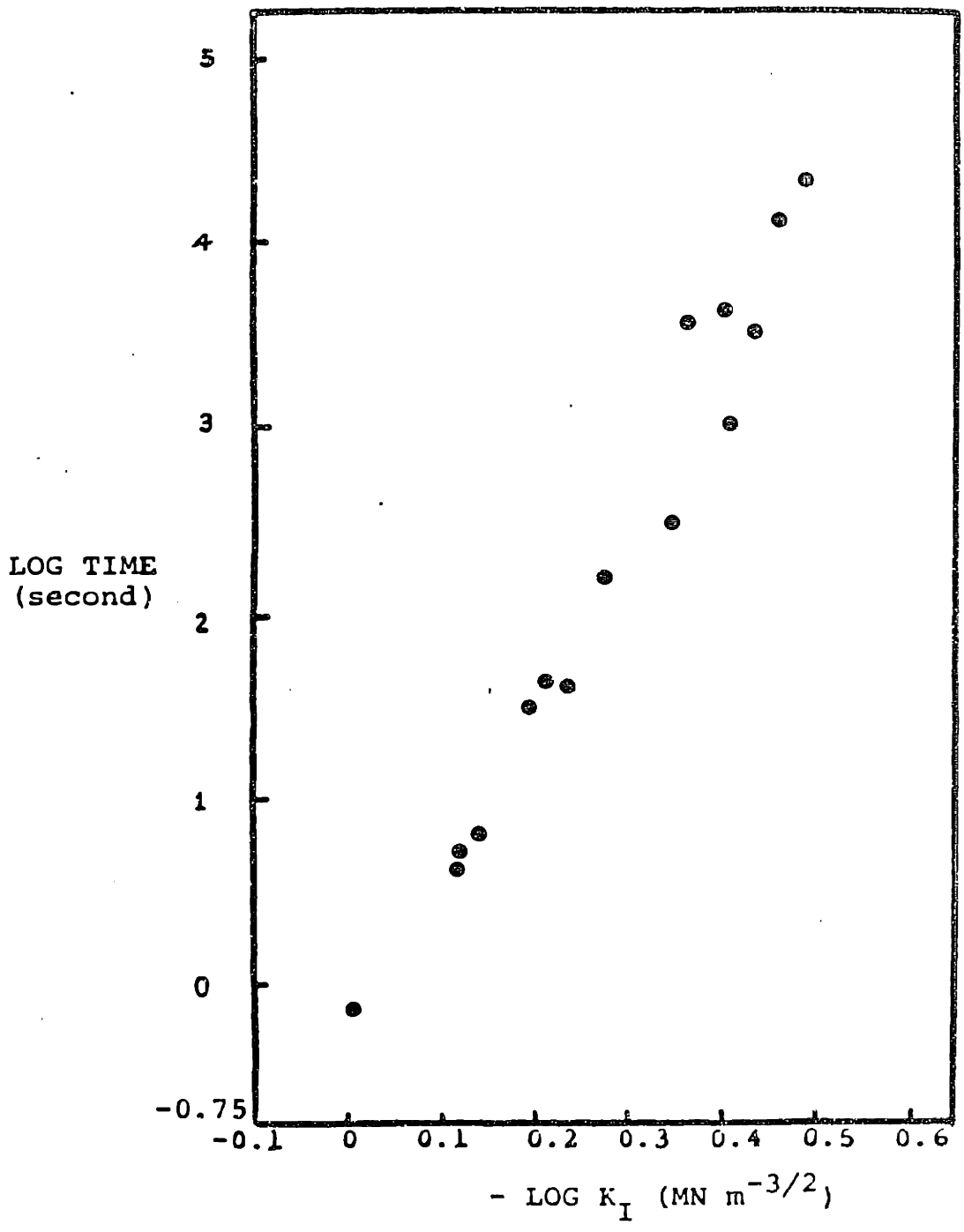

Figure 27 Craze initiation time verses the applied load in pure PVC.

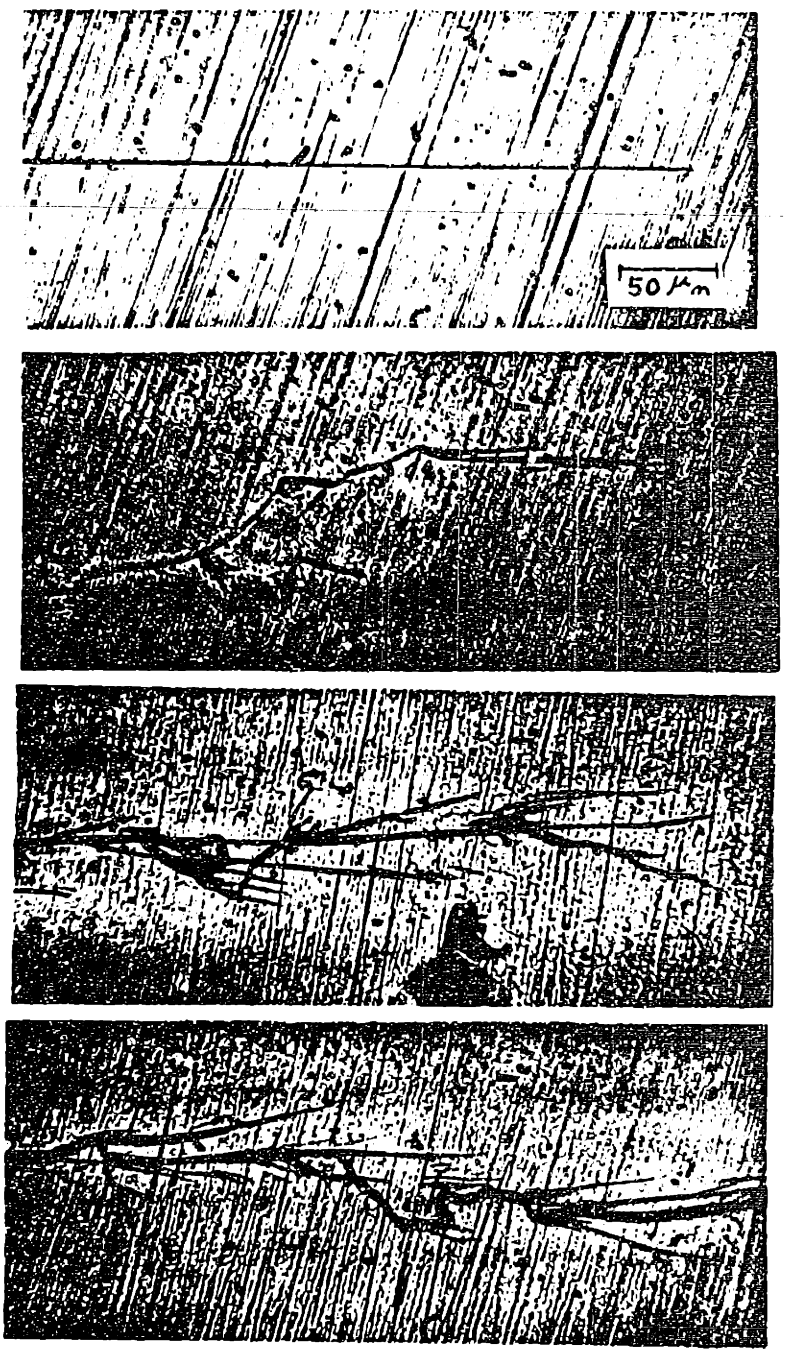

Figure 28 Effect of the load on the formation of multiple crazes during fatigue crack growth.

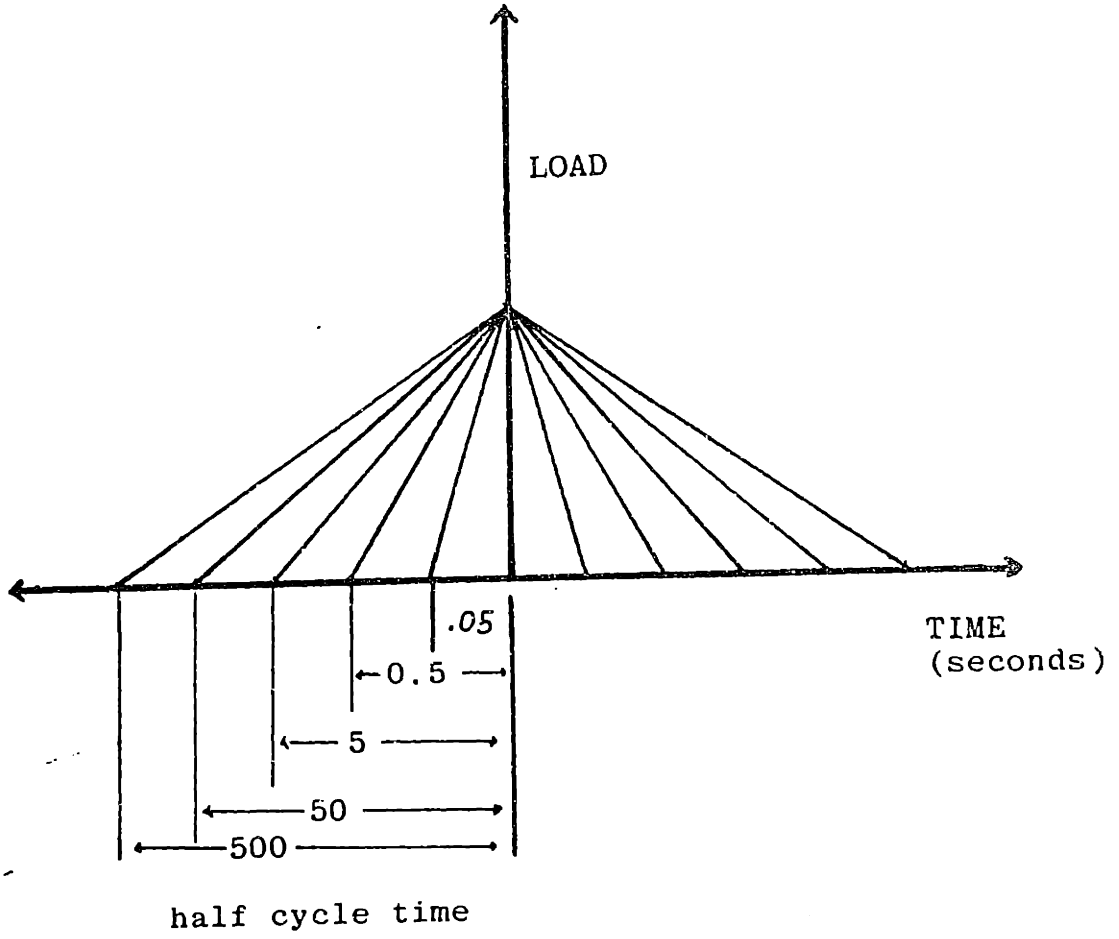

Figure 29 Scheme for testing the effect of time on the growth of crazes.

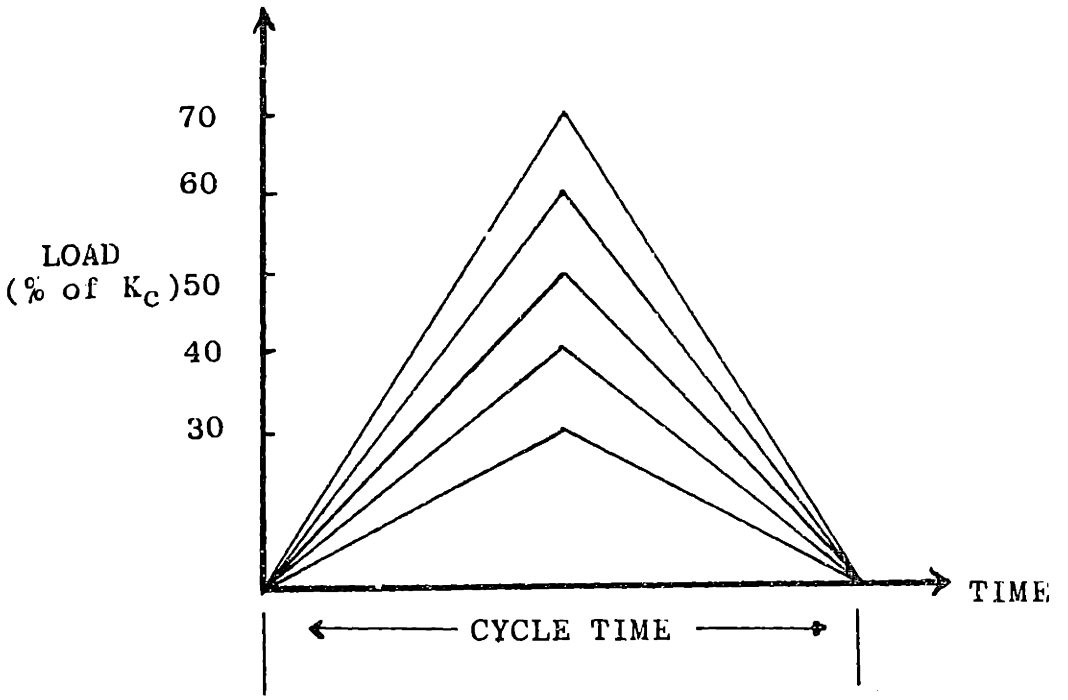

Figure30 Scheme for testing the effect of load on the growth of crazes.

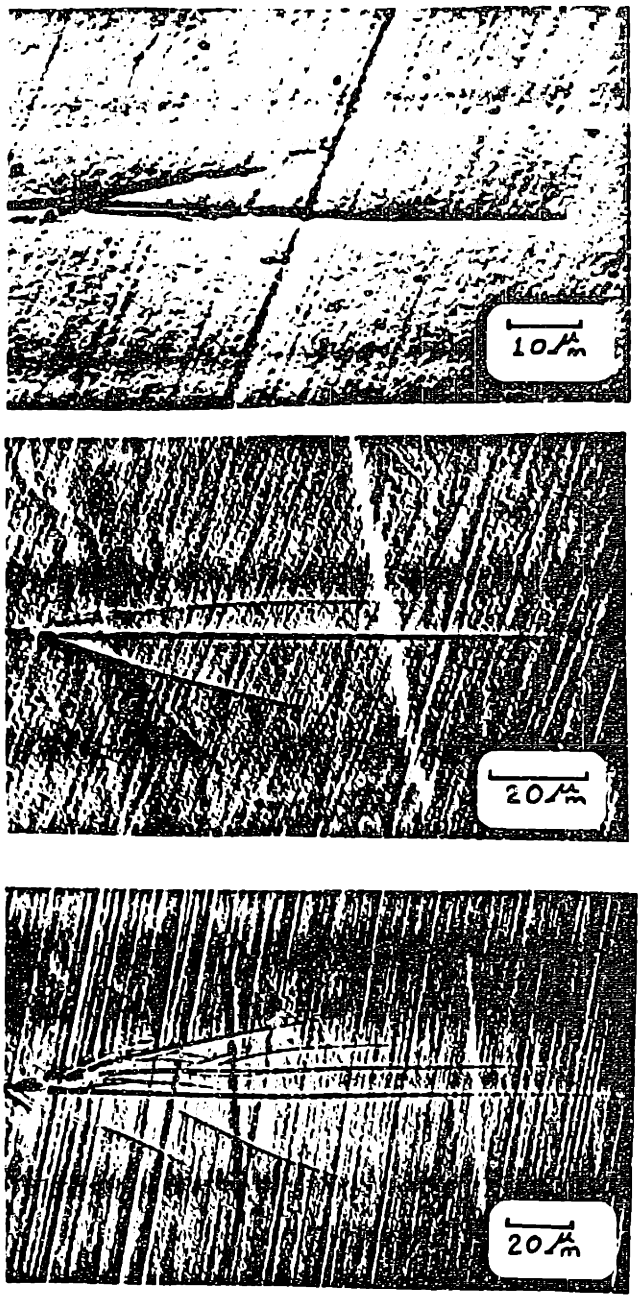

K_I ($MN/m^{3/2}$)

0.93

1.28

1.57

Figure31 Effect of load on the growth of crazes at a loading rate ~ 1 lb/sec.

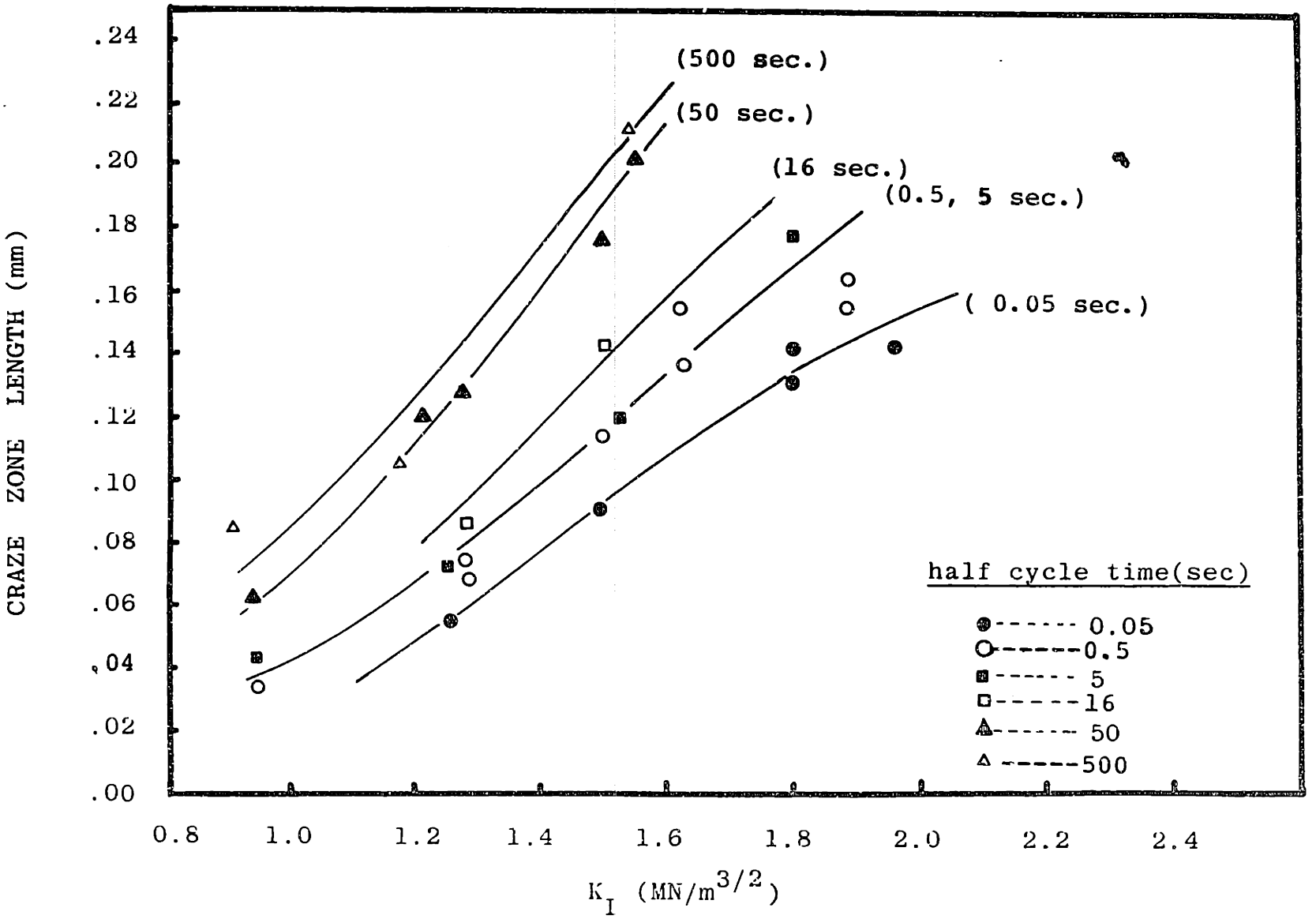

Figure 32 The effects of time and load on the growth of the crazes.

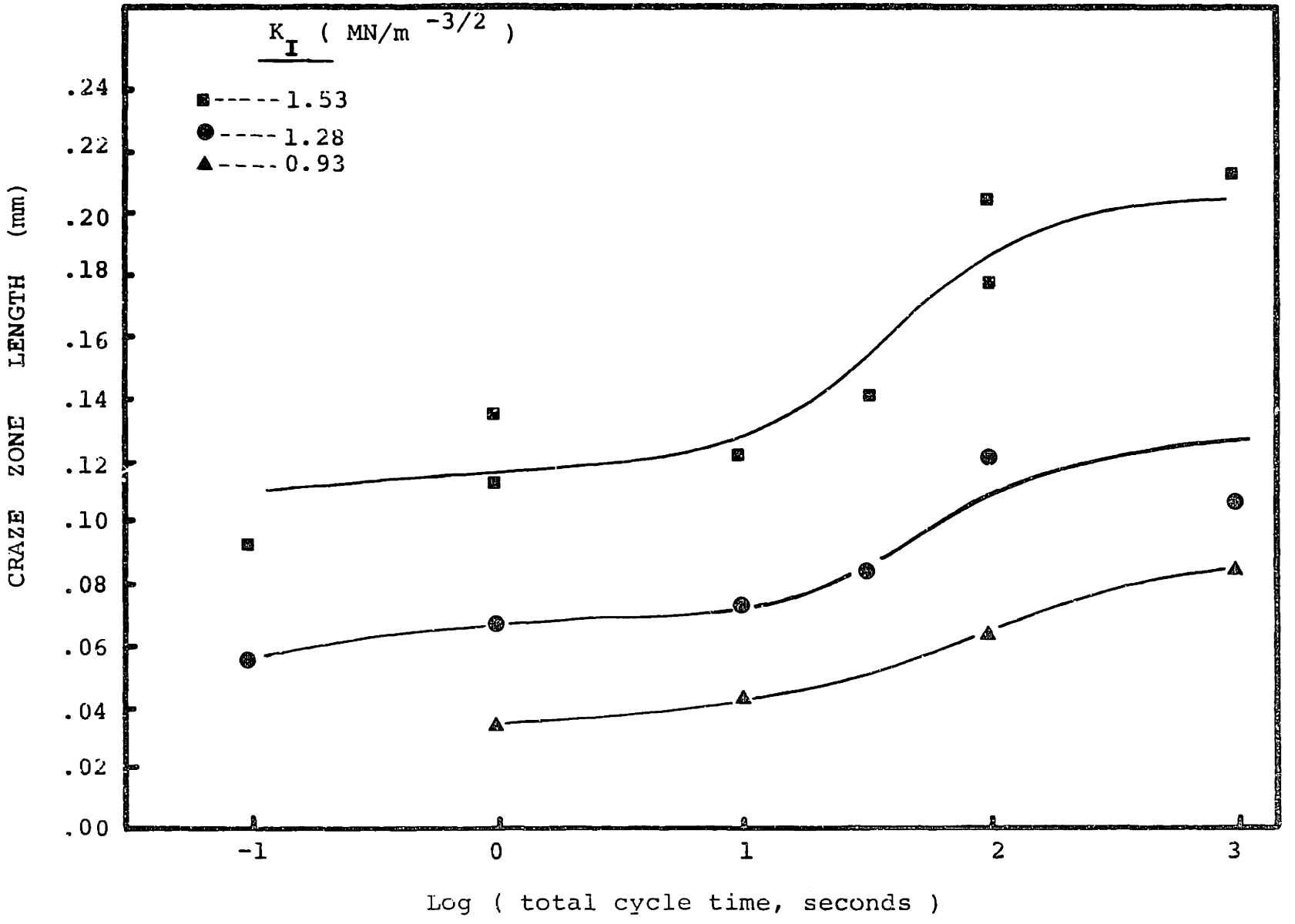

Figure 33. Craze zone length vs. the total cycle time.

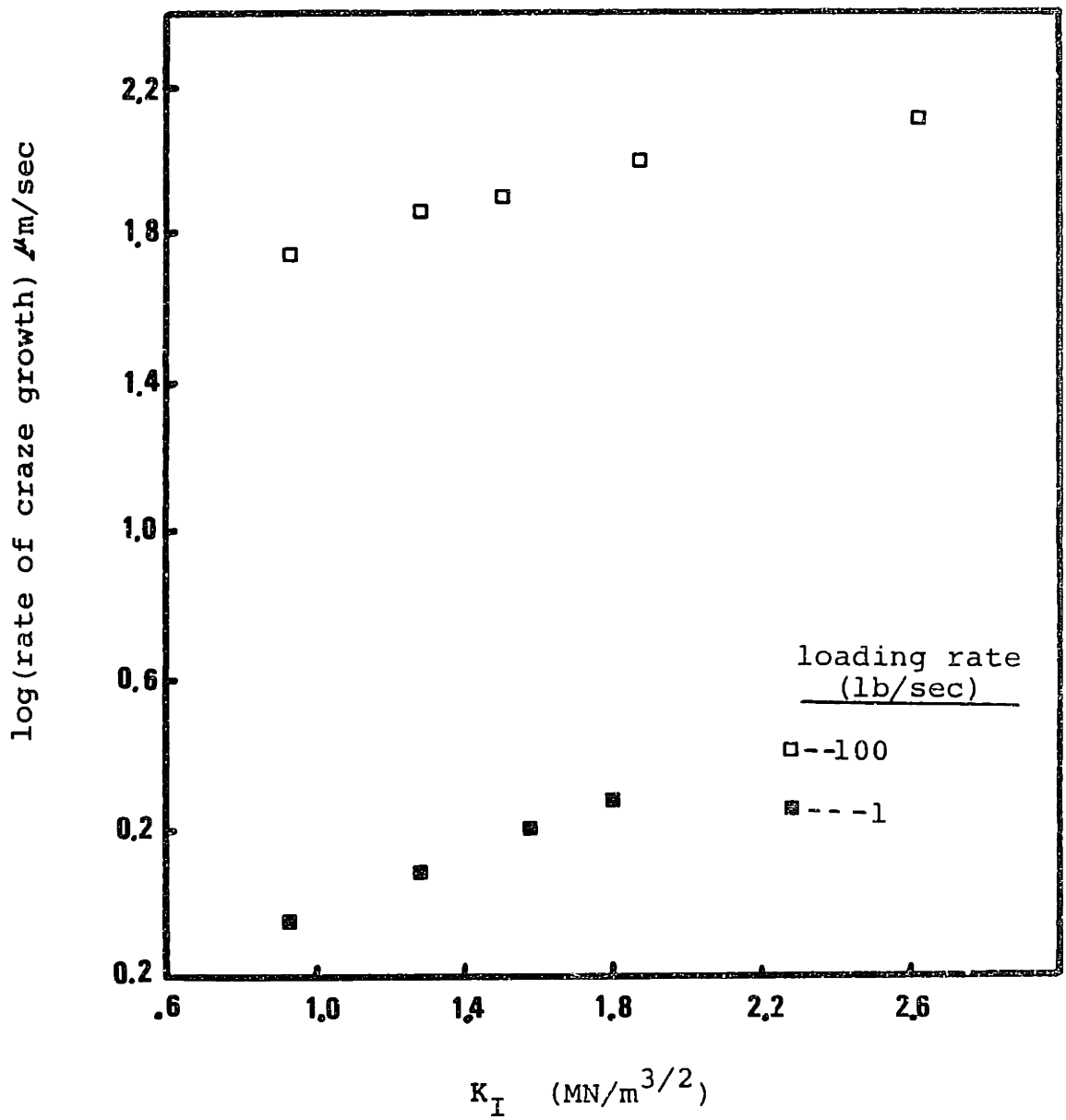

Figure 34 . Effect of loading rate on the rate of craze growth as a function of K_I.

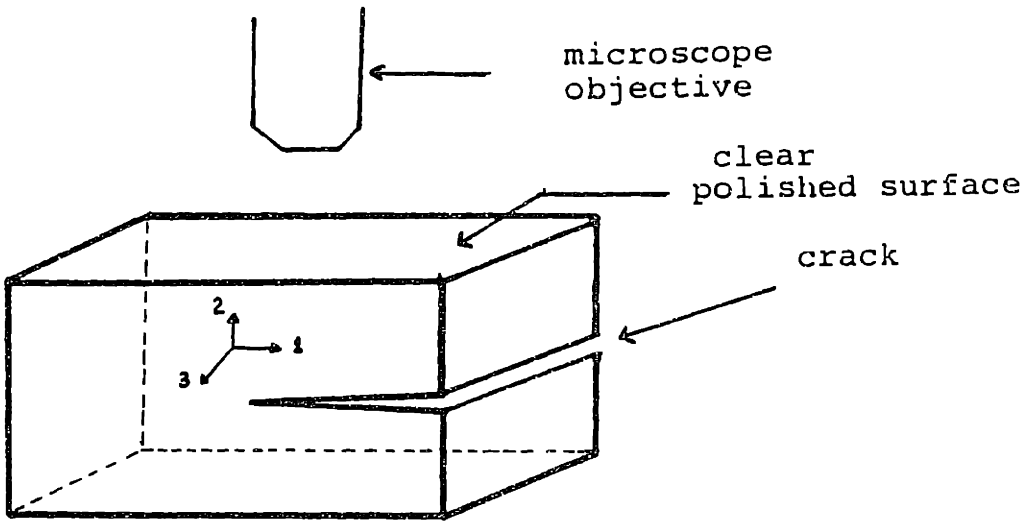

Figure35 set-up for observing the interference fringes at the crack tip.

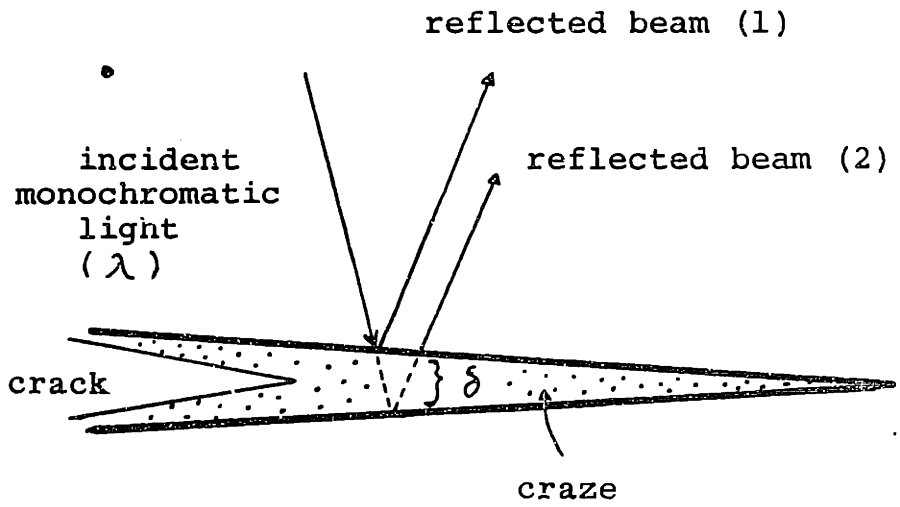

$$\text{for bright fringes: } \delta = \frac{(f+1/2)\lambda}{2\mu} \qquad f=0,1,2\ldots$$

$$\text{for dark fringes: } \delta = \frac{f\lambda}{2\mu} \qquad f=1,2,3\ldots$$

Figure 36 Schematic of the light paths which give rise to the interference patterns of the craze.

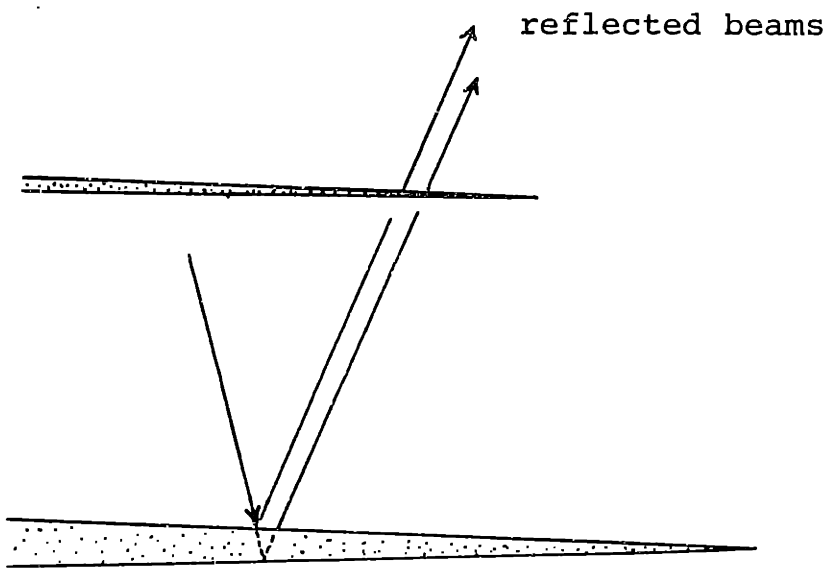

Figure 37. Schematic of the light beams passing through two crazes relatively parallel to each other.

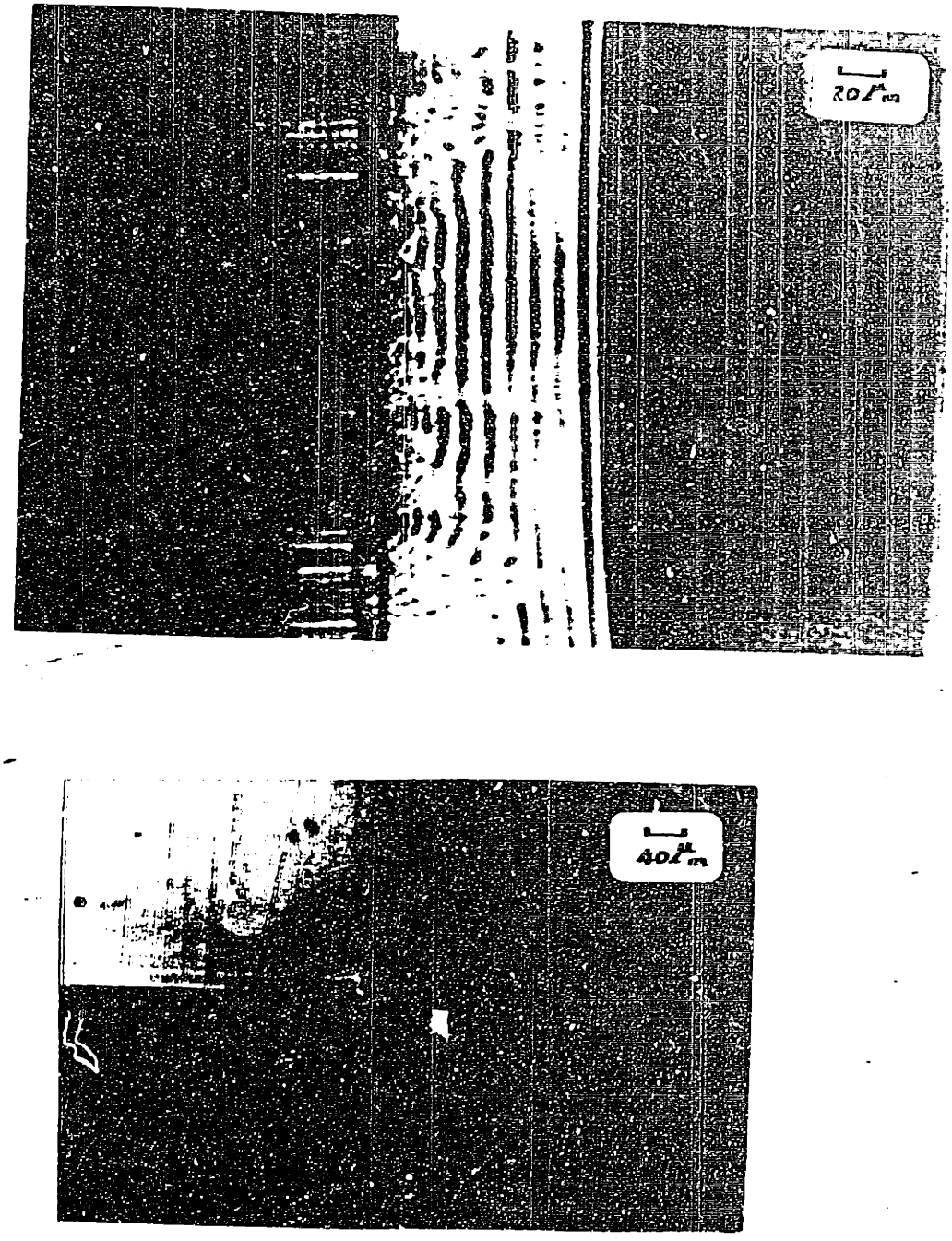

Figure 38. Optical micrographs of the fringe pattern (top) and the side view (bottom) of the craze zone ahead of a notch tip in a specimen previously loaded to 47% K_Q.

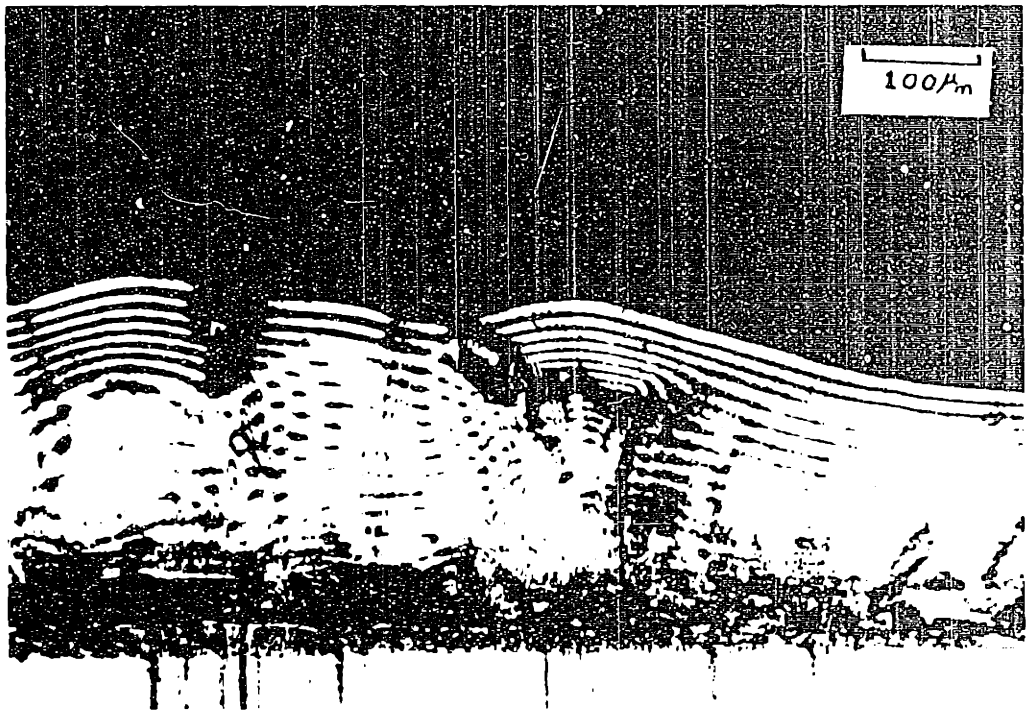

Figure 39 Interference fringes of loaded crack and craze in pure PVC. The specimen was loaded to 2.62MN $m^{-3/2}$ ($\sim 66\%$ K_Q) at a loading rate of 100 lb/sec prior to the interference experiment.

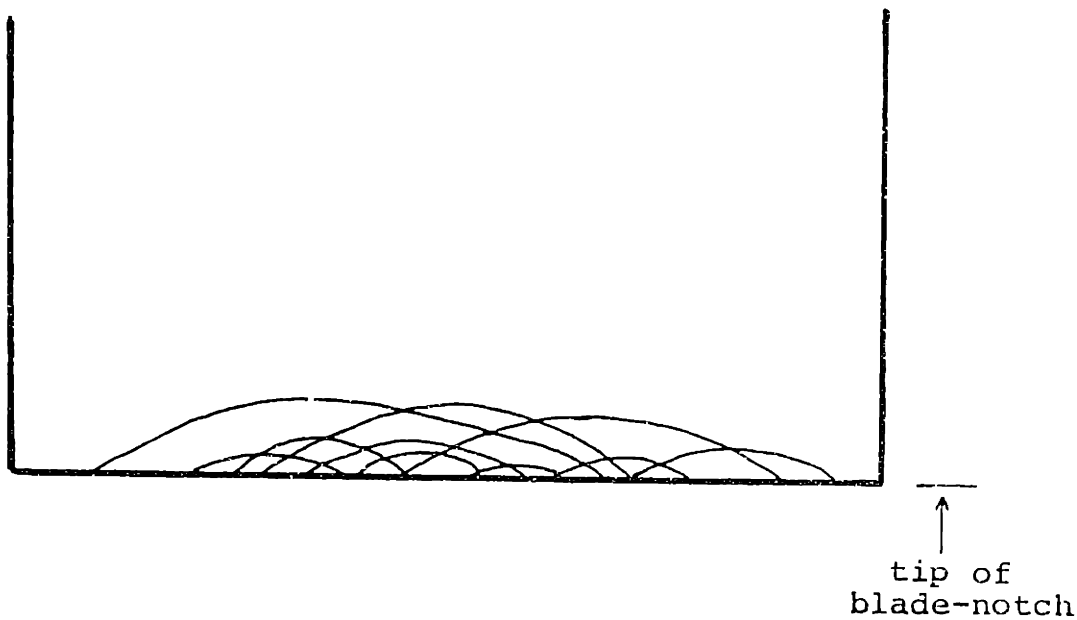

Figure 40. Schematic of the growth pattern of crazes at the tip of a blade-notch in a PVC specimen. The size of the crazes are exaggerated relative to the specimen size.

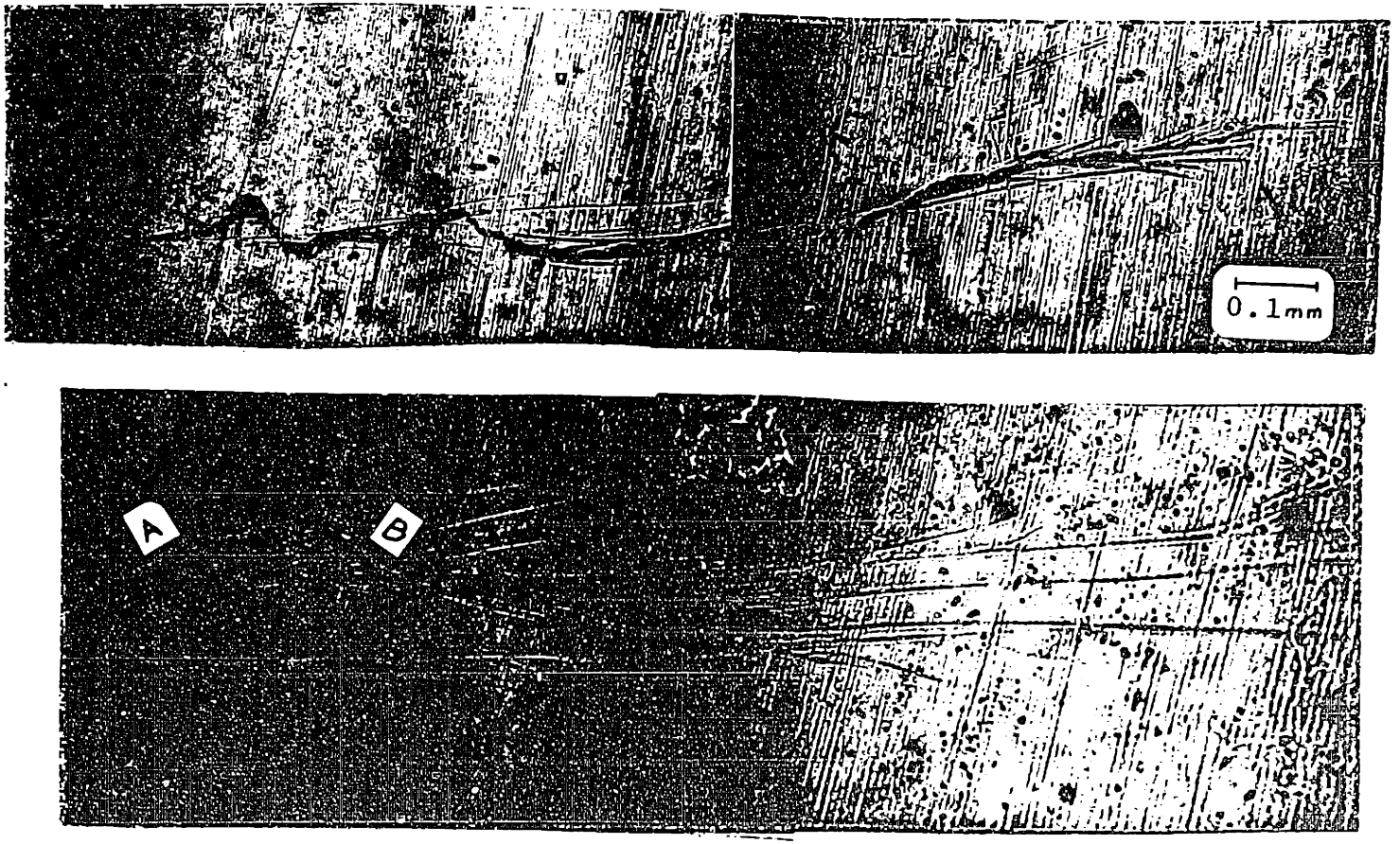

Figure 41 a) Optical micrograph of a crack in pure PVC which has grown stably with multiple crazes forming at the tip. b) A more magnified view of the end of the crack tip. Regions A and B correspond to the SEM micrographs in figures 13 and 42 respectively.

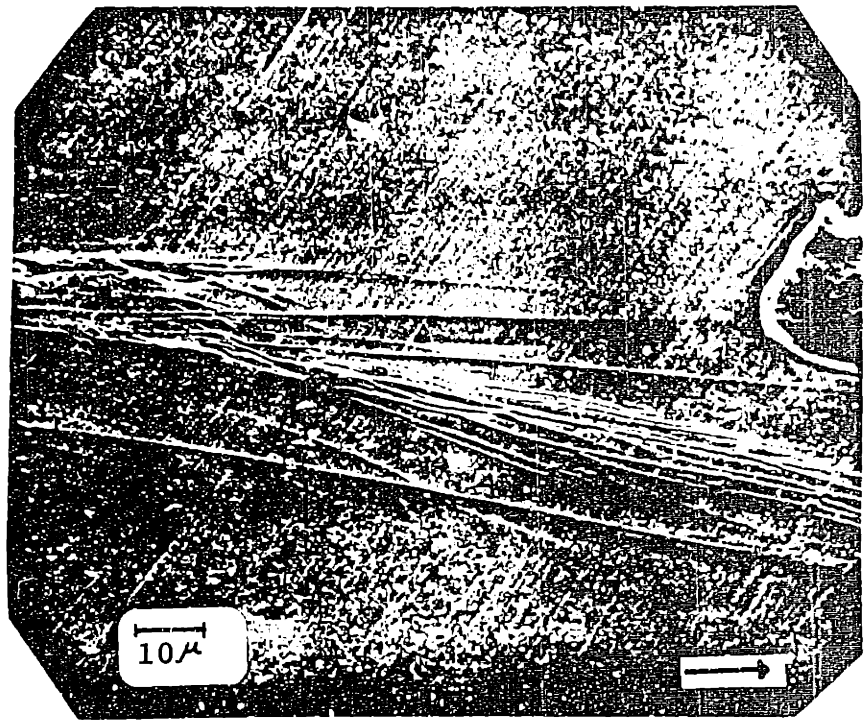

Figure 42. SEM micrographs of the multiple crazes in the stable crack growth zone. Arrow shows the direction of crack propagation.

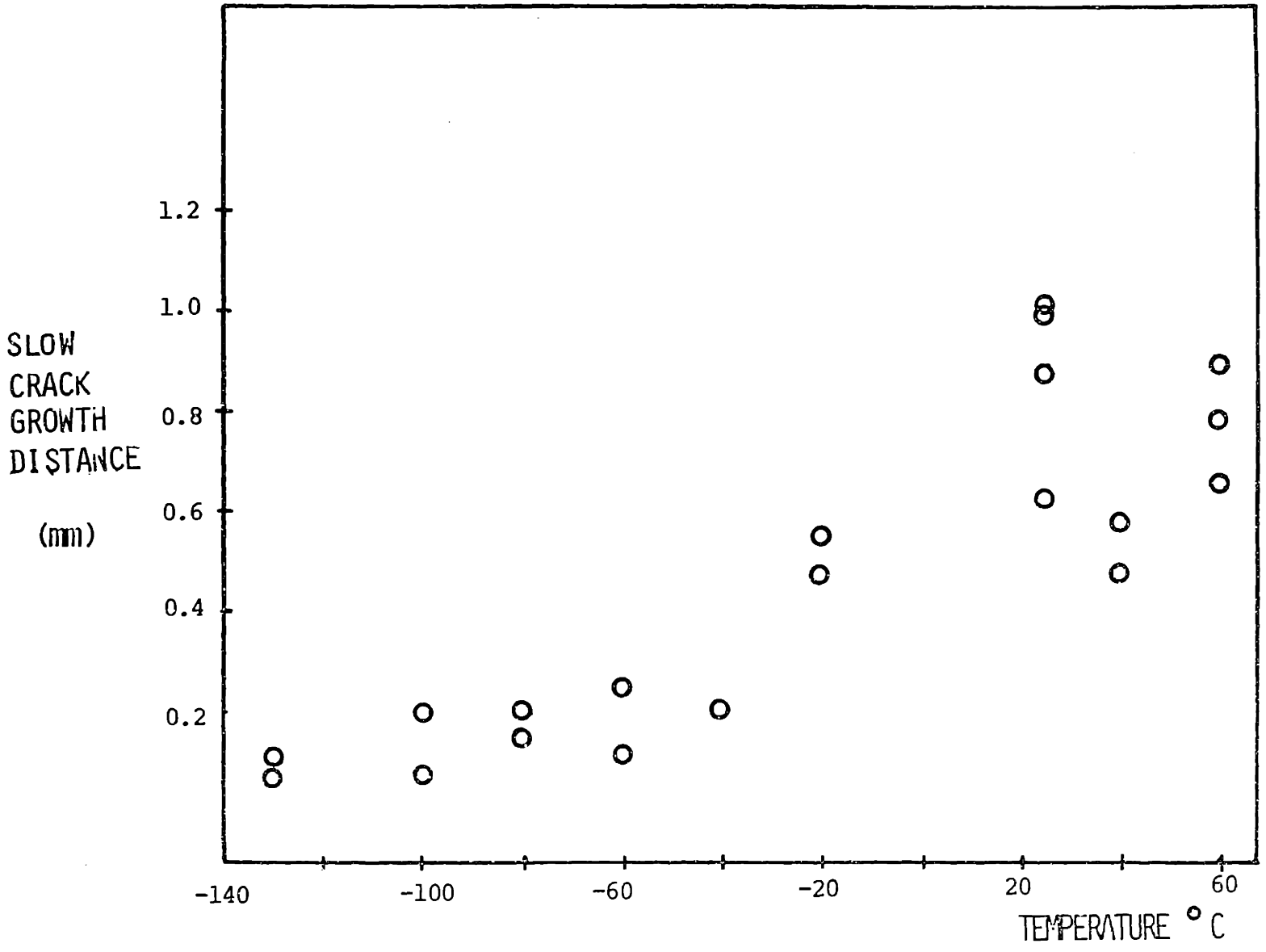

FIGURE. 43

EFFECT OF TEMPERATURE ON THE GROWTH OF THE SLOW CRACK ZONE
LOADING RATE = 500 lb/sec.

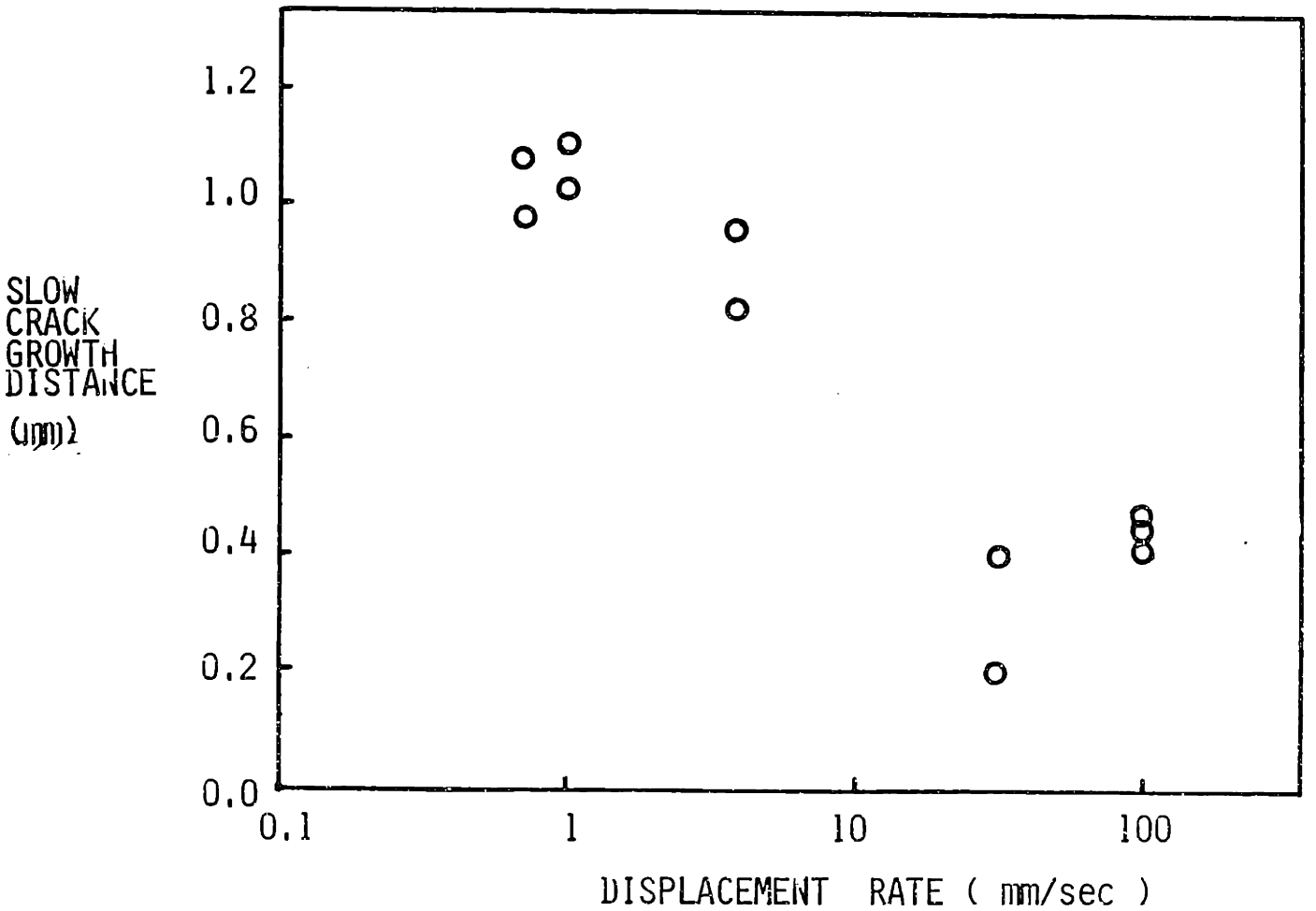

FIGURE 44

EFFECT OF DISPLACEMENT RATE ON THE GROWTH OF THE SLOW CRACK ZONE IN PURE PVC AT ROOM TEMPERATURE.

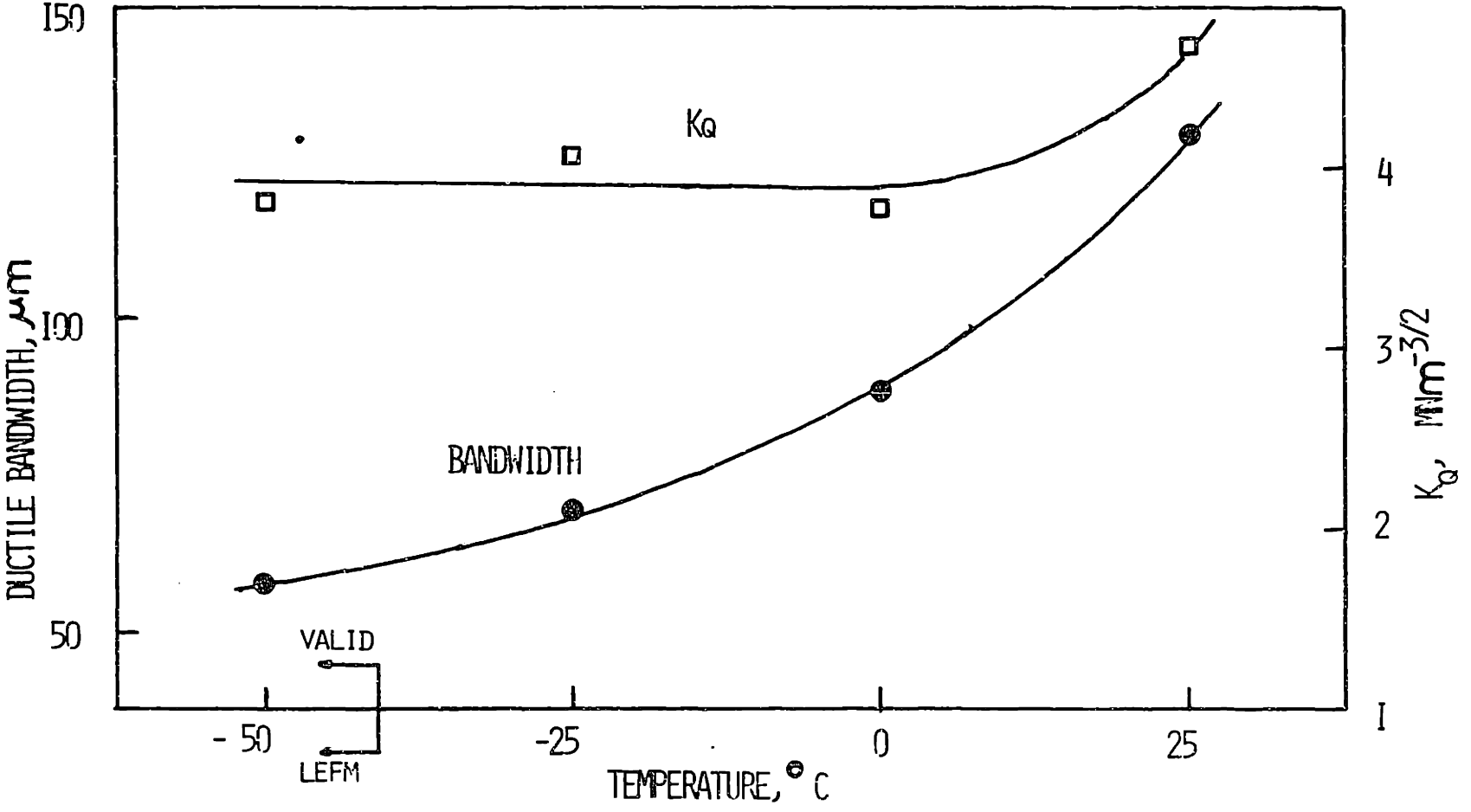

FIGURE 45.

EFFECT OF TESTING TEMPERATURE ON DUCTILE BANDWIDTH AT CRACK TIP IN PVC PIPE M MATERIAL, T_F = 12 ms, CURVED TENSION SPECIMEN, REF.(1).

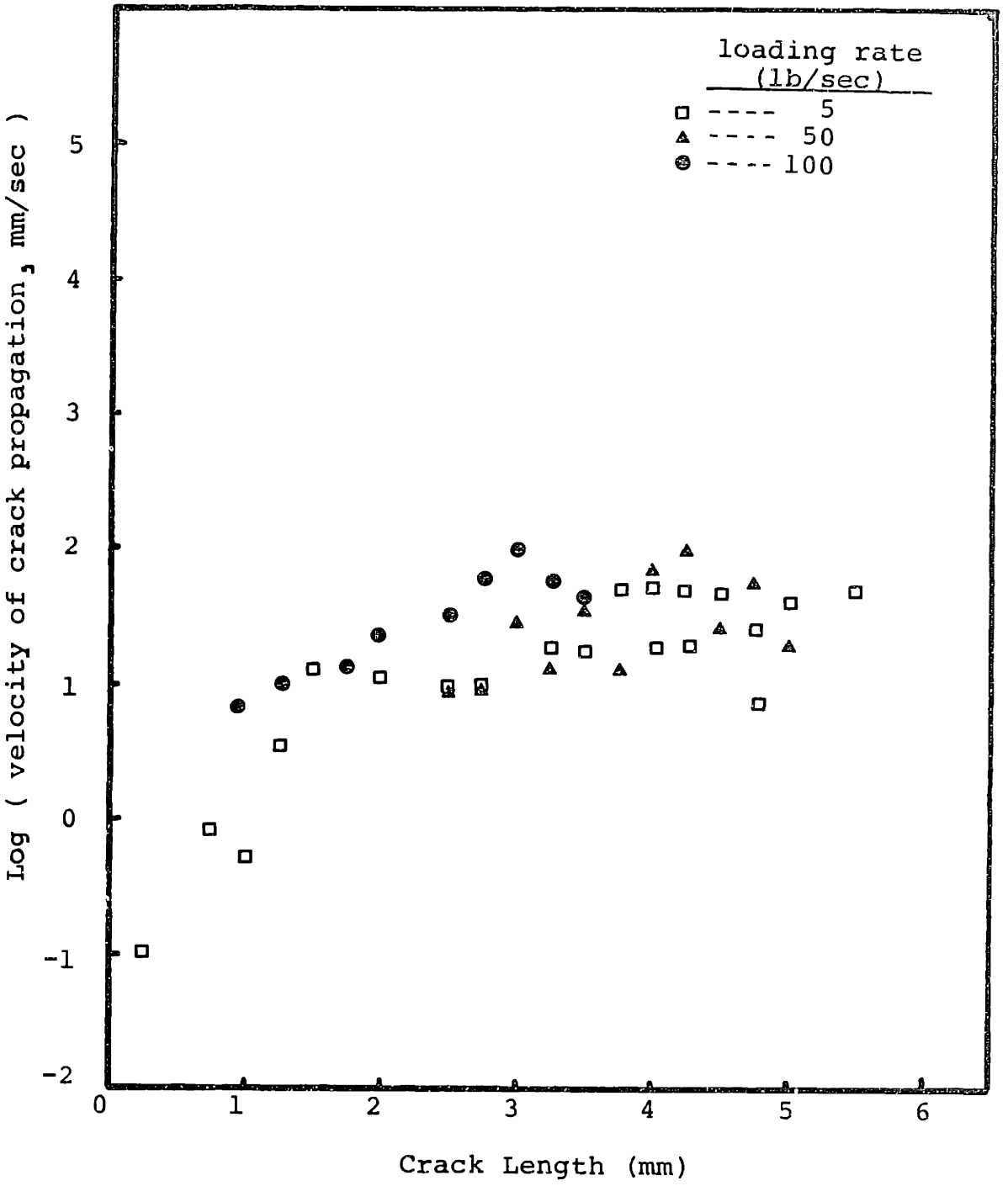

Figure 46 Log crack velocity vs. the instantaneous crack length measured from the initial crack tip.

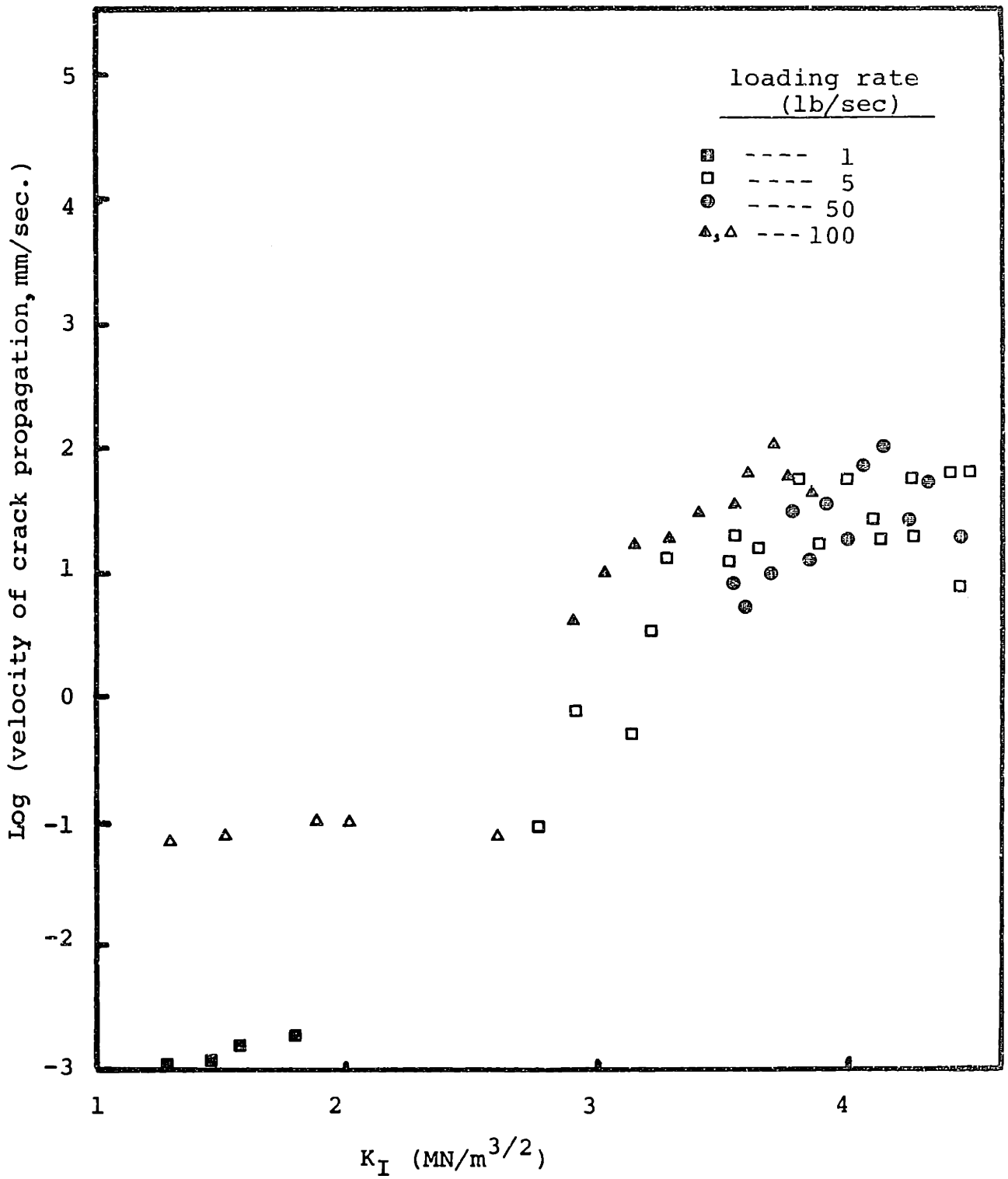

Figure 47. Log crack velocity vs. K_I at the crack tip. The symbols △ and ■ represent the data obtained from the study of the extensional growth rate of the crazes, measured by the microscopy.

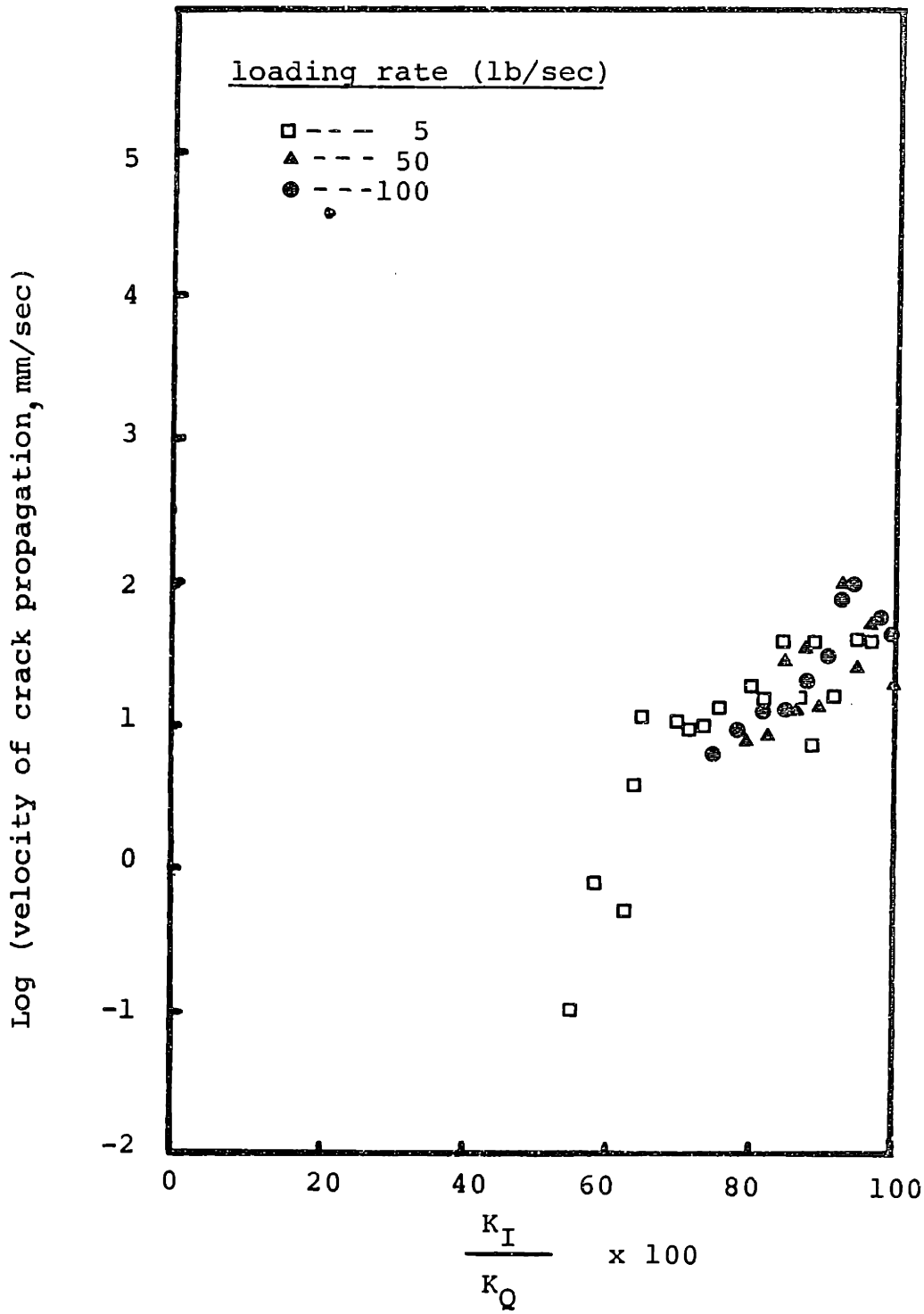

Figure 48. Log of crack propagation velocity vs. K_I/K_Q.

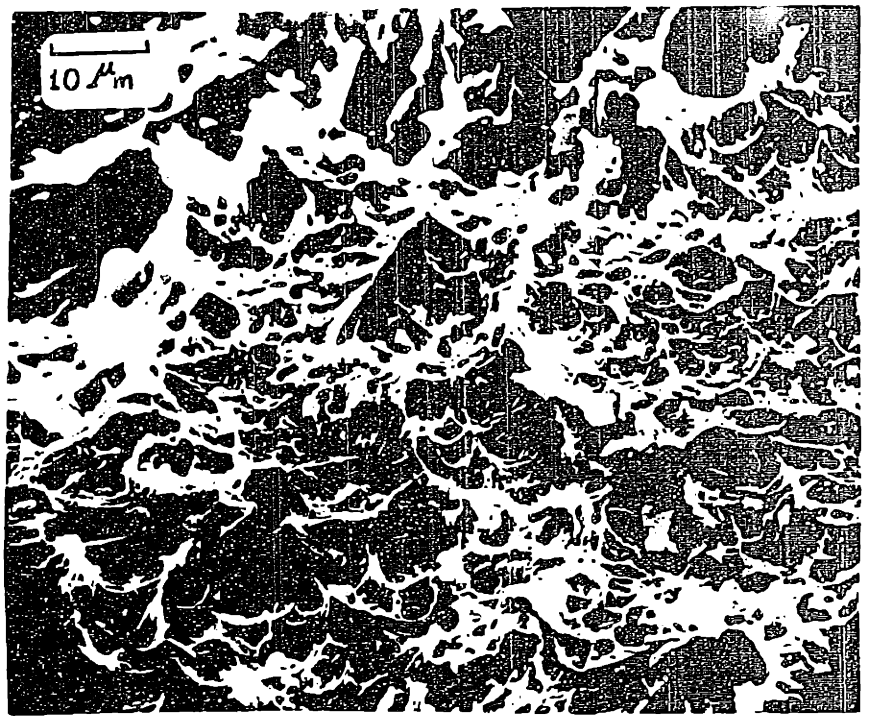

Figure49 Morphology of the ductile band region in PVC pipe materials.

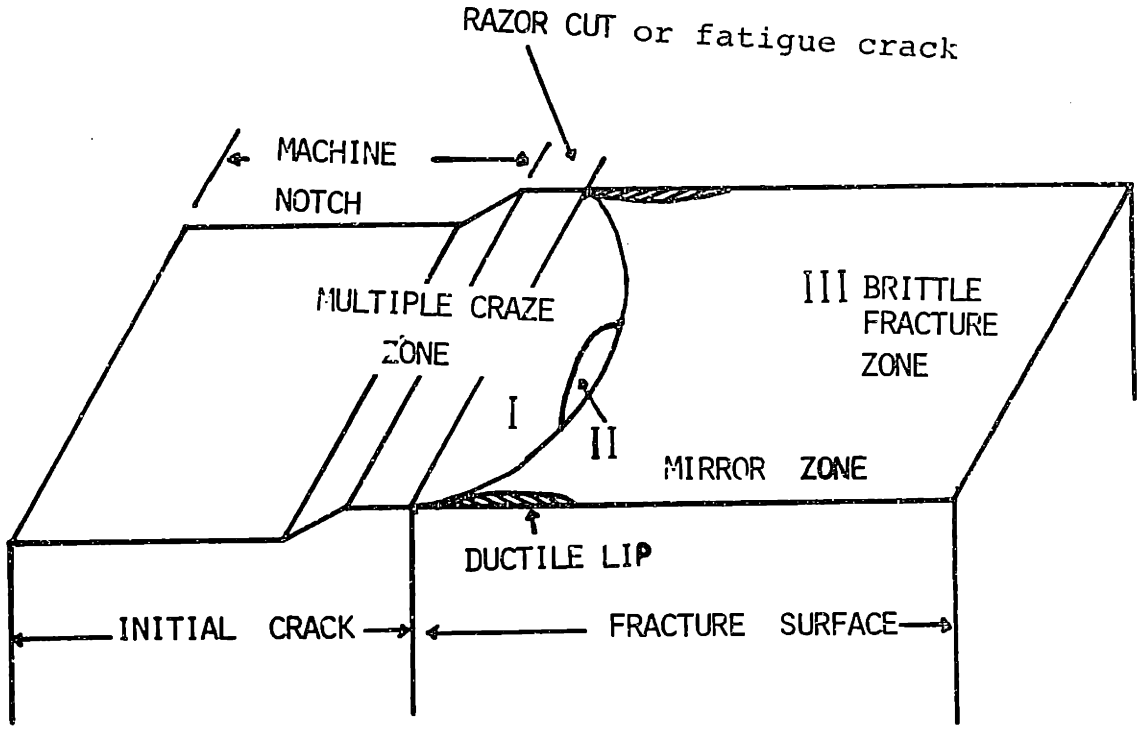

FIGURE 50.

SCHEMATIC REPRESENTATION OF FRACTURE SURFACE OF VALID K_{IC} TEST OF PURE PVC AND C_aCO_3 - PVC MATERIALS.

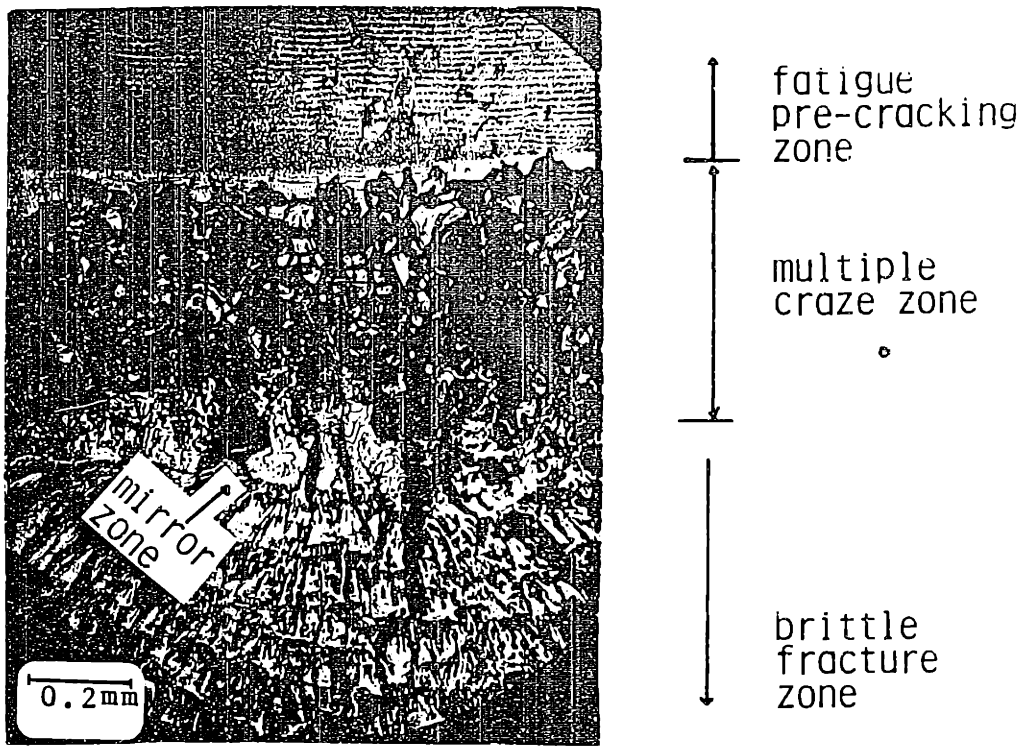

Figure **51 A** Optical micrograph of a fracture surface of a fatigue cracked specimen, pure PVC.

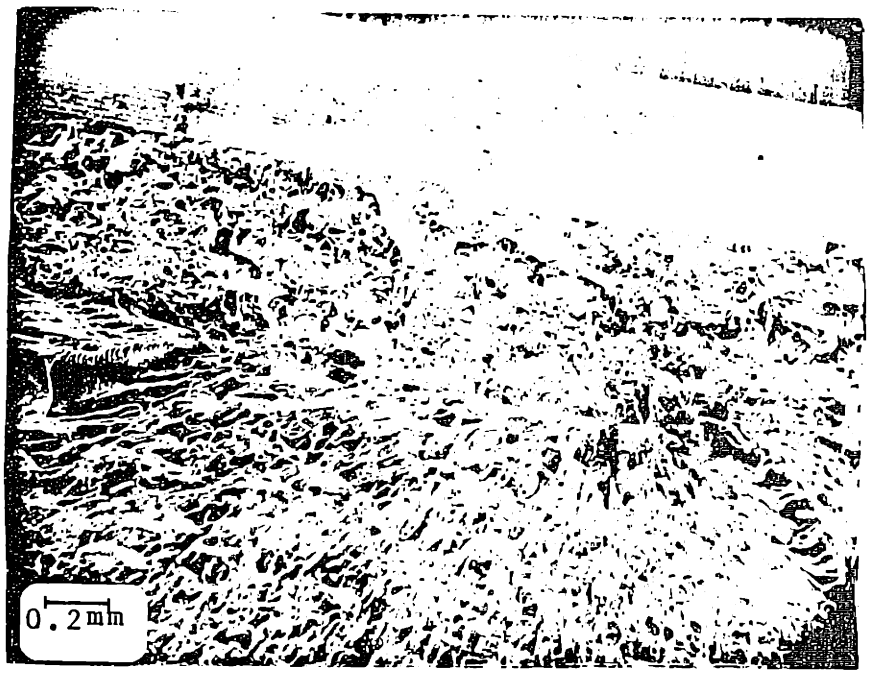

Figure **51 B** SEM micrograph of a fracture surface of a fatigue cracked specimen.

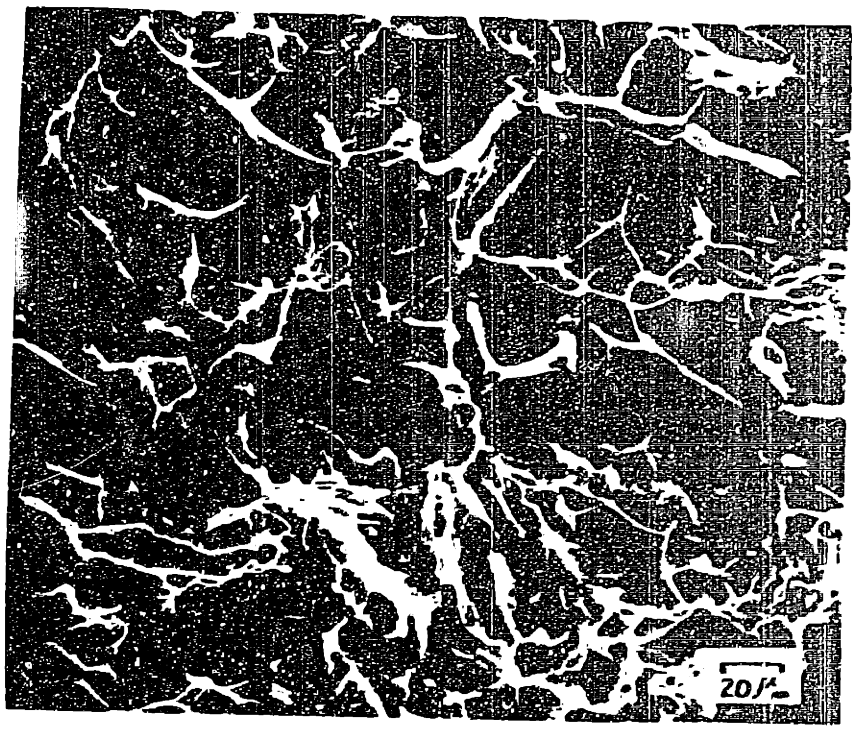

Figure 52 SEM micrograph of the surface morphology of the multiple craze zone in pure PVC specimen fractured at room temperature.

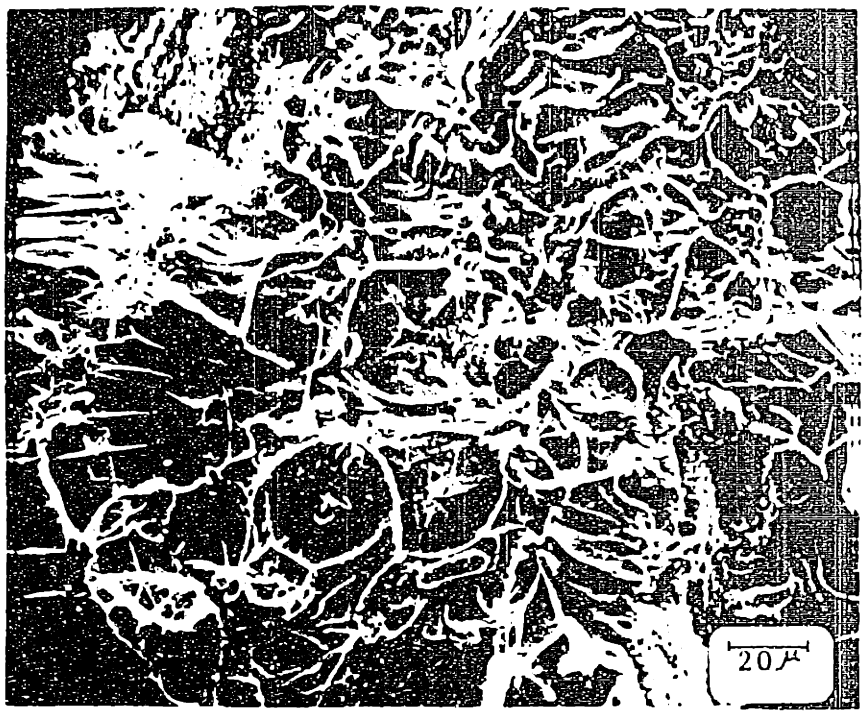

Figure 53 SEM micrograph of the surface morphology of multiple craze zone in $CaCO_3$ filled PVC specimen fractured at room temperature.

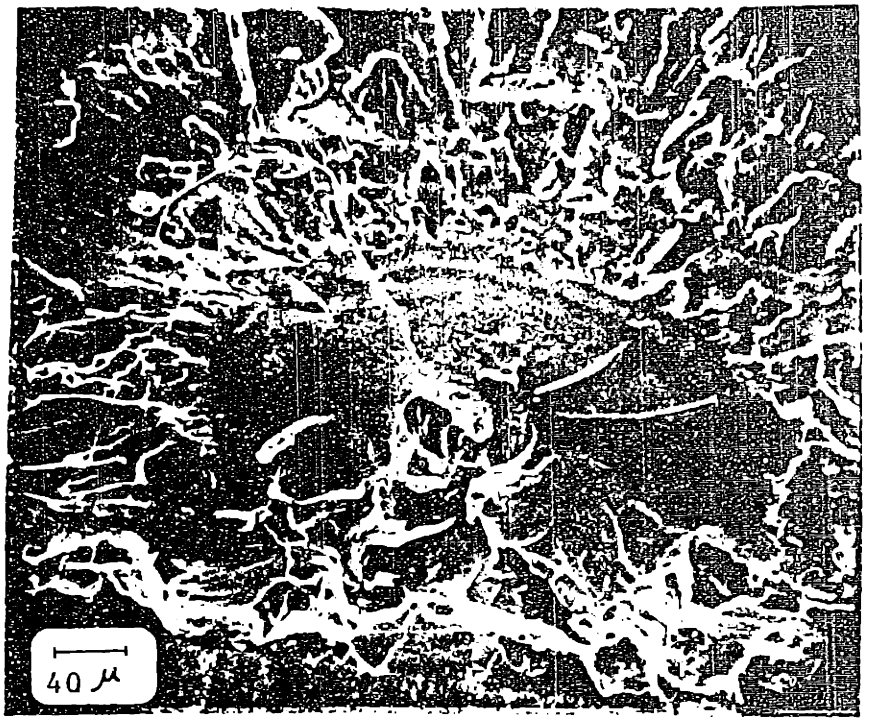

Figure 54 SEM micrograph of the mirror zone on the fracture surface of a pure PVC specimen.

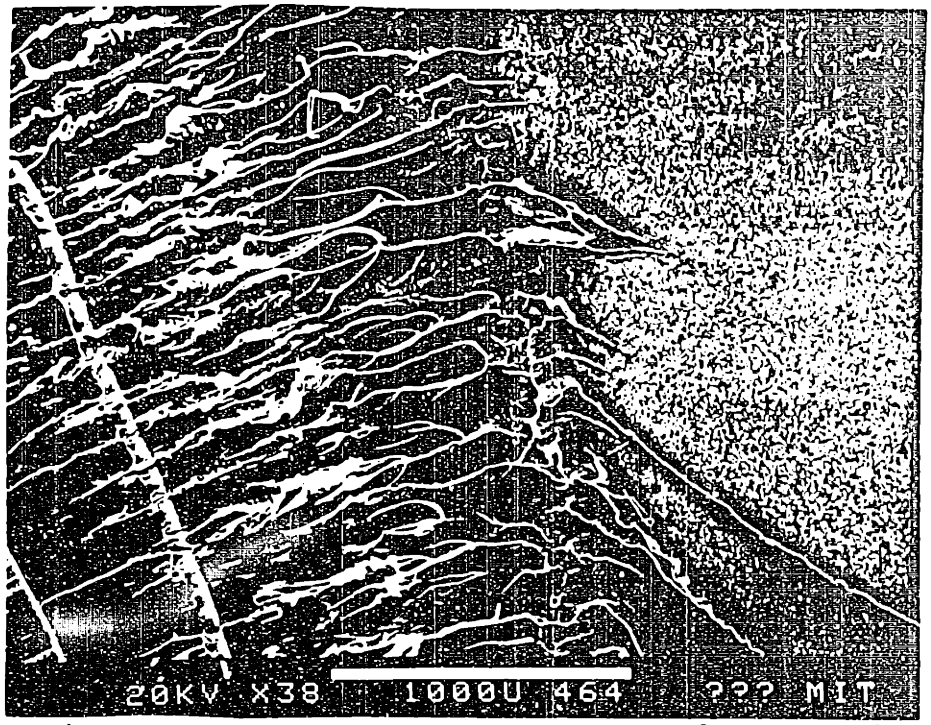

fatigued crack growth zone → | slow crack growth zone → | ← fast crack growth zone →

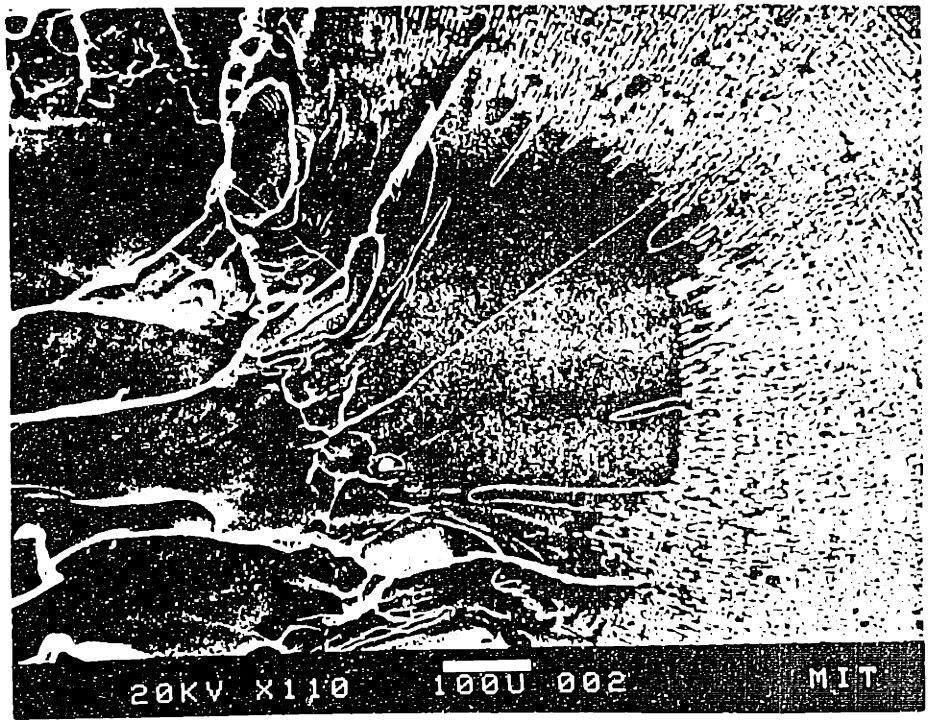

Figure 55 top: Fracture surface morphology of polycarbonate
bottom: Morphology of the fracture origin identified on the fracture surface of polycarbonate.

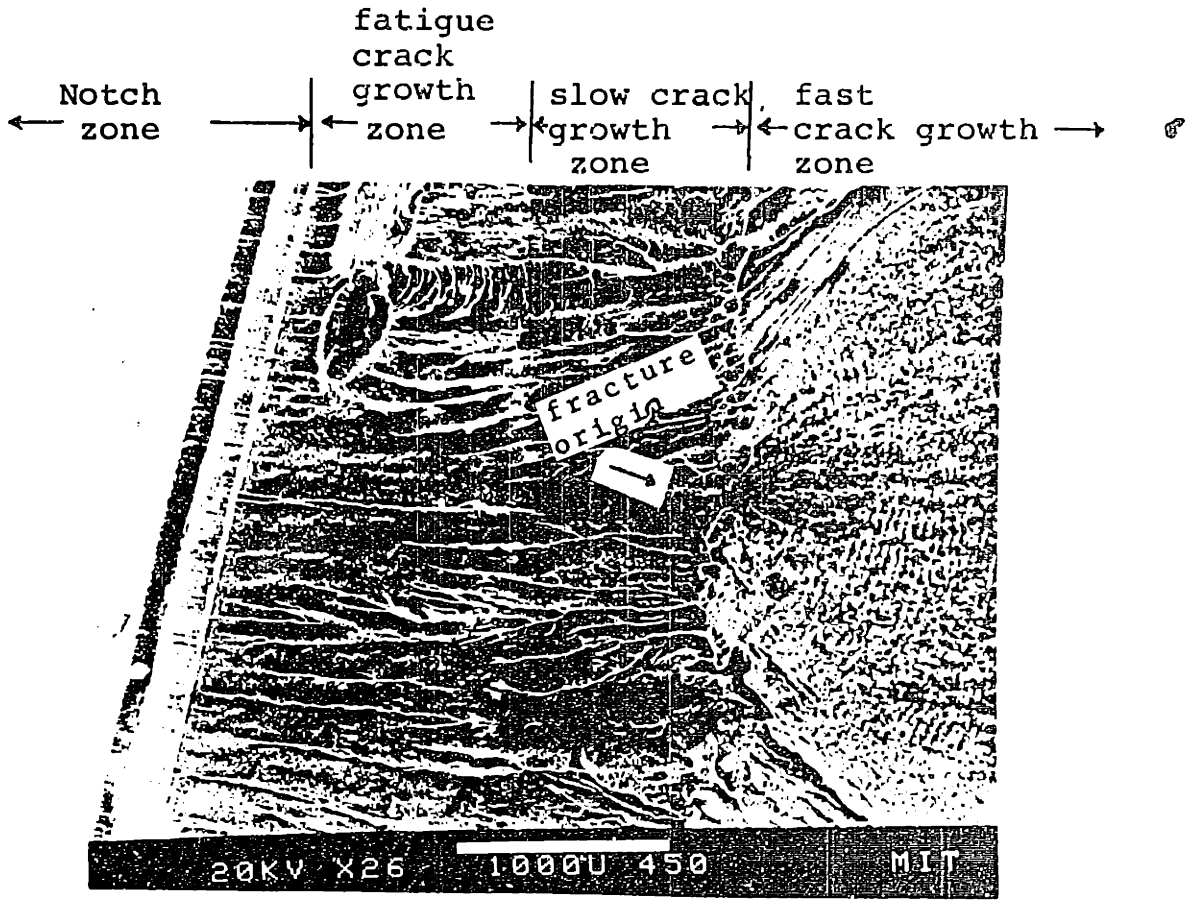

Figure 56 Fracture surface morphology of polysulfone.

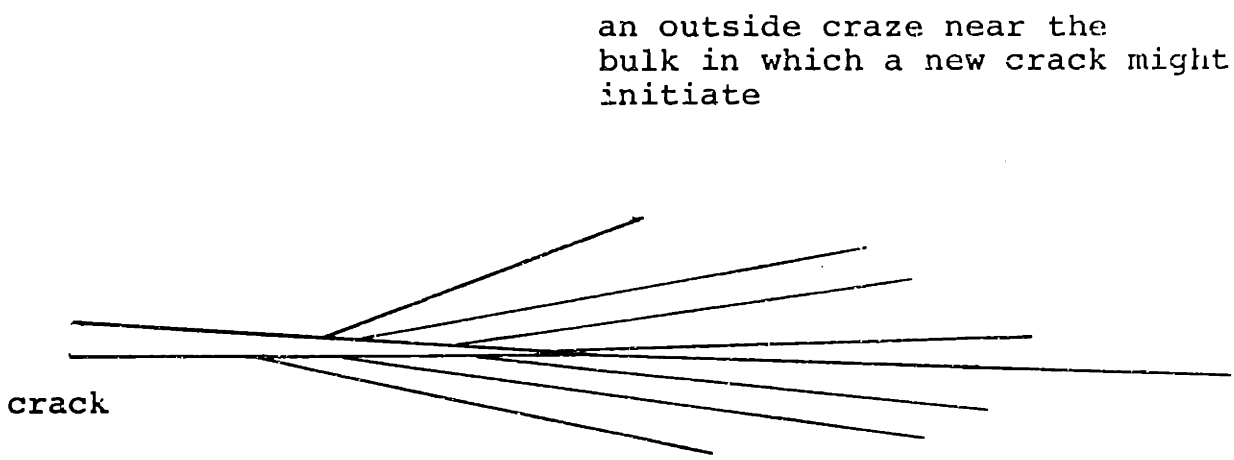

Figure 57. Schematic illustration of the multiple craze zone, showing that a new crack might initiate from one of the secondary crazes near the bulk.

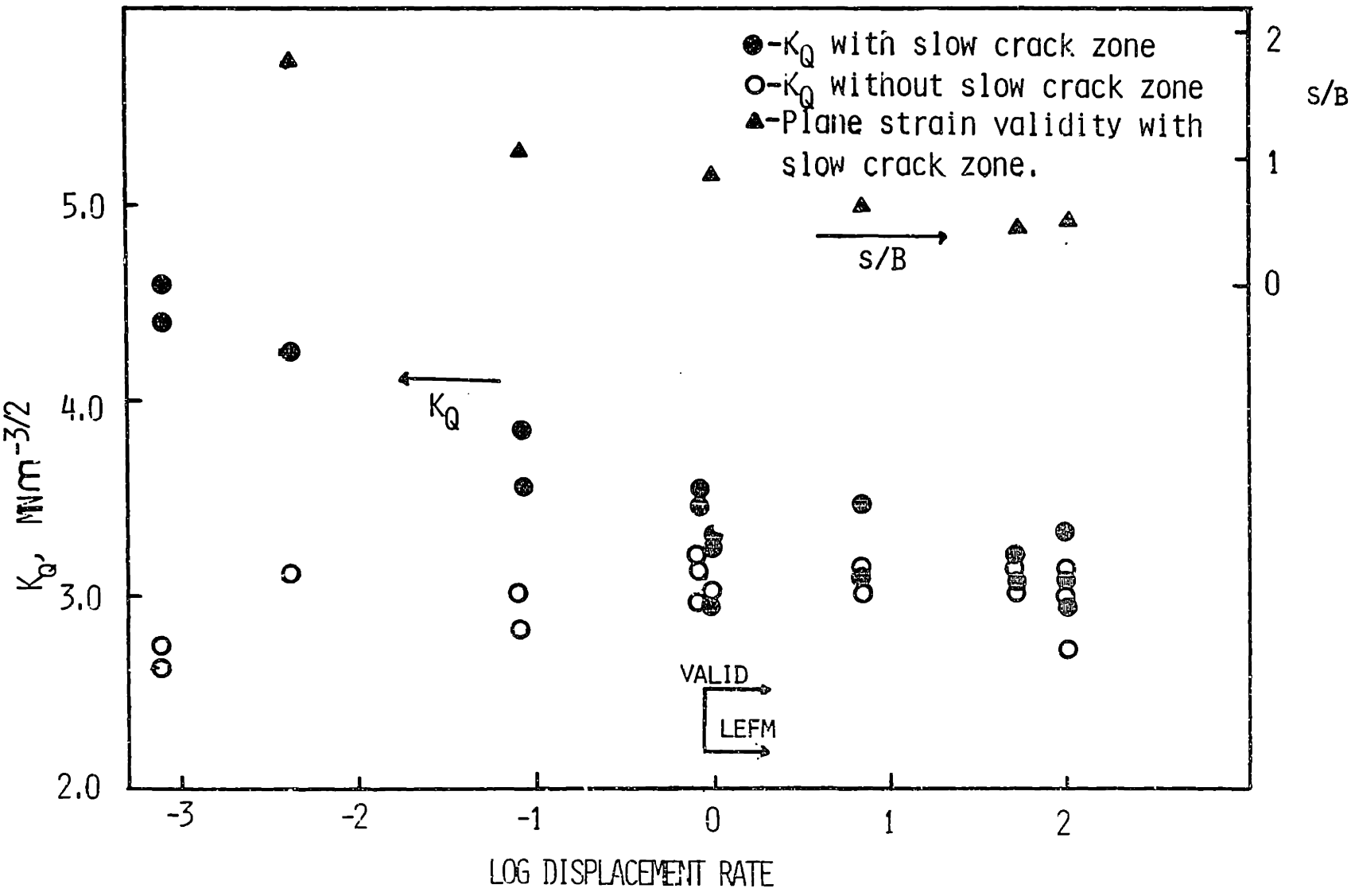

FIGURE 58.

Effect of slow crack zone on K_Q calculation at various displacement rates; room temperature.

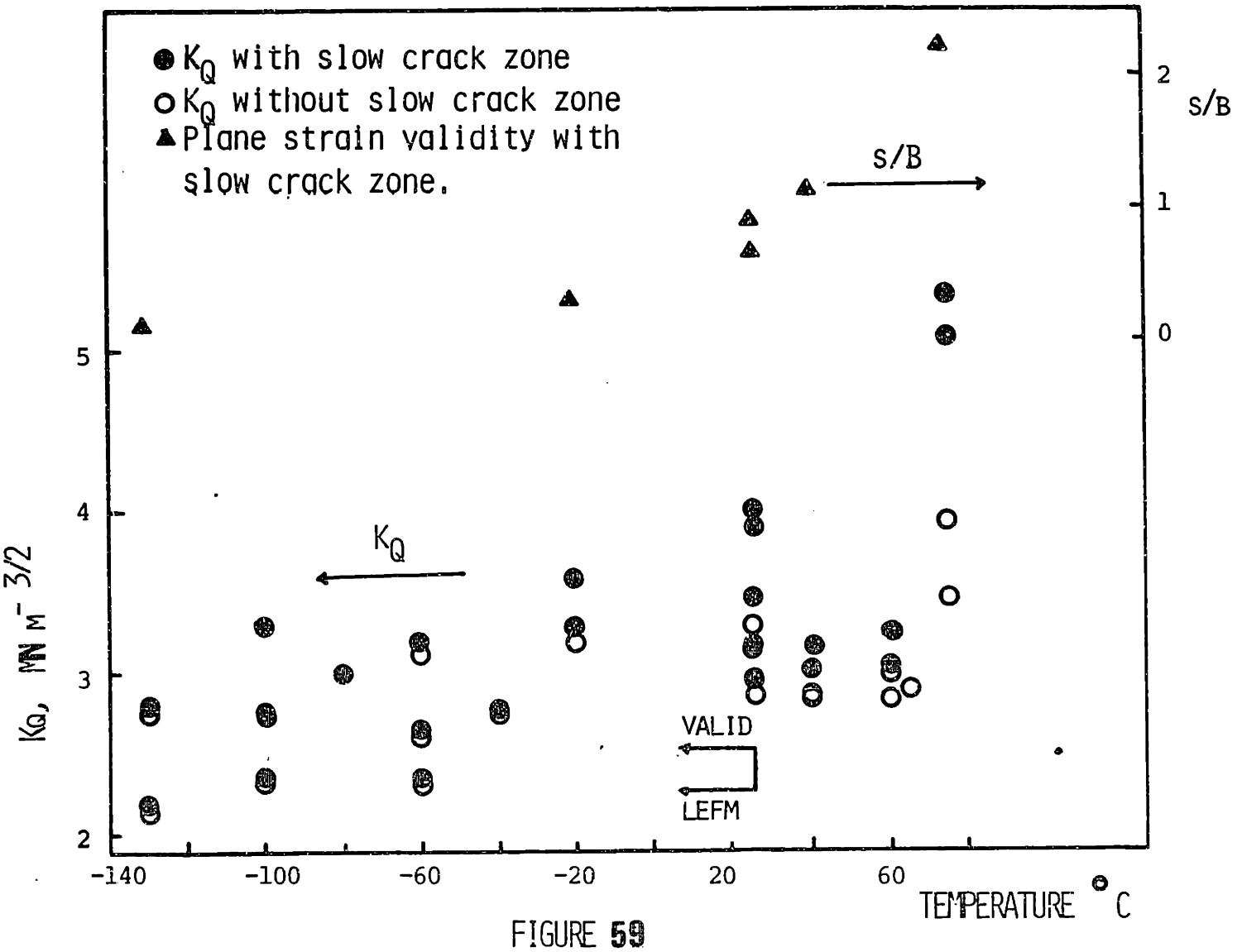

FIGURE 59

Effect of slow crack zone on K_Q calculation at various temperatures; loading rate = 500 lb/sec.

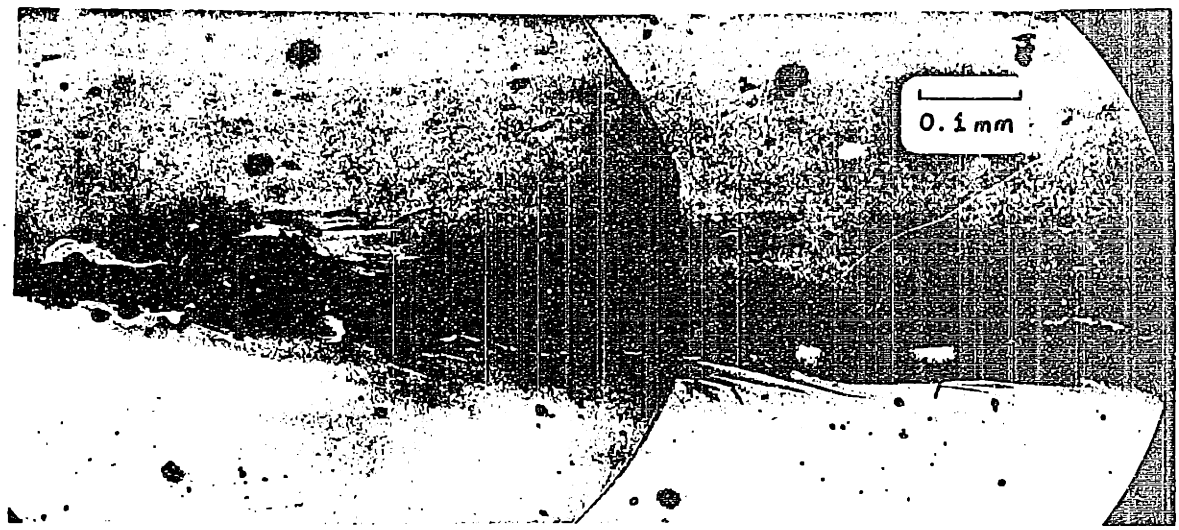

Figure 60, Comparison of the side views of two pure PVC specimens which fractured under the same condition but at different K_c; for the specimen at the top, $K_c = 3.32$ MN/m$^{3/2}$, for the specimen at the bottom, $K_c = 2.89$ MN/m$^{3/2}$.

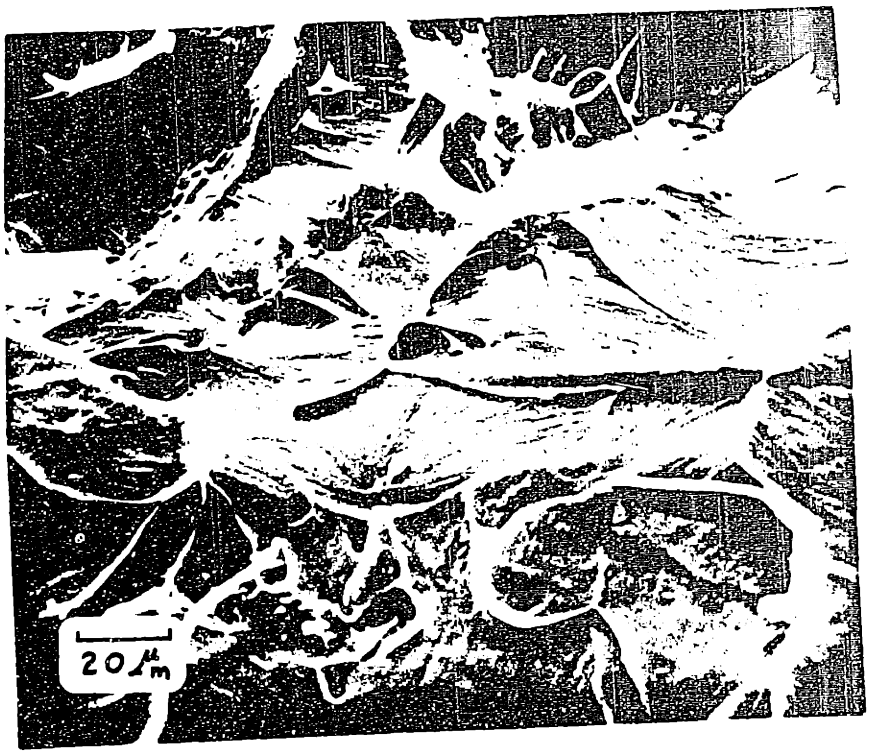

Figure 61 . The morphology of the stable crack growth region in a specimen fractured at -60 C.

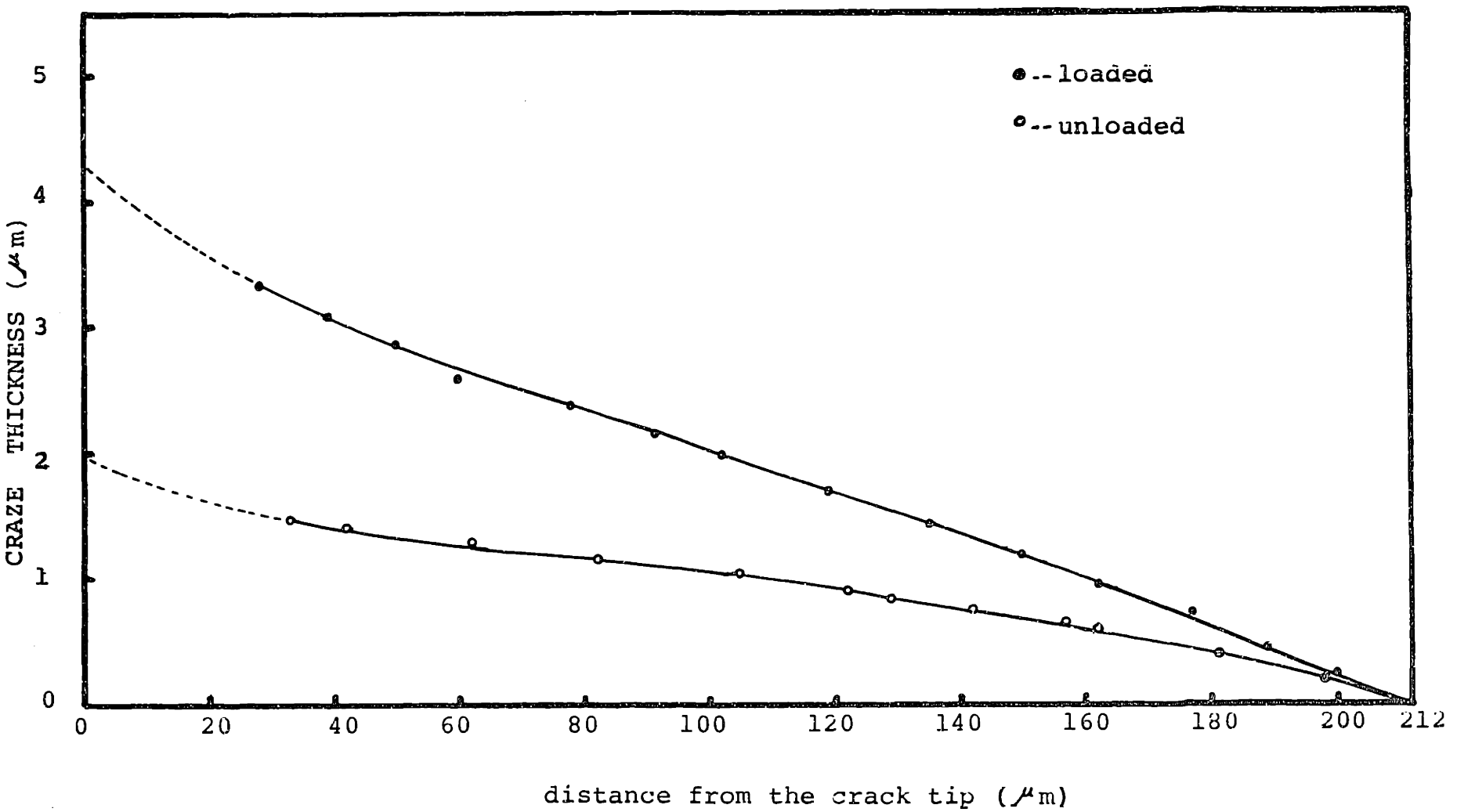

Figure 62 Shape of loaded and unloaded crazes in pure PVC determined from the interference pattern; (●) loaded, (○) unloaded.

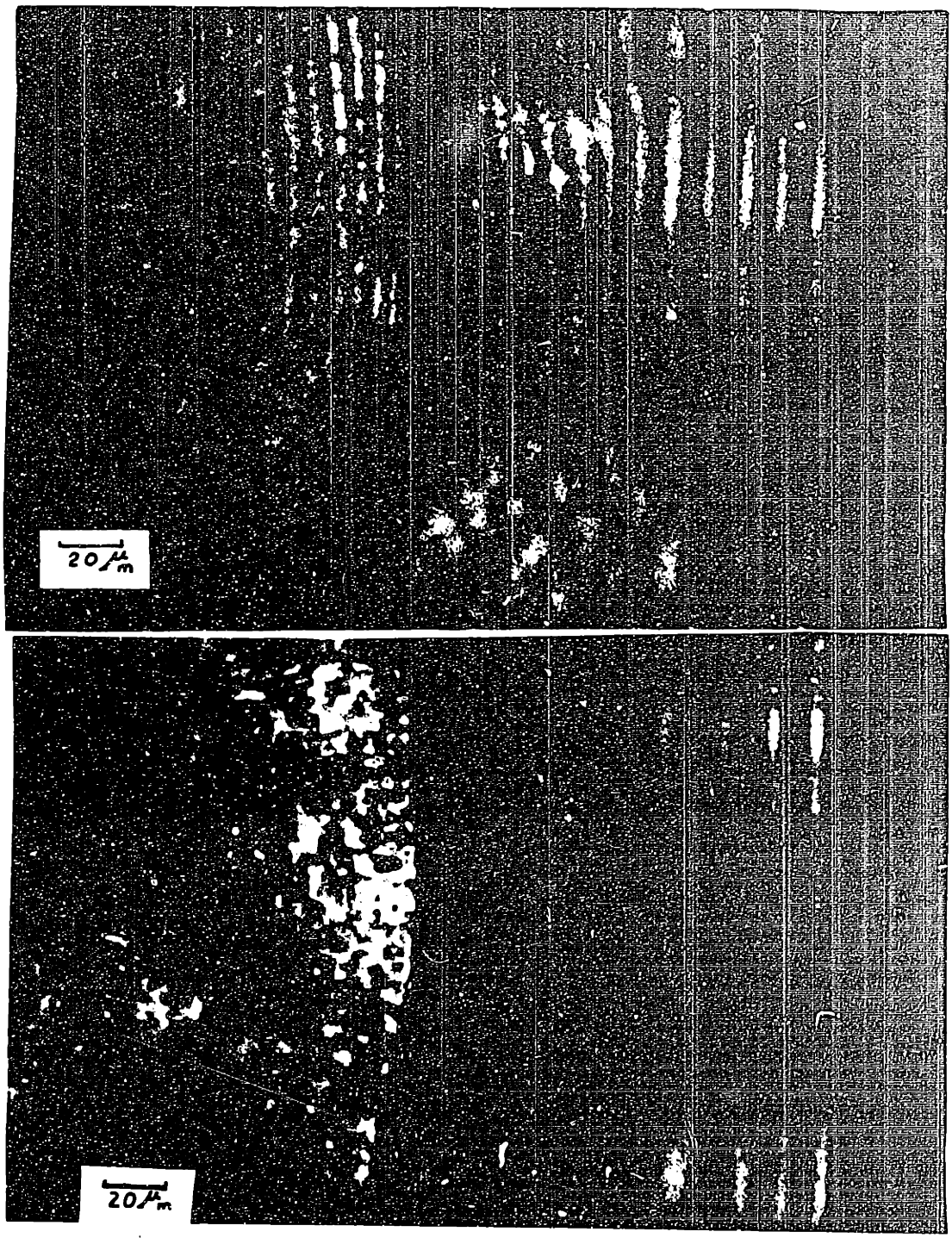

Figure 63 Interference patterns of the craze loaded (top) and unloaded (bottom) at the tip of a crack growing stably.

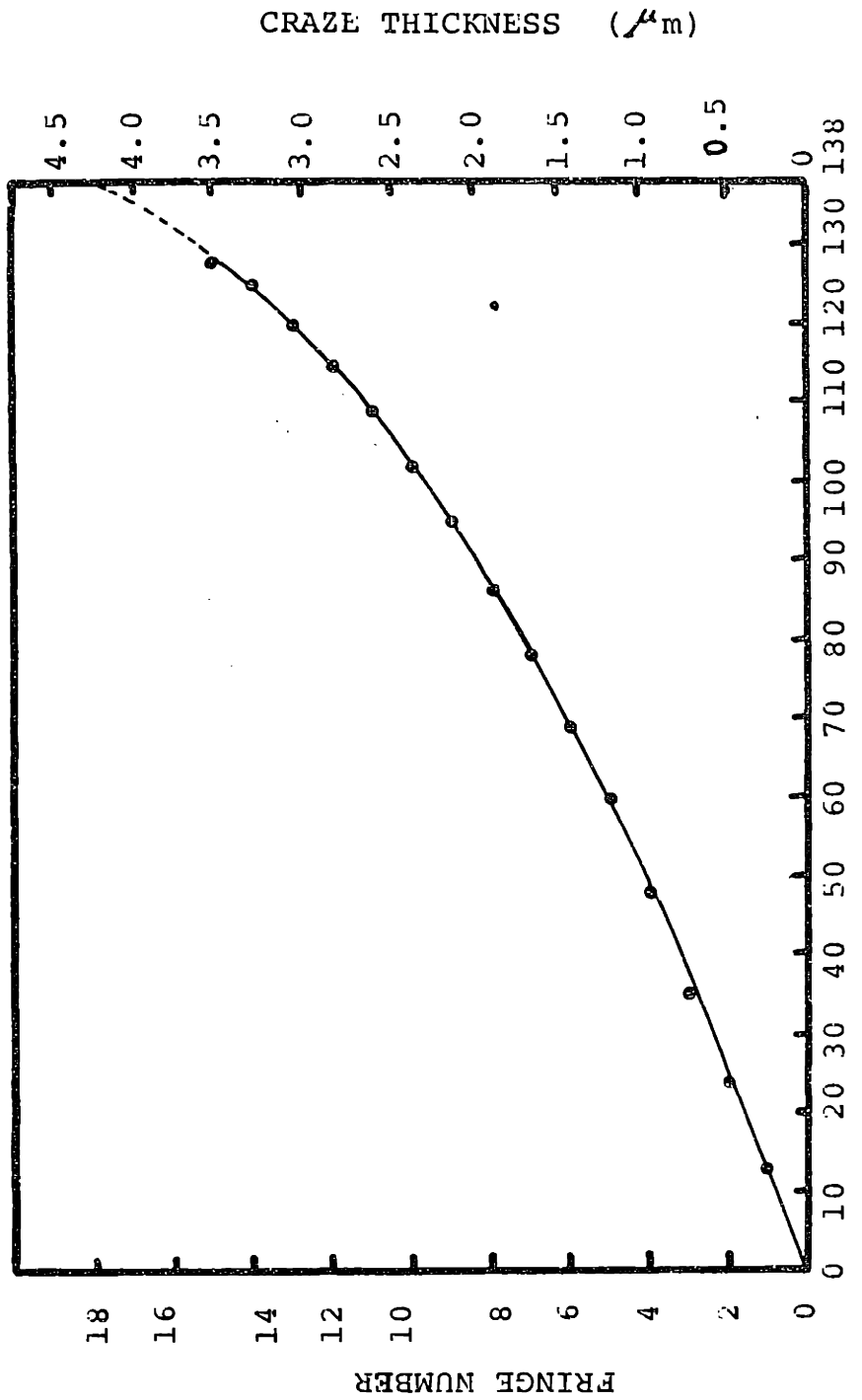

Figure 64 Shape of a loaded craze at the tip of a crack growing stably.

APPENDIX A

Method for Calculating the Refractive Index of a Loaded Craze

According to the theory of interference optics:

$$\delta = \frac{f\lambda}{2\mu} \quad (1)$$

$$\delta_o = \frac{f_o\lambda}{2\mu_o} \quad (2)$$

where δ is the craze thickness of a loaded craze,

δ_o is the crack thickness of an unloaded craze,

f is the fringe number of a loaded craze,

f_o is the fringe number of an unloaded craze,

and λ is the wavelength of the monochromatic light.

Dividing (1) by (2):

$$\delta/\delta_o = f\mu_o/f_o\mu \quad (3)$$

Let $r = \delta/\delta_o$

Then, $r = f\mu_o/f_o\mu$ (4)

Applying the Lorentz-Lorenz relationship:

$$\frac{\mu^2 - 1}{\mu^2 + 2} = P\rho \quad (5)$$

$$\frac{\mu_o^2 - 1}{\mu_o^2 + 2} = P\rho_o \quad (6)$$

where P is the polarizability of the material,

ρ is the densit of a loaded craze,

and ρ_o is the density of an unloaded craze.

Eliminating μ between (5) and (6) and using the relationship in eq.(4) leads to the cubic in r:

$$r^3 + 2Ar^2 - Br + AB = 0$$

where

$$A = (\mu_o^2 - 1)/(\mu_o^2)$$

$$B = \left(\frac{\mu_o f}{f_o}\right)^2$$

The one solution of this cubic with value greater than 1 is used.

With known values of f, f_o and μ_o, together with the value of r calculated, the refractive index of a loaded craze, μ, can be obtained. [25]